Title
Effects of Strong-Column Weak-Beam Ratios on Collapse Capacities of Tall Reinforced Concrete Moment Frame Structures

Author
Cagurangan, Colleen

Publication Date
2015

Peer reviewed|Thesis/dissertation

Effects of Strong-Column Weak-Beam Ratios on Collapse Capacities of Tall Reinforced Concrete Moment Frame Structures

by

Colleen Kirsten Cagurangan

A dissertation submitted in partial satisfaction of the
requirements for the degree of
Doctor of Philosophy

in

Engineering - Civil and Environmental Engineering

in the

Graduate Division

of the

University of California, Berkeley

Committee in charge:

Professor Jack P. Moehle, Chair
Professor Filip C. Filippou
Professor Douglas S. Dreger

Spring 2015

Effects of Strong-Column Weak-Beam Ratios on Collapse Capacities of Tall Reinforced Concrete Moment Frame Structures

Abstract

Effects of Strong-Column Weak-Beam Ratios on Collapse Capacities of Tall Reinforced Concrete Moment Frame Structures

by

Colleen Kirsten Cagurangan

Doctor of Philosophy in Engineering - Civil and Environmental Engineering

University of California, Berkeley

Professor Jack P. Moehle, Chair

The intent of the strong-column weak-beam (SCWB) strength ratio in building codes is to reduce the likelihood of the formation of story mechanisms in reinforced concrete special moment-resisting frames subjected to seismic loading. Previous research has shown that for tall buildings the current code requirement is not sufficient to prevent these undesirable plastic mechanisms from forming and leading to collapse of the structure. Furthermore, nonlinear analyses of structures greater than four stories with strength ratios of 2.0 or greater have shown story mechanisms to still occur. It is unclear whether complete prevention of story mechanisms is possible or even necessary in tall buildings. To achieve a complete building mechanism, the required SCWB ratio would lead to dimensions that would be deemed unacceptable to project sponsors.

To determine the effects that SCWB strength ratios have on collapse mechanisms and collapse capacities of buildings, several structures with differing SCWB ratios and heights were analyzed: namely, 12-, 18- and 24-story structures each with 1.2, 1.4, 1.6, 1.8, and 2.0 SCWB ratios, for a total of 15 structures. Numerical modelling of these perimeter frame structures was done in Opensees. A nonlinear static analysis and an incremental dynamic analysis (IDA) using 30 ground motions were performed on each structure. Fragility curves were obtained using the maximum likelihood method from the results of the IDA. The probability of collapse given a maximum credible event, P(C|MCE), of each structure was subsequently obtained. Maximum beam and column end rotations occurring during the IDA were plotted to examine the types of mechanisms formed.

To Tym.

Contents

List of Figures

List of Tables

Acknowledgments

I would first like to thank my husband, Christopher Cagurangan. Without his invariable love and support this thesis would not have been possible. It has been a long road, and I am blessed to have found someone so patient, understanding and willing to accompany me on this journey.

I would like to express my gratitude to my PhD advisor, Professor Jack Moehle. It is only with his understanding and guidance that I have been able to complete this PhD program. He has generously imparted his knowledge and wisdom, enabling me to develop my researching skills. I would like to thank Professor Filip Filippou for being a wonderful, enthusiastic professor and mentor. I am grateful to have had the opportunity to study at UC Berkeley and learn from such amazing faculty as he.

I would like to thank Silvia Mazzoni for spending so much time teaching me the ins and outs of Opensees and getting my computer models up and running. I am also very grateful to Frank McKenna, who has helped me out of more Opensees problems than I can count. He provided the technical support I needed to complete my research.

I have met several wonderful colleagues along the way, who have become dear friends. I would like to acknowledge my one-time officemate and great friend, Gabriel Hurtado, with whom I have shared many of the ups and downs. He has always been there to discuss issues both professional and personal. I would like to thank Margarita Constantinides for her friendship; she has been able to truly sympathize with the laughter and tears that come with the PhD program.

I am grateful this program has afforded me the opportunity to meet people from near and far. Carlos Arteta has been a great friend, helping me both academically and emotionally during the final months of this dissertation. Beyhan Bayhan, though he may be far away, is still near and dear to my heart. A big thank you to these friendships that have made the PhD bearable and even pleasurable.

Chapter 1

Introduction

1.1 Motivation

The intent of the strong-column weak-beam (SCWB) strength ratio in building codes is to reduce the likelihood of the formation of story mechanisms in reinforced concrete special moment resisting frames subjected to seismic loading. The current ACI 318 provisions, (ACI 318-14, 2014), require a column-to-bream strength ratio of 1.2 or greater as summed at the joints. Previous research (Dooley & Bracci, 2001; Haselton et al., 2011; Ibarra & Krawinkler, 2005) has shown that for tall buildings this is not sufficient to prevent these undesirable plastic mechanisms from forming and leading to collapse of the structure. Furthermore, nonlinear analyses of structures greater than four stories with strength ratios of 2.0 or greater have shown story mechanisms to still occur (Haselton et al., 2011; Ibarra & Krawinkler, 2005). It is unclear whether complete prevention of story mechanisms is possible or even necessary in tall buildings. To achieve a complete building mechanism, the required SCWB ratio may be greater than is acceptable to the project sponsor.

1.2 Objective

The objective of this study is to investigate the role SCWB ratios have on the performance of tall buildings. Collapse capacities of structures have been used as a way to quantify and compare their performances. It has been shown that SCWB ratios have a significant effect on collapse capacity, thus this study will investigate the performance of tall buildings with varying SCWB strength ratios subjected to far-field ground motions scaled to collapse of the structure using an incremental dynamic analysis approach and to present the reader with information as to how much of an increase in performance one can expect given an increase in the SCWB strength ratio. This will be achieved through the review of previous research and the analytical modeling and analyses of the various structures.

1.3 Scope

This study encompasses reinforced-concrete special moment-resisting-frame structures ranging in height from 12- to 24-stories. All buildings have perimeter frames as lateral force resisting systems. Any lateral resistance provided by the gravity framing is neglected. SCWB ratios range from 1.2 (as prescribed by the current code) to 2.0 (any higher would seem unreasonable to expect a practitioner to implement). This study is limited to one plan configuration from which all structures are built, situated on a firm-soil site Class C.

1.4 Organization

Chapter 2 provides a review of previous literature on the subject of SCWB strength ratios, giving an overview of some of the building code requirements currently in use, summarizing the findings of SCWB ratio recommendations to date as well as the previously investigated effects of SCWB ratios on performance. Chapter 2 also reviews the hysteretic model and collapse capacity method used in the evaluation of the structures.

Chapter 3 provides the methodology used in this study: the layout of the structure, the mathematical model, seismic analysis and design of the model, and the analysis of the results of the incremental dynamic analysis.

Chapter 4 introduces the buildings under investigation, providing the plan layout and frame details and ultimately the SCWB strength ratios for each structure.

Chapter 5 presents and discusses the results from the collapse capacity analysis of each structure, including collapse capacity, collapse margin ratio, collapse fragility curves, and failure mechanisms for each structure. A comparison of two definitions of SCWB ratios to measure performance of a structure is also presented.

Chapter 6 summarizes the research done and explores future research possibilities.

Chapter 2

Literature Review

2.1 Strong-Column Weak-Beam Ratios in Use

The intent of the strong-column weak-beam (SCWB) provisions found in many codes is to reduce yielding of columns above the ground floor in moment-resisting frames, thus avoiding excessive local ductility demands and the subsequent formation of story mechanisms. There is, however, little consensus among the codes and current literature as to what that strength ratio should be to create a strong-column weak-beam condition.

Recommendations for the strength ratio differ among various building codes. The Canadian Standards Association (CSA, 2004) only requires that the sum of the nominal moments of the columns taken at the center of the joint be greater than or equal to the sum of the probable moments of the beams taken at the center of the joint, that is a SCWB ratio of one. ACI 318-14 (2014) states that at the face of a joint the sum of the nominal moments of the columns framing into the joint shall be greater than the sum of the flexural strengths of the beams by a factor of 1.2, while the Eurocode (Eurocode 8, 2004) requires a factor of 1.3 for the column-to-beam design flexural strength ratio.

Also with a minimum SCWB ratio of 1.3, a more involved approach is taken by the New Zealand building code (NZS:3101, 2006; Paulay & Priestley, 1992). The upper floors are more significantly effected by the higher modes than the lower floors, as are buildings with longer periods, therefore the dynamic magnification factor is varied over the height of the structure and according to the period of the building as follows.

For columns of one-way frames:

$$\begin{gathered} \omega_{max} = 0.5T_1 + 0.85 \\ \text{where} \\ 1.3 \leq \omega_{max} \leq 1.8 \end{gathered} \tag{2.1}$$

with ω_{max} applied starting at a third of the building height up to two floors below the top level, and varies linearly from 1.0 at the ground level to ω_{max}, and from the top floor down to ω_{max}, as shown in Figure 2.1.

Though a specific SCWB ratio has yet to be agreed upon, there is agreement that current SCWB code requirements do not inhibit story mechanisms from occuring, especially in taller buildings, and that the higher the column yielding extends in the structure, the better the

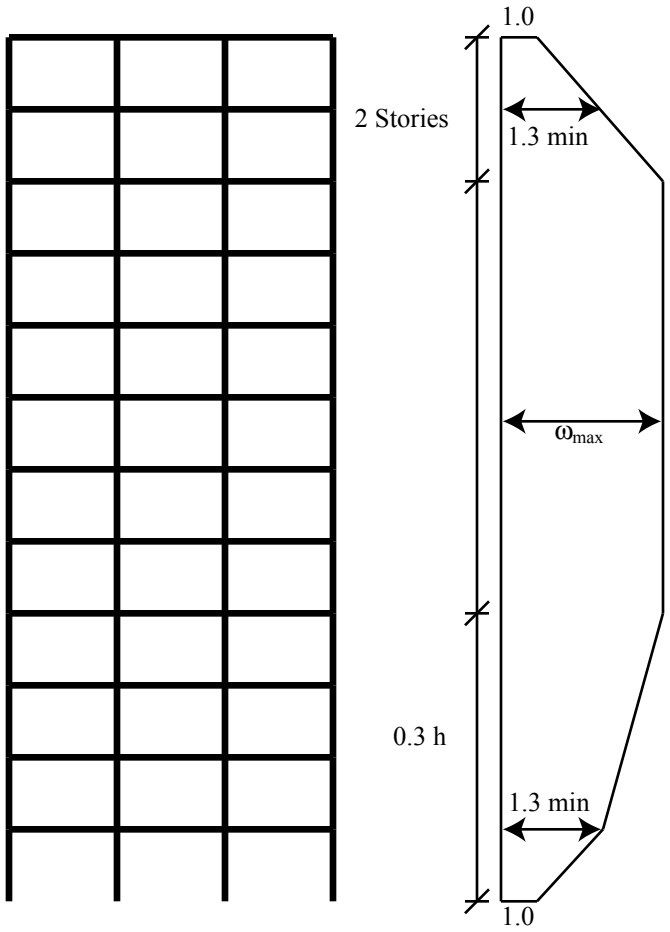

Figure 2.1: New Zealand Standards Dynamic Magnification Factor, ω

structure can be expected to perform. Among those suggesting higher SCWB ratios, the Structural Engineering Association of California recommends a higher ratio of about two in their Blue Book article, *Reinforced Concrete Structures*, while Durrani and Wight (1985) recommend 1.5. Dooley and Bracci (2001) studied the response of three- and six-story buildings to 20 design level ground motions and found that a "minimum strength ratio of 2.0 might be more appropriate" and that increasing strength not stiffness was more beneficial. Using a column-to-beam strength ratio of 1.2, the probability of forming a story mechanism was approximately 90%. Increases beyond 2.0 did little to improve performance.

Kuntz and Browning (2003) took a top down approach, reducing girder strengths from the top floor to as far down as the middle of the structure in structures four to sixteen stories tall. The reduction value, R_g, varied from approximately 1.6 to 2.7 in the upper girders, with a general trend of increased R_g with increase in number of stories. This alternatively can be thought of as increasing the α factor (similar to the SCWB ratio) up the height of the structure.

Haselton et al. (2011) also studied the effects that the SCWB ratio has on the seismic

performance and the risk of collapse of buildings. Using ground motions scaled to a rare event level spectral shape and studying four-story and 12-story structures, they found 1.2 is fine for four-story buildings, but that a complete building mechanism was not realized until a ratio of 2.0 was used. For the 12-story structure, the building performance continued to improve through to a ratio of 3.0, beyond which no studies were performed. They suggested the SCWB ratio could be height dependent, and that it may help to vary the SCWB ratio over the height of the structure, with larger ratio starting at the lowest level. This is contradictory to the findings of Kuntz and Browning (2003).

Ibarra and Krawinkler (2005) studied the global collapse of frame structures nine to 18 stories tall. Their models with infinitely strong columns exhibited very large column moments when the beams reached their bending strength. They found the SCWB ratio would need to be greater than three to avoid hinges occurring in the columns. They also modeled structures with more conventional SCWB ratios of 2.4, 1.2 and 1.0. Compared to the infinitely strong column models, these structures had greatly reduced collapse capacities with columns forming plastic hinges long before the collapsing mechanism occurred.

It is apparent that current SCWB design criteria should be reviewed (Ibarra & Krawinkler, 2005; Haselton, Goulet, et al., 2008; Building Seismic Safety Council of the National Institute of Building Sciences, 2009).

2.2 Hysteretic Model

To simulate the behavior of structures undergoing large ground motions, models are constructed in Opensees, the Open System for Earthquake Engineering Simulation (McKenna et al., 2000). These models need to account for the high degree of nonlinearity the structures are expected to experience. By design, the moment-resisting frames of these structures are expected to yield in moment either in the beams or columns, thus modeling the nonlinearity comes down to modeling the moment-rotation relationships at the end of the elements.

Many hysteretic models have been proposed, but the model employed here was developed by Ibarra and Krawinkler (2005). Building on the Clough material, their model incorporates strength deterioration and cyclic deterioration of strength and stiffness. The backbone curve of their model is shown in Figure 2.2 and is defined by the following:

- The initial stiffness - K_e
- The hardening stiffness - $K_s = \alpha_s K_e$
- The post capping stiffness - $K_c = \alpha_c K_e$
- The yield moment - M_y
- The residual strength branch - $M_r = \lambda M_y$
- The capping plastic rotation - Θ_{cp}
- The post capping rotation - Θ_{pc}

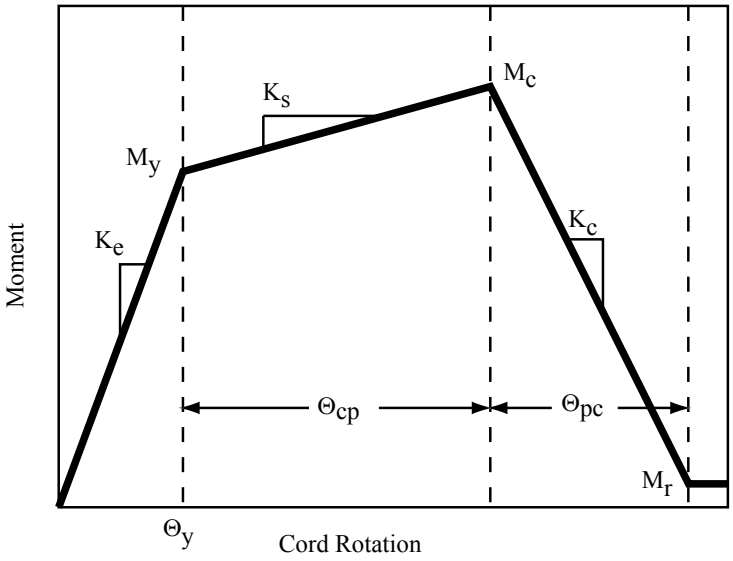

Figure 2.2: Moment-Rotation model developed by Ibarra, Medina, and Krawinkler. (Adapted from Haselton and Deierlein)

Several equations have been proposed for estimating the various quantities needed to describe this moment-rotation relationship. In particular, Fardis and Haselton calibrated empirical equations based on large databases of monotonic and cyclic uniaxial tests (Fardis & Biskinis, 2003; Haselton, Liel, Lange, & Deierlein, 2008).

Fardis and Biskinis (2010) derived the following expressions.

For members with rectangular or T-compression zone sections, the yield curvature is the smaller of:

$$\begin{aligned} \phi_y &= \frac{f_y}{E_s(1-\xi_y)d} \\ \phi_y &= \frac{\epsilon_c}{\xi_y d} \approx \frac{1.8 f_c}{E_c \xi_y d} \end{aligned} \tag{2.2}$$

where ξ_y is defined as:

$$\xi_y = \left(\alpha^2 A^2 + 2\alpha B\right)^{1/2} - \alpha A \tag{2.3}$$

If the yield curvature is governed by the steel, then A and B are given as:

$$\begin{aligned} A &= \frac{b}{b_w}\left(\rho_1 + \rho_2 + \rho_v + \frac{N}{b d f_y}\right) + \frac{1}{\alpha}\frac{t}{d}\left(\frac{b}{b_w} - 1\right) \\ B &= \frac{b}{b_w}\left(\rho_1 + \rho_2 \delta' + \frac{\rho_v(1+\delta')}{2} + \frac{N}{b d f_y}\right) + \frac{1}{2\alpha}\left(\frac{t}{d}\right)^2\left(\frac{b}{b_w} - 1\right) \end{aligned} \tag{2.4}$$

Otherwise:

$$A = \frac{b}{b_w}\left(\rho_1 + \rho_2 + \rho_v - \frac{N}{\epsilon_c E_s b d}\right) + \frac{1}{\alpha}\frac{t}{d}\left(\frac{b}{b_w} - 1\right)$$
$$B = \frac{b}{b_w}\left(\rho_1 + \rho_2\delta' + \frac{\rho_v(1+\delta')}{2}\right) + \frac{1}{2\alpha}\left(\frac{t}{d}\right)^2\left(\frac{b}{b_w} - 1\right) \tag{2.5}$$

Finally, the yield moment is given as:

$$\begin{aligned}\frac{M_y}{bd^3} =& \phi_y \left[E_c\left[\frac{\xi_y^2}{2}\left(\frac{1+\delta'}{2} - \frac{\xi_y}{3}\right)\frac{b_w}{b} + \left(1 - \frac{b_w}{b}\right)\left(\xi_y - \frac{t}{2d}\right)\left(1 - \frac{t}{2d}\right)\frac{t}{2d}\right]\right. \\ &\left. + \frac{E_s\left(1-\delta'\right)}{2}\left[\left(1-\xi_y\right)\rho_1 + \left(\xi_y - \delta'\right)\rho_2 + \frac{\rho_v}{6}\left(1-\delta'\right)\right]\right]\end{aligned} \tag{2.6}$$

Along with the above equations, Fardis and Biskinis (2003) also developed predictive equations for monotonic and cyclic rotations. For one, the ultimate rotation is given as:

$$\begin{aligned}\Theta_u = \alpha_{st}\left(1 - 0.43a_{cy}\right)\left(1 + 0.5a_{sl}\right)\left(0.3^{\nu}\right)\ldots \\ \left(\frac{max(0.01,\omega')}{max(0.01,\omega)}c_{units}f_c\right)^{.225}\left(\min\left(9, \frac{L_s}{h}\right)\right)^{.35} 25^{(\alpha\rho_s\frac{f_{yw}}{f_c})}\end{aligned} \tag{2.7}$$

Haselton, Liel, et al. (2008) also developed empirical equations based on the element model developed by Ibarra, Medina, and Krawinkler (2005) and implemented in Opensees by Altoontash (2004). Haselton, Liel, et al. (2008) used the cyclic and monotonic tests from the Structural Performance Database by the Pacific Earthquake Engineering Research Center to calibrate the variables needed for the element model. In addition to developing these predictive equations, they also included the standard deviations of those calibrations.

The following are the results of their calibrations. Starting with the capacity of the plastic rotation:

$$\Theta_{cp} = 0.12\left(1 + 0.55a_{sl}\right)\left(0.16\right)^{\nu}\left(0.02 + 40\rho_{sh}\right)^{0.43}\left(0.54\right)^{0.01c_{units}f_c'}\left(0.66\right)^{0.1s_n}\left(2.27\right)^{10.0\rho} \tag{2.8}$$

where a_{sl} is the bond-slip indicator, ν is the axial load ratio, ρ_{sh} is the transverse reinforcement ratio, s is stirrup spacing, d_b the longitudinal rebar diameter, f_y the longitudinal rebar yielding strength, and c_{units} is a conversion variable from MPa to ksi units. Finally, s_n is a rebar buckling coefficient given by:

$$s_n = \left(\frac{s}{d_b}\right)\left(\frac{c_{units}f_y}{100}\right)^{0.5} \tag{2.9}$$

To account for imbalances in top and bottom longitudinal reinforcement, Equation 2.8 is factored by

$$\left(\frac{max\left(0.01, \frac{\rho' f_y}{f_c'}\right)}{max\left(0.01, \frac{\rho f_y}{f_c'}\right)}\right)^{0.225} \tag{2.10}$$

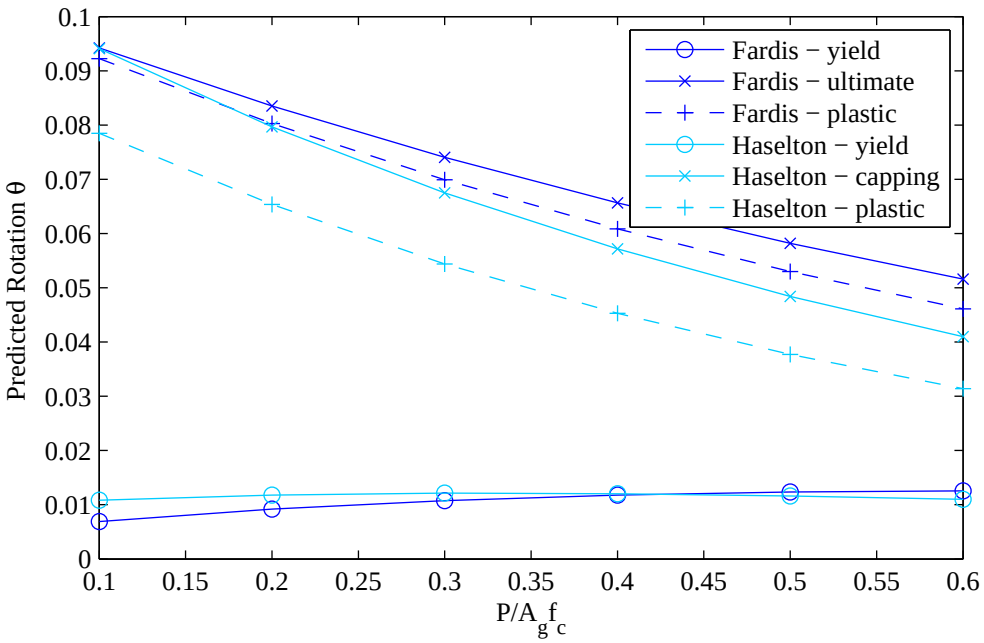

Figure 2.3: A comparison of the rotations predicted by Haselton and Fardis

adopted from Ibarra et al. (2005).

For the post-capping rotation:

$$\Theta_{pc} = (0.76)\,(0.031)^{\nu}\,(0.02 + 40\rho_{sh})^{1.02} \leq 0.10 \tag{2.11}$$

A comparison of these predicted rotation equations can be seen in Figure 2.3.

To predict the capping moment capacity:

$$M_c/M_y = (1.25)\,(0.89)^{\nu}\,(0.91)^{0.01 c_{units} f'_c} \tag{2.12}$$

Assuming zero deterioration for both the accelerated stiffness and unloading stiffness modes, Haselton, Liel, et al. (2008) gave a simplified equation for the cyclic energy-dissipation capacity:

$$\lambda = (170.7)\,(0.27)^{\nu}\,(0.10)^{s/d} \tag{2.13}$$

For c, the exponent defining the rate of cyclic deterioration, Ibarra and Krawinkler assume a value of 1.0, believing it to have little effect on the response of the structure (Ibarra & Krawinkler, 2005).

The last value needed to describe the backbone curve is the initial stiffness. Many suggestions are available for approximating the initial stiffness of a reinforced concrete member. FEMA 356 (2000) states that for columns with an axial load ratio ≥ 0.5, the flexural stiffness shall be $0.7E_cI_g$, where the axial load ratio is ≤ 0.3 the flexural stiffness shall be $0.5E_cI_g$ with a linear transition between the two. Haselton and Deierlein (2008) also developed an equation to predict the ratio for the effective stiffness, which includes a term for shear span:

$$\frac{EI_y}{EI_g} = -0.07 + 0.59\left(\frac{P}{A_g f'_c}\right) + 0.07\left(\frac{L_s}{H}\right) \quad 0.2 \leq \frac{EI_y}{EI_g} \leq 0.6 \tag{2.14}$$

Elwood and Eberhard examined the results of 221 column tests and concluded that FEMA overestimated the lower bound (Elwood & Eberhard, 2009). They proposed an equation to estimate the column flexural stiffness, but for the purposes of this study, a simplified version proposed by Elwood et al. (2007) as an update to ASCE/SEI 41 is used, namely:

$$EI_{eff}/EI_g = \begin{cases} 0.3 & \text{if } \frac{P}{A_g f'c} \leq 0.1 \\ \frac{P}{A_g f'c} + 0.2 & \text{if } 0.1 \leq \frac{P}{A_g f'c} \leq 0.5 \\ 0.7 & \text{if } \frac{P}{A_g f'c} \geq 0.0.5 \end{cases} \tag{2.15}$$

2.3 Collapse Capacity

Vamvatsikos and Cornell (2002) proposed incremental dynamic analysis (IDA) as a method for determining the collapse capacity of a structure. IDA is the analysis method in which a structure is subjected to one or more ground motions scaled incrementally to create curves of an engineering demand parameter versus an intensity measure. The ground motions are scaled until a collapse occurs. Collapse can be defined in various ways, but for the purpose of this research, the structure is considered to have collapsed when the limit state of maximum story drift exceeds 10% (Vamvatsikos & Cornell, 2002; FEMA P695, 2009). The spectral acceleration at the first period of the structure has been chosen as the intensity measure. Thus the median collapse capacity is the spectral acceleration at which half of the ground motions have caused collapse.

The results from the IDA can be expressed in terms of a collapse fragility curve. First, it is assumed that a lognormal distribution represents well the nonlinear response data (Ibarra & Krawinkler, 2005; Shome, 1999). The collapse capacity data are fitted to a continuous distribution using the method of maximum likelihood (Ang & Tang, 1973). The maximum likelihood estimators for $\hat{\lambda}$ and $\hat{\xi}$ for the lognormal distribution are given as:

$$\hat{\lambda} = \frac{1}{n-1} \sum_{i=1}^{n} \ln\, x_i \tag{2.16}$$

$$\hat{\xi^2} = \frac{1}{n-1} \sum_{i=1}^{n} \left(\ln\, x_i - \hat{\lambda} \right)^2 \tag{2.17}$$

resulting in the lognormal probability density function

$$f(x) = \frac{1}{\sqrt{2\pi}\xi x} \exp\left[-\frac{1}{2} \left(\frac{\ln\, x - \lambda}{\xi} \right)^2 \right] \tag{2.18}$$

Chapter 3

Methodology

To determine the effects that SCWB strength ratios have on collapse capacities of buildings, several buildings with differing SCWB ratios and heights are analyzed. Median collapse capacity values are obtained for each structure as a point of comparison among SCWB ratios as well as a comparison against MCE ground motion intensities. The following methodology used to obtain these values is based on that given for performance evaluation set forth in FEMA P695.

3.1 Building Description

For this study of reinforced-concrete frame structures, three building heights are selected: 12-, 18-, and 24-stories. For each height, several buildings are designed with varying SCWB ratios. All designs are developed from a single floor plan: a perimeter reinforced concrete moment-resisting-frame structure. Figures 3.1 and 3.2 show a typical floor plan and elevation. The height of the first story is 15 ft and the height of the remaining floors is 13 ft. The gravity system consists of an 8 in. concrete slab at each level supported by columns spaced at 20 ft on center. The lateral force resisting system consists of two four-bay moment-resisting frames in each direction. As seen in the plan view, the frames are configured such that the exterior columns are not required to act in biaxial bending. The buildings were designed thus so that this study could build on work done by Haselton and Deierlein (2008).

3.2 Mathematical Model

To investigate the effects of the SCWB ratios on structures of various heights, models are developed in OpenSees (McKenna et al., 2000). A balance between accuracy and efficiency of the model is desired as each structure must undergo multiple nonlinear dynamic analyses to complete an incremental dynamic analysis (IDA) and obtain the collapse capacity. The building is condensed to a single lateral-load resisting frame (in the longer direction) and a P-delta column. The lateral-load resisting frame carries the gravity load within its tributary area, while the P-delta column carries the weight of half the structure minus the load carried by the frame. The stiffness contributed by the gravity framing is ignored. The slabs are assumed to act as rigid diaphragms, which is simulated in Opensees by tying together all

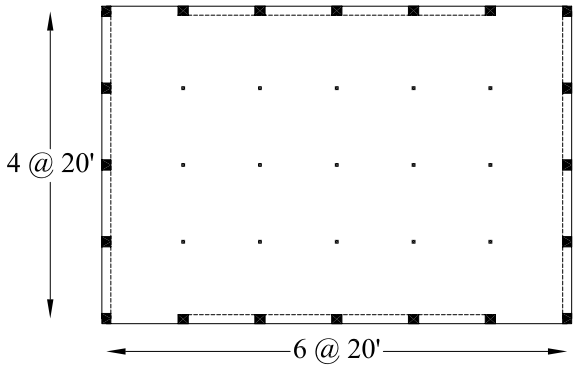

Figure 3.1: A plan view of a typical floor.

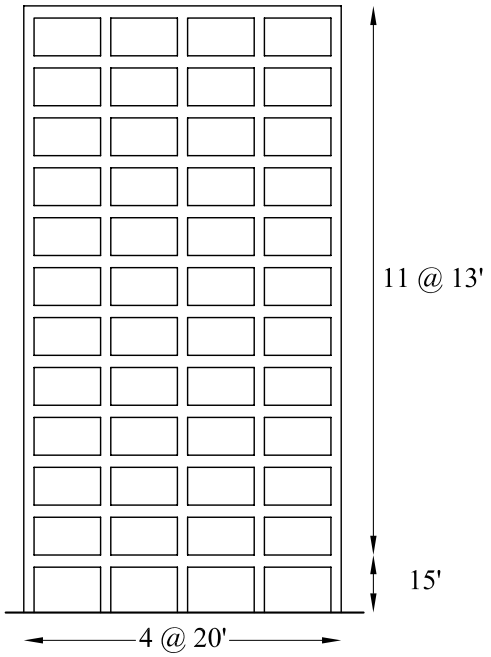

Figure 3.2: Elevation of the 12-Story Moment-Resisting-Frame

nodes on each floor using the multi-point equalDOF constraints command. The base of the columns are assumed to be fixed and are modeled as such.

Beam Model Selection

Several assumptions were made in modeling the beams. The distributed load and consequent bending moments were accounted for in the design but not modeled in the analysis, though gravity loads were accounted for as lumped masses and loads at the beam-column nodes. It was also assumed the beam elements would not experience significant changes in the axial force while undergoing lateral loading from a ground motion. In addition, plastic hinges were determined by static analysis to form at the ends of the beams and the possibility of yielding in mid-span need not be considered. Nonlinear shear was not modeled.

Fardis and Haselton, (Fardis & Biskinis, 2003; Haselton, Liel, et al., 2008) developed predictive equations to dictate the moment-rotation relationship of the element. This relationship can be modeled using the ModIMKPeakOriented material model developed by Ibarra et al. (2005) and implemented in Opensees by Lignos and Krawinkler (2012). Six quantities describe the material model: initial stiffness K_y, yielding moment, M_y, strain hardening ratio proportional to the initial stiffness, α_s, residual moment factor, $ResFac$, post-capping stiffness ratio, α_c, and plastic rotation capacity, θ_{cp}.

To implement the moment-rotation relationship and, subsequently, the material model, each beam is constructed of five components: two semi-rigid elastic elements create the joint offsets equivalent to half the width of the column, two zero-length springs accommodate the plastic hinges and an elastic beam-column element models the center portion of the beam. Setting aside the joint offsets, the beam is now represented by three elements in series, thus modifications to the moment-rotation relationship must be made such that the original stiffness of the beam is maintained. Assuming the beam will be subjected to double-curvature bending, the stiffness is $K_{mem} = 6EI_{beam}/L_{beam}$. Using a spring to beam-column element stiffness ratio of $n = 10$, as suggested by Ibarra et al. (2005), such that the spring stiffness is larger than the beam-column element, $K_s = nK_{bc}$, the stiffness of the individual components with regard to the original element can now be determined. As presented in Ibarra et al. (2005), the following modifications are required for the ModIMKPeakOriented material model for the springs:

$$\begin{aligned} K_{bc} &= \frac{n+1}{n} K_{mem} \\ K_s &= (n+1) K_{mem} \end{aligned} \tag{3.1}$$

The strain-hardening and post-capping slopes become

$$\alpha_s = \frac{\alpha}{1 + n(1-\alpha)} \tag{3.2}$$

The cyclic deterioration parameter becomes

$$\gamma_s = (n+1)\gamma_{mem} \tag{3.3}$$

The plastic rotation capacity of the spring becomes

$$\theta_{cp,s} = \theta_{cp} - \frac{(M_c - M_y)L_{beam}}{6EI_{beam}} \tag{3.4}$$

Lastly, from Zareian and Medina (2010), for the stiffness-proportional damping of the beam-column element:

$$\beta_{bc} = \frac{n+1}{n}\beta \tag{3.5}$$

with the damping of the spring set to zero.

Column Model Selection

Ideally, the element chosen to represent the columns would be able to model the change in axial forces (and thus change in stiffness) under seismic excitation as well as allow for the moment-rotation relationship to be explicitly defined. Such an element does not currently exist in OpenSees. Although fiber models are able to represent effects of varying axial loads, simulation using such models would be prohibitively slow. Therefore, it was decided to use the previously discussed predictive equations. They represent a large base of knowledge and are easily implemented. Therefore, the change in axial load is ignored and the column is modeled in a manner similar to the beams; an elastic beam-column element with a zero-length spring at each end. No joint offsets were implemented in the columns and nonlinear shear was not modeled. Second-order P-Delta effects were taken into account through the P-Delta type of geometric transformations for the columns.

Joints

Joints were modeled by offsetting the beam ends by a distance equal to the total joint width. This was done so that the beam-with-hinges element would model the appropriate moment for use in the moment-curvature relationship. Using rigid joint offsets equal to half the width of the joint would have accounted for the joint flexibility, acknowledging that joints do not behave as rigid blocks. However, offsetting the joints by only half the width places the plastic hinge section of the beam inside the joint, and the local force recorders would overestimate the moment (and subsequent rotation) occurring in the plastic hinge region. Implementing a more complex model of the joints is not practical in the analysis of a tall structure. The increase in the number of nodes and elements would be too large, and the computational cost would outweigh the increase in accuracy gained by those models.

Figure 3.3 depicts an example the moment-curvature response in the springs of the ends of the elements framing into the middle joint of the second floor of the 12-story, 1.8 SCWB ratio structure from the 1100838 ground motion. This particular ground motion caused a failure mechanism incorporating the first two floors. The figure shows the corresponding yielding occurring in the beams necessary for this collapse mechanism.

3.3 Earthquake Analysis

Seismic Ground Motion Values

This study uses the building site identified by the Tall Buildings Initiative (TBI), (Moehle et al., 2011). The TBI set of ground motions contain the appropriate range of frequency content for the assessment of tall structures. A full description of the location and faults can

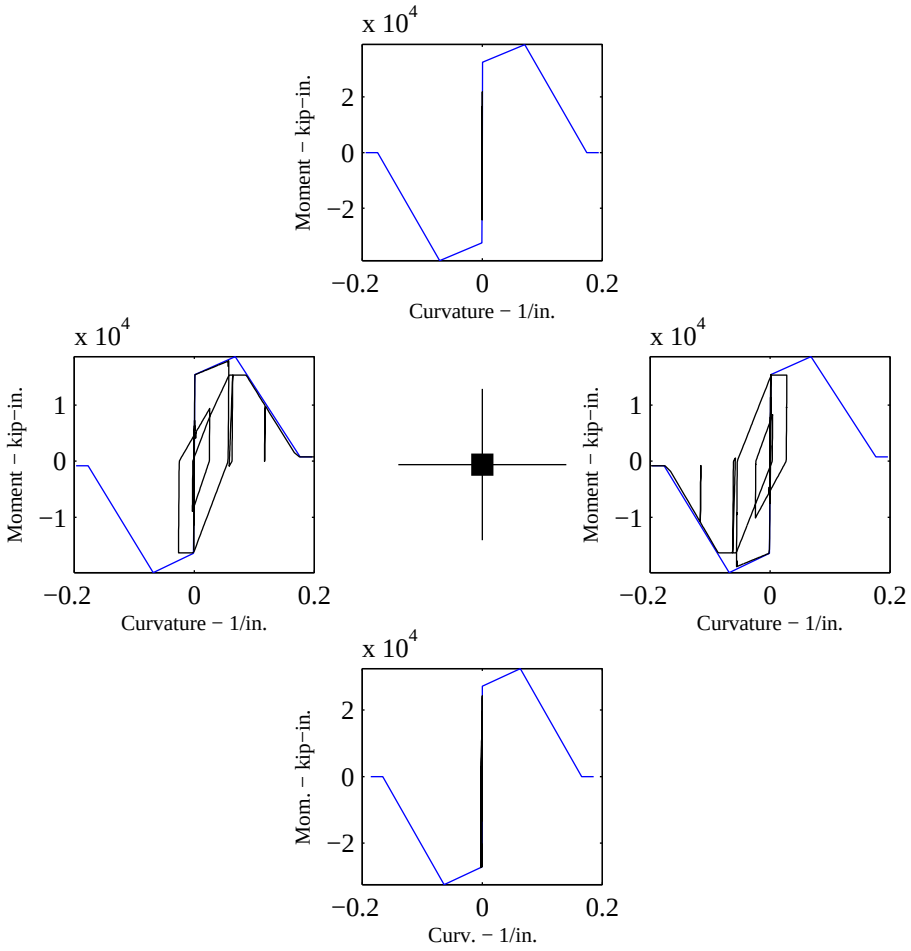

Figure 3.3: Moment-curvature of element ends framing into second floor, third column joint

be found in Moehle et al. (2011). The building is presumed to be located in Los Angeles at latitude: 34.05, longitude: -118.25 on a site classified as a Site Class C soil type. From the 2005 ASCE 7 standard, the mapped acceleration parameters are given as $S_S = 2.159$ and $S_1 = 0.723$. Adjusting for the appropriate site class, the maximum considered earthquake (MCE) spectral response acceleration parameters become $S_{MS} = F_a S_S = (1.0)(2.159) = 2.159$ and $S_{M1} = F_v S_1 = (1.3)(0.723) = 0.94$. The MCE is reduced by 2/3 to obtain the design response spectrum shown in Figure 3.4, where $S_{DS} = 1.44$ and $S_{D1} = 0.627$.

Ground Motions

The five sets of 15 pairs of ground motions from the TBI were chosen for the dynamic analysis of the models. These were obtained by the TBI through probabilistic seismic hazard disaggregation of the site defined above. The selection and scaling of the ground motions from the Next Generation Attenuation database had the following criteria: the maximum source distance was 100 km, the maximum shear wave velocity was between 180 to 1200 m/s,

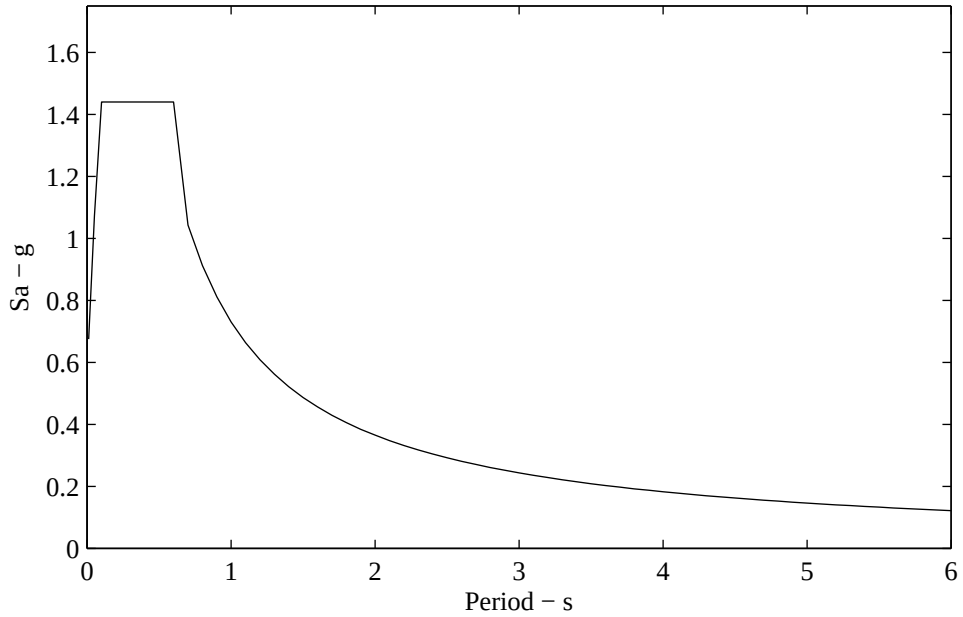

Figure 3.4: DBE response spectrum

damping was 5%, the error between the target spectrum and the geometric mean spectrum of the recording was weighted for periods between 3.0 and 7.0 s, no more than two recordings from a given event were used, and the sampling rate was decreased to 25 samples per second (Moehle et al., 2011). The five sets represent five seismic hazard levels ranging in return periods of 25, 43, 475, 2475, and 4975 years; the sets were named SLE-25-NEW, SLE-43-NEW, DBE-NEW, MCE-NEW, and OVE-NEW respectively. For the sake of simplicity, NEW will be omitted in future references to these sets. Tables 3.1, 3.2, and 3.3 provide lists of the ground motions of the last three sets. Also for each of the three sets, response spectra plots for the 30 ground motions from the 15 pairs along with their median and target spectra can be seen in Figures 3.5, 3.6, and 3.7. The 15 pairs of ground motions are each treated as two individual, unrelated ground motions and are applied to the two-dimensional frame in 30 separate scenarios.

Design

The initial design of each building was done using the modal response spectrum analysis method per ASCE/SEI 7-05 (American Society of Civil Engineers, 2006). This will be elaborated upon in chapter 4.

Nonlinear Static (Pushover) Analysis

A nonlinear static (pushover) analysis is performed on each structure to obtain various values needed for the collapse evaluation. An inverted triangular load pattern is applied to the side of the structure to produce the pushover curves. As an example, Figure 3.8 shows the

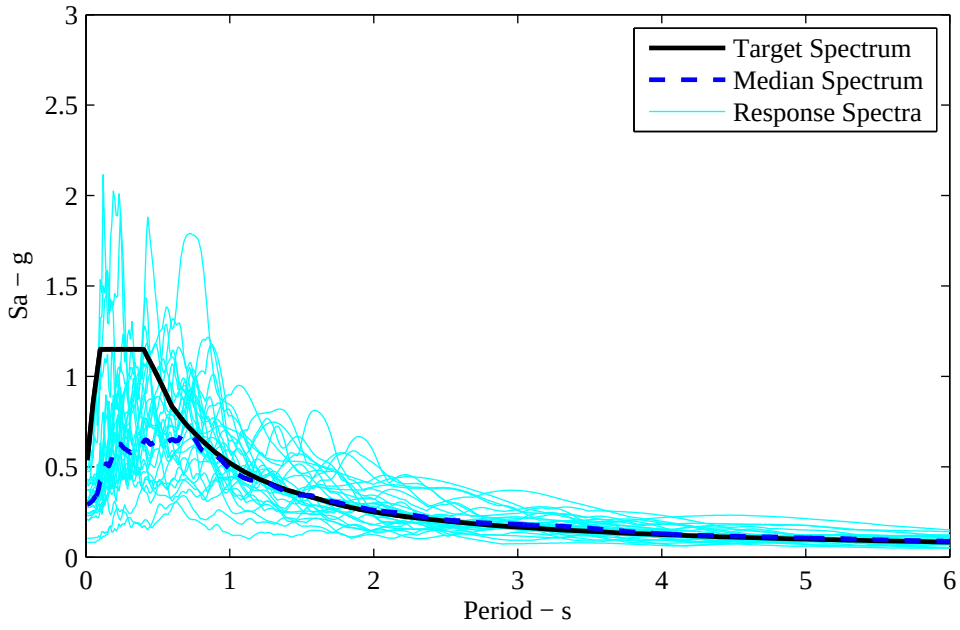

Figure 3.5: DBE response spectra

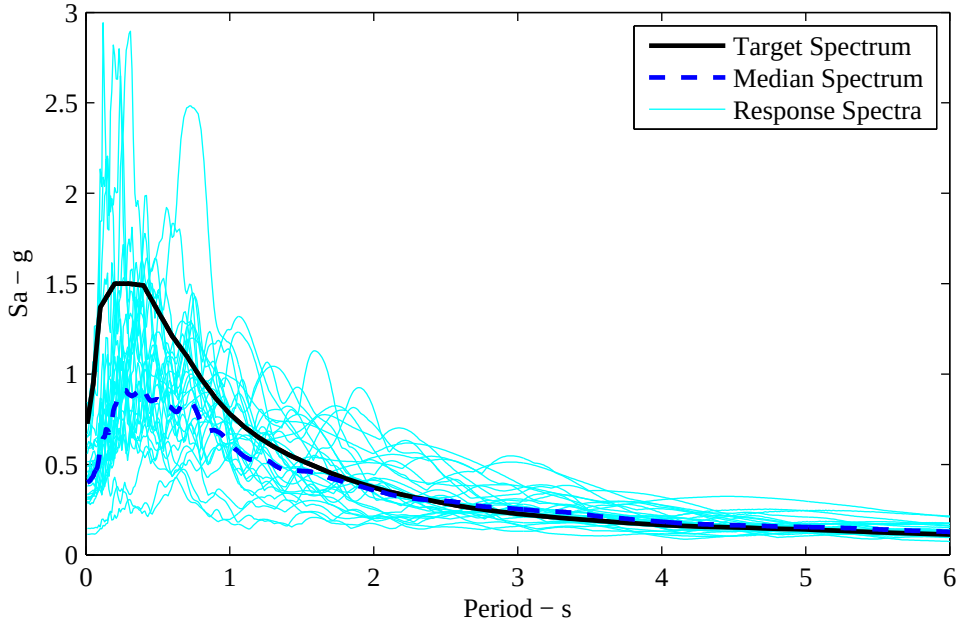

Figure 3.6: MCE response spectra

Table 3.1: Selected ground motions for DBE set

Event	Magnitude (M_w)	Station Name	Horizontal Component 1	Horizontal Component 2	Distance (km)	Scaling Factor
Chi-Chi, Taiwan 1999	7.62	CHY067	1101223.th	2101223.th	83.56	4.06
		TAP026	1101423.th	2101423.th	95.85	4.16
Landers 1992	7.28	Barstow	1100838.th	2100838.th	34.86	2.33
		Yermo Fire Station	1100900.th	2100900.th	23.62	1.36
Hector Mine 1999	7.13	Mecca - CVWD Yard	1101810.th	2101810.th	91.96‘	3.66
Kocaeli, Turkey 1999	7.51	Bursa Tofas	1101155.th	2101155.th	60.43	2.65
		Zeytinburnu	1101177.th	2101177.th	51.98	3.65
Denali, Alaska 2002	7.9	TAPS Pump Station #10	1102114.th	2102114.th	0.18	0.72
Imperial Valley-06	6.53	Delta	1100169.th	2100169.th	22.03	1.69
Cape Mendocino 1992	7.01	Fortuna - Fortuna Blvd	1100827.th	2100827.th	15.97	2.69
St Elias, Alaska 1979	7.54	Yakutat	1101629.th	2101629.th	80.0	1.25
Tabas, Iran 1978	7.35	Tabas	1100143.th	2100143.th	1.79	0.56
Hector Mine 1999	7.13	Mentone Fire Station #9	1101811.th	2101811.th	91.15	4.84
Duzce, Turkey 1999	7.14	Duzce	1101605.th	2101605.th	0.0	0.69
Loma Prieta 1989	6.93	Dumbarton Bridge West End FF	1100757.th	2100757.th	35.31	3.33

Table 3.2: Selected Ground Motions for MCE Set

Event	Magnitude (M_w)	Station Name	Horizontal Component 1	Horizontal Component 2	Distance (km)	Scaling Factor
Chi-Chi, Taiwan 1999	7.62	TAP052	1101436.th	2101436.th	98.51	3.84
		TCU067	1101504.th	2101504.th	0.64	1.29
Landers 1992	7.28	Barstow	1100838.th	2100838.th	34.86	3.24
		Yermo Fire Station	1100900.th	2100900.th	23.62	1.9
Kocaeli, Turkey 1999	7.51	Bursa Tofas	1101155.th	2101155.th	60.43	3.68
		Hava Alani	1101163.th	2101163.th	58.33	3.71
Denali, Alaska 2002	7.9	TAPS Pump Station #10	1102114.th	2102114.th	0.18	1.0
Imperial Valley-06	6.53	Delta	1100169.th	2100169.th	22.03	2.35
Hector Mine 1999	7.13	Indio - Riverside Co Fair Grnds	1101792.th	2101792.th	74.0	3.69
Cape Mendocino 1992	7.01	Fortuna - Fortuna Blvd	1100827.th	2100827.th	15.97	3.73
St Elias, Alaska 1979	7.54	Yakutat	1101629.th	2101629.th	80.0	1.74
Tabas, Iran 1978	7.35	Tabas	1100143.th	2100143.th	1.79	0.78
Duzce, Turkey 1999	7.14	Duzce	1101605.th	2101605.th	0.0	0.96
		Mudurnu	1101619.th	2101619.th	34.3	4.96
Loma Prieta 1989	6.93	Dumbarton Bridge West End FF	1100757.th	2100757.th	35.31	4.62

Table 3.3: Selected Ground Motions for OVE Set

Event	Magnitude (M_w)	Station Name	Horizontal Component 1	Horizontal Component 2	Distance (km))	Scaling Factor
Landers 1992	7.28	Barstow	1100838.th	2100838.th	34.86	4.28
		Yermo Fire Station	1100900.th	2100900.th	23.62	2.51
Chi-Chi, Taiwan 1999	7.62	TCU122	1101546.th	2101546.th	9.35	2.04
		TCU082	1101515.th	2101515.th	5.18	1.69
Kocaeli, Turkey 1999	7.51	Bursa Tofas	1101155.th	2101155.th	60.43	4.86
		Hava Alani	1101163.th	2101163.th	58.33	4.91
Denali, Alaska 2002	7.9	TAPS Pump Station #10	1102114.th	2102114.th	0.18	1.33
Hector Mine 1999	7.13	Indio - Riverside Co Fair Grnds	1101792.th	2101792.th	74.0	4.88
SIMULATION	NA	NA	1900001.th	2900001.th	1.0	1.0
			1900002.th	2900002.th	1.0	1.0
			1900003.th	2900003.th	1.0	1.0
			1900004.th	2900004.th	1.0	1.0
			1900005.th	2900005.th	1.0	1.0
			1900006.th	2900006.th	1.0	1.0
			1900007.th	2900007.th	1.0	1.0

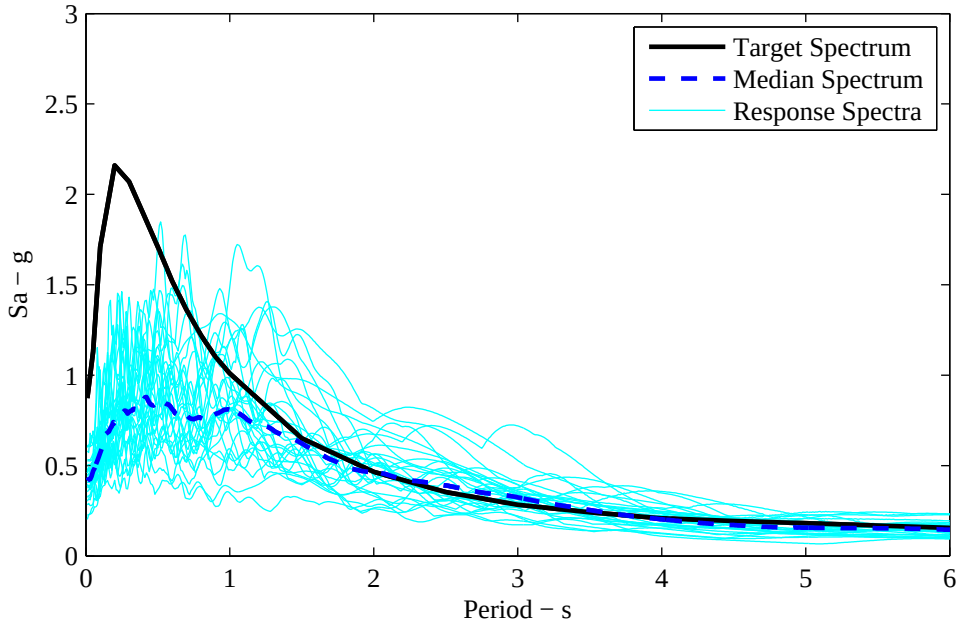

Figure 3.7: OVE response spectra

pushover curve for the 12-story, 1.2 SCWB ratio structure. FEMA P695 (2009) derives from this graph some of the quantities needed for the collapse assessment, including the maximum base shear, V_{max}, and the ultimate displacement, δ_u. The ultimate displacement is defined as the displacement of the roof when the base shear has dropped to 80% of V_{max}. The period based ductility of the structure, μ_T, is defined as the ratio of the ultimate roof displacement to the effective yield displacement and is used later to adjust the collapse fragility curve to account for the spectral shape.

$$\mu_T = \frac{\delta_u}{\delta_{y,eff}} \tag{3.6}$$

FEMA P695, however, does not use the plot to obtain the yield displacement but rather defines the yield displacement as:

$$\delta_{y.eff} = C_O \frac{V_{max}}{W} \left[\frac{g}{4\pi^2}\right] (max\,(T, T_1))^2 \tag{3.7}$$

where W is the weight of half of the structure, g is the gravity constant, T is the fundamental period as defined by ASCE/SEI 7-05, ($T = C_u T_a = C_u C_t h_n^x$; for concrete moment-resisting frames, $C_t = 0.016$ and $x = 0.9$) and T_1 is the fundamental period computed from the nonlinear models. C_O is calculated as

$$C_O = \phi_{1,r} \frac{\sum_1^N m_x \phi_{1,x}}{\sum_1^N m_x \phi_{1,x}^2} \tag{3.8}$$

Shown as the dashed blue line in Figure 3.8, this method of calculating the yield displacement overestimates the initial stiffness of the structure. Therefore, for the purpose of

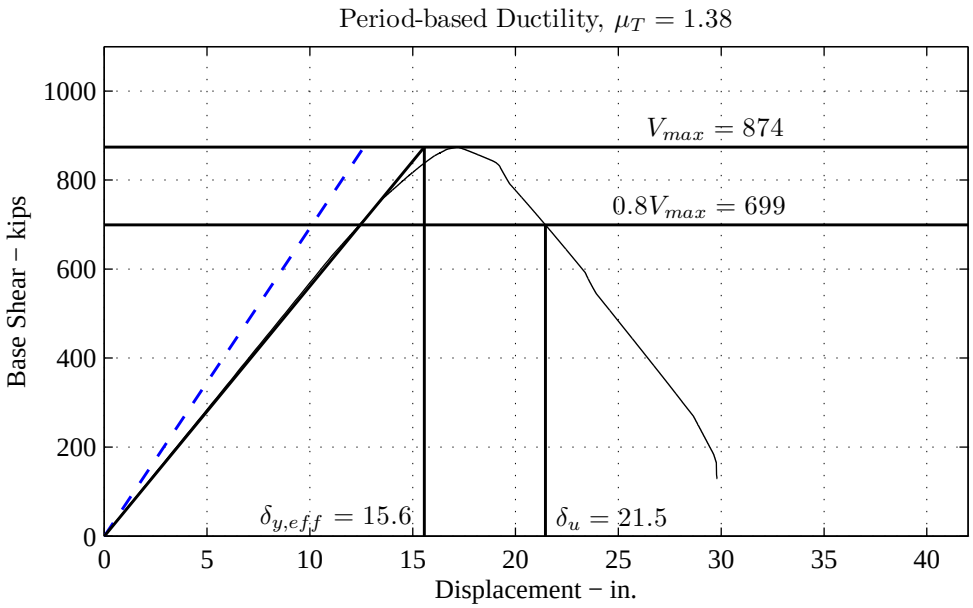

Figure 3.8: Nonlinear static pushover curve for the 12-story structure

this study, the yield displacement is obtained by passing a line through the plot at $0.7V_{max}$ and defining δ_y as the point at which the line intersects V_{max}.

Incremental Dynamic Analysis

The incremental dynamic analysis (IDA) discussed earlier is performed using the OVE set of ground motions, the strongest of the sets. Each ground motion is scaled up to the point at which a small increase in Sa results in a large increase in maximum interstory drift for that individual record. At this juncture, the plot of the IDA curve becomes a flat line. The building is considered to have collapsed under a given scaled ground motion when the resulting maximum interstory drift ratio meets or exceeds 10%. (It is recognized that this is an unreasonably large value, but is simply being used to define failure, though failure would most probably occur sooner.) The corresponding Sa is the collapse capacity of that structure for that ground motion.

3.4 Analysis of Results

Median Collapse Intensity and Collapse Margin Ratio

From the IDA comes the median collapse capacity, $\hat{S}_{CT}$, the spectral acceleration at which one-half of the ground motions have caused the structure to collapse as defined above. $\hat{S}_{CT}$ can be found by calculating the exponent of $\hat{\lambda}$ from Equation 2.16. The MCE level spectral acceleration, S_{MT}, is taken from the MCE target spectrum at the period of the building derived from the eigenvalue analysis. Taking the ratio of the two values, one obtains the

collapse margin ratio, CMR:

$$CMR = \frac{\hat{S}_{CT}}{S_{MT}} \tag{3.9}$$

Accounting for Uncertainty

Four types of uncertainty are accounted for in the development of the collapse fragility curve: record-to-record variability, design requirements, test data, and archetype or modeling uncertainty.

Record-to-record variability comes inherently from the selection of ground motions. Due to the use of a ground motion set other than the set provided in FEMA P695, the uncertainty from record variability, β_{RTR}, is taken directly from the results of the IDA, and not as $\beta_{RTR} = 0.40$ given for the Far-Field ground motion record set.

The three remaining contributors of uncertainty are determined by quality ratings outlined in FEMA P695. A value of $\beta_{DR} = 0.10$ is chosen for the design requirements uncertainty based on a high level of confidence in the extensively used design code implemented in the design of the structures. Reinforced concrete is a thoroughly-tested and widely used material thus enabling an uncertainty value of 0.10 for β_{TD}. Lastly, the archetype design space consists of just one model, namely the structure under consideration, so it therefore represents the entire design space. In addition, the model represents well the nonlinear behavior of the plastic hinges. It does not, however, model every aspect of the building, including joints, foundations and axial-flexural interaction in columns. It is rated good, with $\beta_{MDL} = 0.20$.

The above four values are combined through the square root of the sum of the squares to obtain a total value of uncertainty, β_{TOT}:

$$\beta_{TOT} = \sqrt{\beta_{RTR}^2 + \beta_{DR}^2 + \beta_{TD}^2 + \beta_{MDL}^2} \tag{3.10}$$

Figure 3.9 depicts the change in the fragility curve when additional uncertainty is added to the inherent record-to-record uncertainty. Note, as the uncertainty increases, so does the probability of collapse given an MCE hazard level, which decreases the CMR. The median collapse intensity does not change.

Accounting for Spectral Shape

Baker and Cornell (2006) suggests that in addition to magnitude and distance the shape of the response spectrum should be considered when selecting ground motions for dynamic response history analysis. They have shown that accounting for spectral shape given a specific site and structure affects the collapse capacity of that structure. However, this additional parameter is dependent upon knowledge of the period of the structure, and therefore consideration of spectral shape becomes difficult when one wishes to use the same set of ground motions for buildings of various heights, as in the case of this study. To circumvent this problem, Baker and Cornell (2006) developed a method by which the fragility curve can be adjusted after the IDA has been performed. This method, as outlined in FEMA P695, uses the period-based ductility, defined previously, and the period of the structure to pick a scaling factor to adjust the CMR. Figure 3.10 shows the impact of accounting for spectral shape on the fragility curve. Adjusting the collapse margin ratio moves the curve to

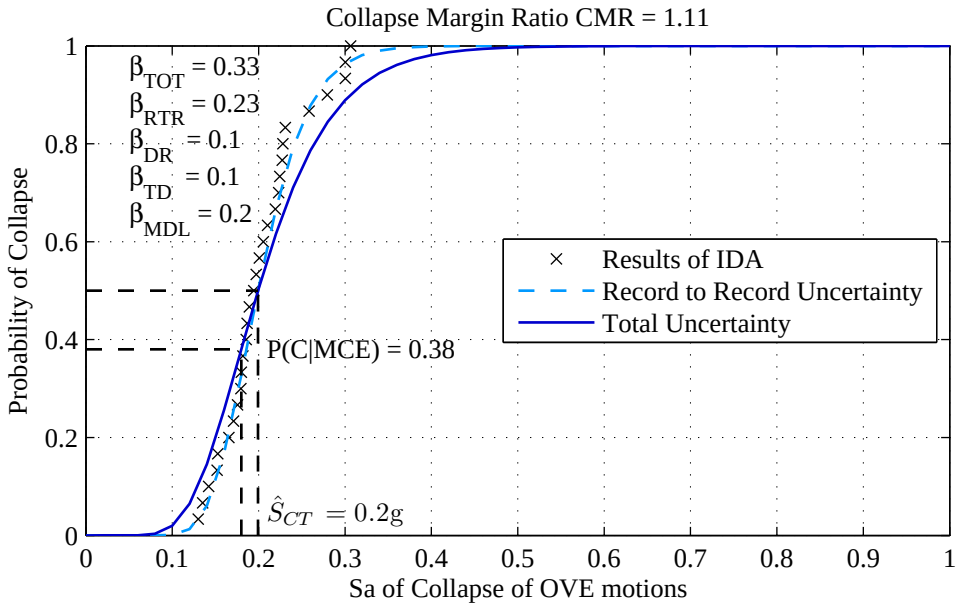

Figure 3.9: Collapse fragility curves demonstrating effects of changes in uncertainty

the right, increasing the median collapse intensity and decreasing the probability of collapse given an MCE level event.

3.5 Performance Evaluation

To determine the benefit of and appropriate value for the SCWB strength ratios, several buildings are evaluated using the method given above. Several building heights are selected, and for each height several iterations of the same building are designed and analyzed with increasing SCWB ratios. Having obtained values for the collapse capacity and CMR as measures of performance of each structure, one can evaluate a structure and draw comparisons as SCWB ratios change. Assuming increases in SCWB ratios equates to increased performance, the question becomes how much of an increase in performance must occur for the increase in SCWB ratios to be justified.

The definition by which the SCWB ratio is calculated can also be evaluated. The following are two ways SCWB ratios can be defined. The SCWB ratio can be defined as the summation of the moment strengths of the columns at each joint divided by the sum of the strengths of the beams at the same joint, as is the definition in ACI-318 (ACI 318-14, 2014). Alternatively, the ratio can be defined as the summation of all the moment strengths of the columns framing into the bottom of the joints divided by the sum of all the moment strengths of the beams framing into the joints at the level. This method will be referred to as the alternate method. Using similar buildings with identical SCWB ratios, but distributing the column and beam strengths differently, one can examine whether requiring the SCWB ratio rule to comply at each joint or whether averaging over the floor would be a better measure of the performance of the structure.

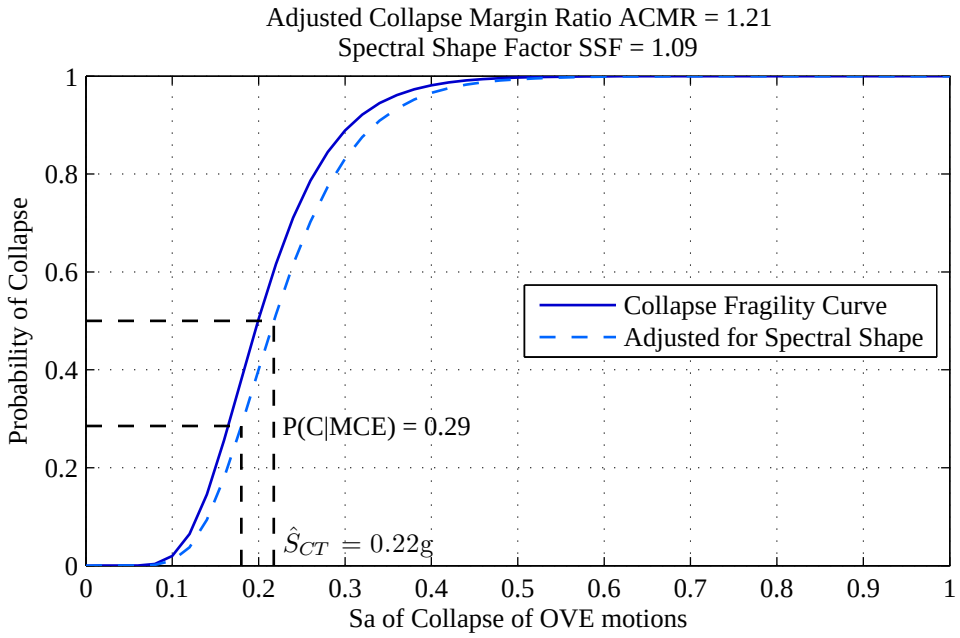

Figure 3.10: Collapse fragility curves accounting for spectral shape

Chapter 4

Buildings under Investigation

Fifteen buildings are examined for this study: five SCWB ratios (1.2, 1.4, 1.6, 1.8, and 2.0) at three different heights (12−, 18−, and 24−stories). All buildings share the same floor plan. The lateral force resisting system consists of two four-bay independent special moment-resisting perimeter frames in each direction. The gravity system consists of an 8 in. concrete slab at each level supported by columns spaced at 20 ft on center. Figure 4.1 depicts the plan view. For this study, only one lateral frame (Figure 4.2) is modeled, namely the frame in the longer direction, such that all columns have the same gravity load and no column experiences biaxial bending.

To design the frames, the demands are obtained from a modal response spectrum analysis per ASCE/SEI 7-05 (American Society of Civil Engineers, 2006) of an elastic model in OpenSees. This version of the code includes the minimum base shear provision. The results from each modal pushover are combined using the complete quadratic combination (CQC) rule. The modal base shear (V_t) ends up less than 85% of the calculated base shear (V), so the results are multiplied by $0.85\frac{V}{V_t}$.

The frame members are designed according to ACI 318-08 (ACI 318-08, 2008). Some

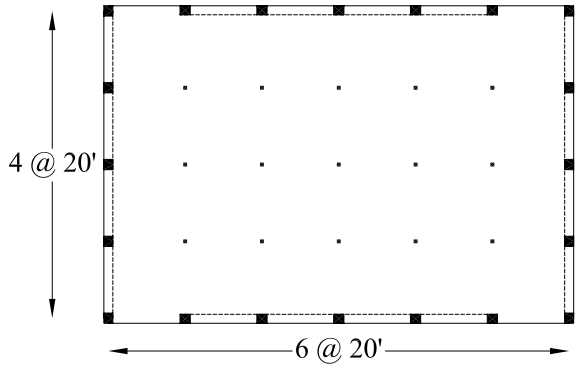

Figure 4.1: Plan view of a typical floor.

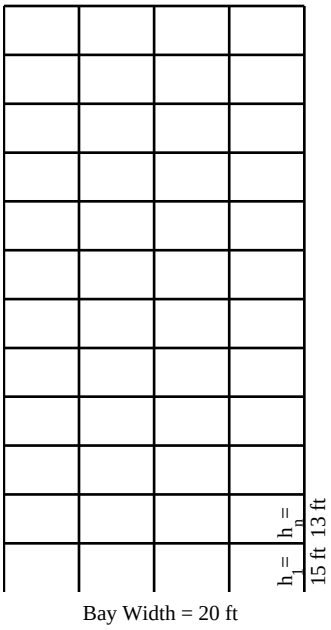

Figure 4.2: Elevation of 12-Story Structure

simplifications are made in the design process to facilitate the design of fifteen buildings. The inelastic numerical models use the exact reinforcement ratios required to meet the beam moment demands from the modal pushover analysis rather than selecting a number and size of reinforcement bars greater than or equal to the needed reinforcement ratio. To account for this missing overstrength usually inherent in the design of a building, the moment demands on the beams are multiplied by 1.2. Because the moment strength of the beams drive the design of the shear strength in the beams and the moment, and thus shear strength, in the columns, this approximate overstrength factor carries over to the design of the rest of the building. No other overstrength factors are used.

Another simplification is to assume moment demands from the beams distribute equally between the upper and lower columns framing into the joint. To design the columns to withstand the moment demands from the beams and the axial force from the modal pushover analysis, the moment-axial interaction diagram is simplified to two lines, the points of which are (0, Pmin), (Mmax, Pb) and (0, Pmax). The reinforcement ratio can then be solved for directly, forming the triangle within which the demands need to fall. This conservative approach introduces another layer of overstrength in the design. The shear strength of the columns is calculated assuming no contribution from the concrete.

Comparing the design base shear to that from the nonlinear pushover demonstrates the extent of the overstrength incorporated into the design. Table 4.1 compares V, the design base shear, to V_{max}, the maximum base shear from the nonlinear pushover analysis.

Table 4.1: Comparison of Design Base Shear and Maximum Pushover Base Shear

Building	Design Base Shear *kips*	Pushover Shear Strength *kips*
12-Story	415	874
18-Story	706	1270
24-Story	978	1640
30-Story	1292	2280

4.1 12-Story Structures

The gravity columns for the 12-story structures measure 24 x 24 in. Figures 4.4 through 4.8 show the dimensions and properties for the beams and columns of the lateral load resisting frames. The reinforcement ratios for the exterior columns of the lateral load resisting frames are initially controlled by the minimum reinforcement ratio. Only when the SCWB ratio exceeds 1.6 does the strength needed for the SCWB ratio determine the reinforcement ratio of these columns. The demands from the modal pushover analysis dictate the reinforcement ratios for the bottom exterior columns; these joints always exceed the target SCWB ratio. The fundamental period of the 12-story structure is 3.65 sec and only decreases slightly as the SCWB ratios increase. Figure 4.3 shows the SCWB ratios achieved at each joint given the design constraints, as well as the mean SCWB ratio of each floor, and the SCWB ratio calculated according to the alternate method.

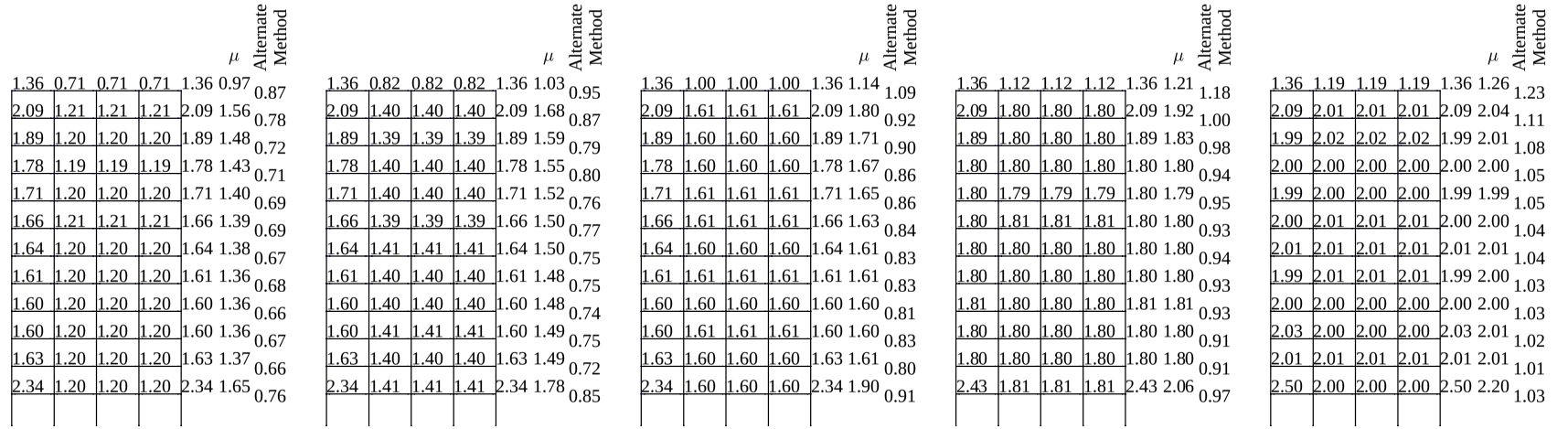

Figure 4.3: SCWB Ratios calculated using an alternate method, calculated at each joint and averaged over each floor of the 12-Story Structure

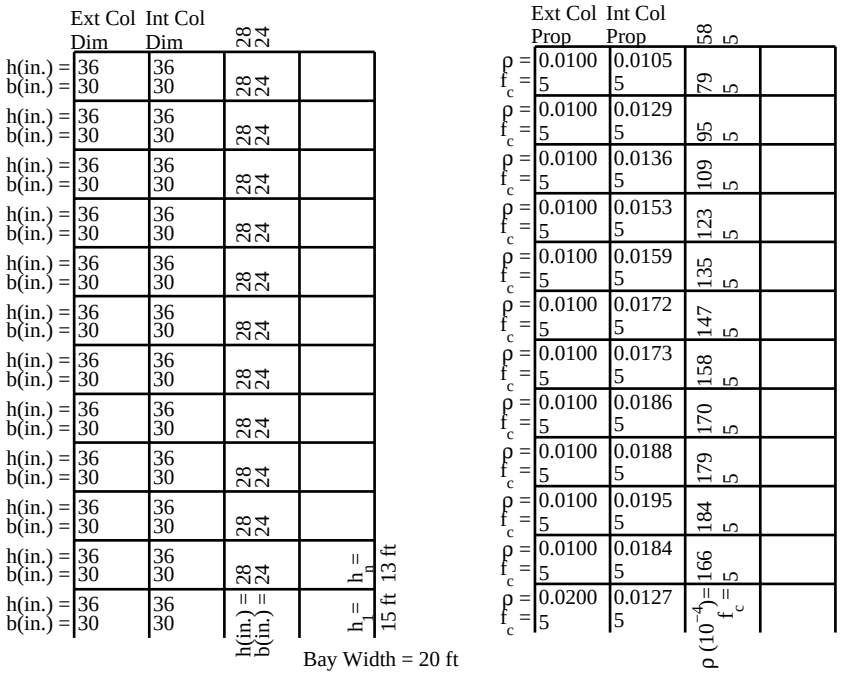

(a) Dimensions (b) Properties

Figure 4.4: Dimensions and Properties of the 12-Story, 1.2 SCWB ratio Structure

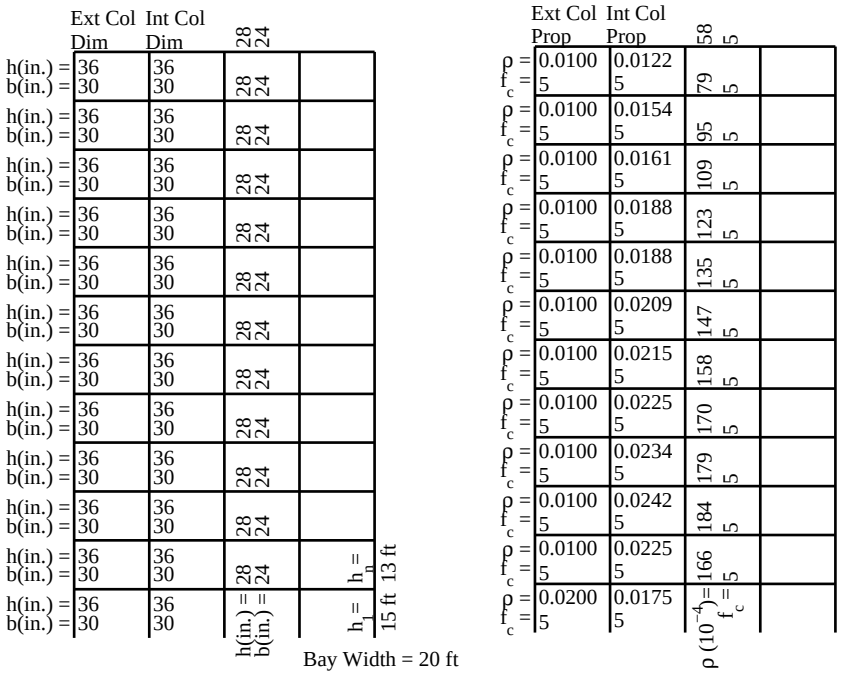

(a) Dimensions (b) Properties

Figure 4.5: Dimensions and Properties of the 12-Story, 1.4 SCWB ratio Structure

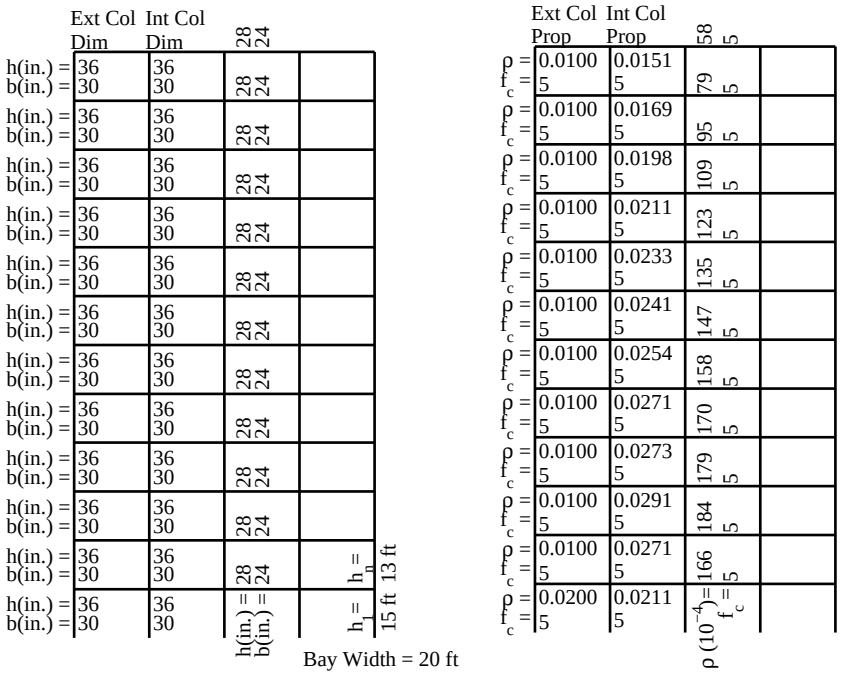

(a) Dimensions (b) Properties

Figure 4.6: Dimensions and Properties of the 12-Story, 1.6 SCWB ratio Structure

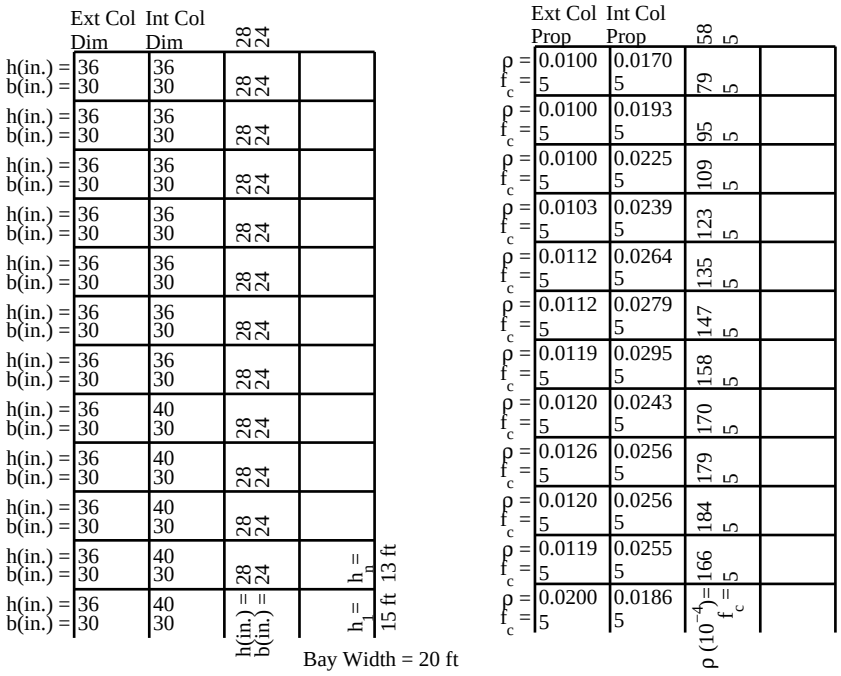

(a) Dimensions (b) Properties

Figure 4.7: Dimensions and Properties of the 12-Story, 1.8 SCWB ratio Structure

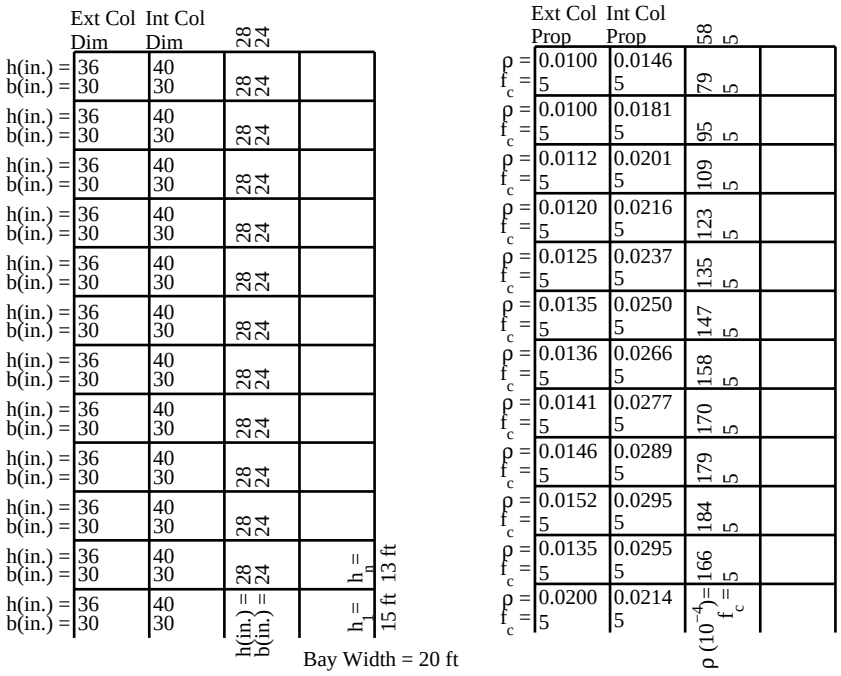

(a) Dimensions (b) Properties

Figure 4.8: Dimensions and Properties of the 12-Story, 2.0 SCWB ratio Structure

4.2 18-Story Structures

The gravity columns for the 18-story structures measure 26 x 26 in. over the first six stories, then decrease to 24 x 24 in. for the remainder of the stories. Figures 4.10 through 4.14 show the dimensions and properties for the beams and columns of the lateral load resisting frames. The reinforcement ratios for the upper exterior columns of the lateral load resisting frames of these buildings are also initially controlled by the minimum reinforcement ratio. Only when the SCWB ratio reaches 1.8 does the strength needed for the SCWB ratio start to determine the reinforcement ratio for the top half of the exterior columns. The demands from the modal pushover analysis dictate the reinforcement ratios for the bottom exterior columns; these joints always exceed the target SCWB ratio. The fundamental period of the 18-story structure is 3.94 sec. Figure 4.9 shows the SCWB ratios for each joint, as well as the mean SCWB ratio of each floor, and the SCWB ratio calculated according to the alternate method.

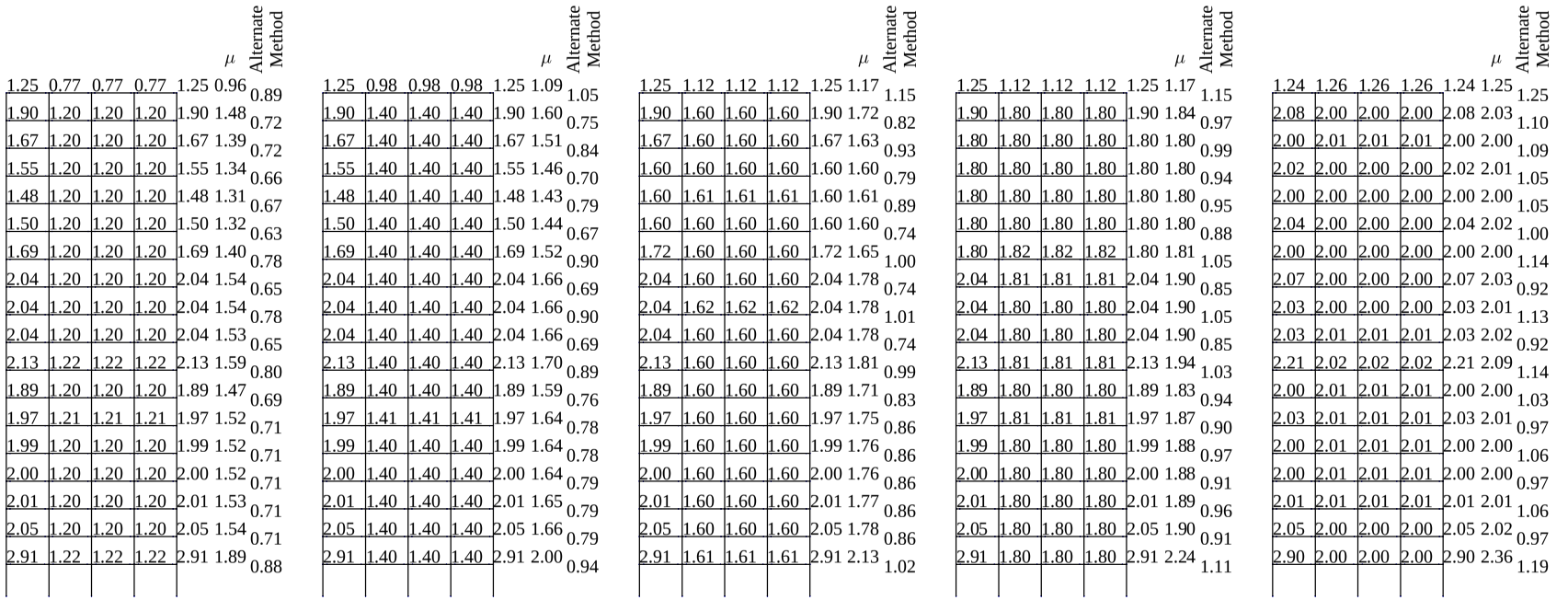

(a) 1.2 SCWB ratio (b) 1.4 SCWB ratio (c) 1.6 SCWB ratio (d) 1.8 SCWB ratio (e) 2.0 SCWB ratio

Figure 4.9: SCWB Ratios calculated using an alternate method, calculated at each joint and averaged over each floor of the 18-Story Structure

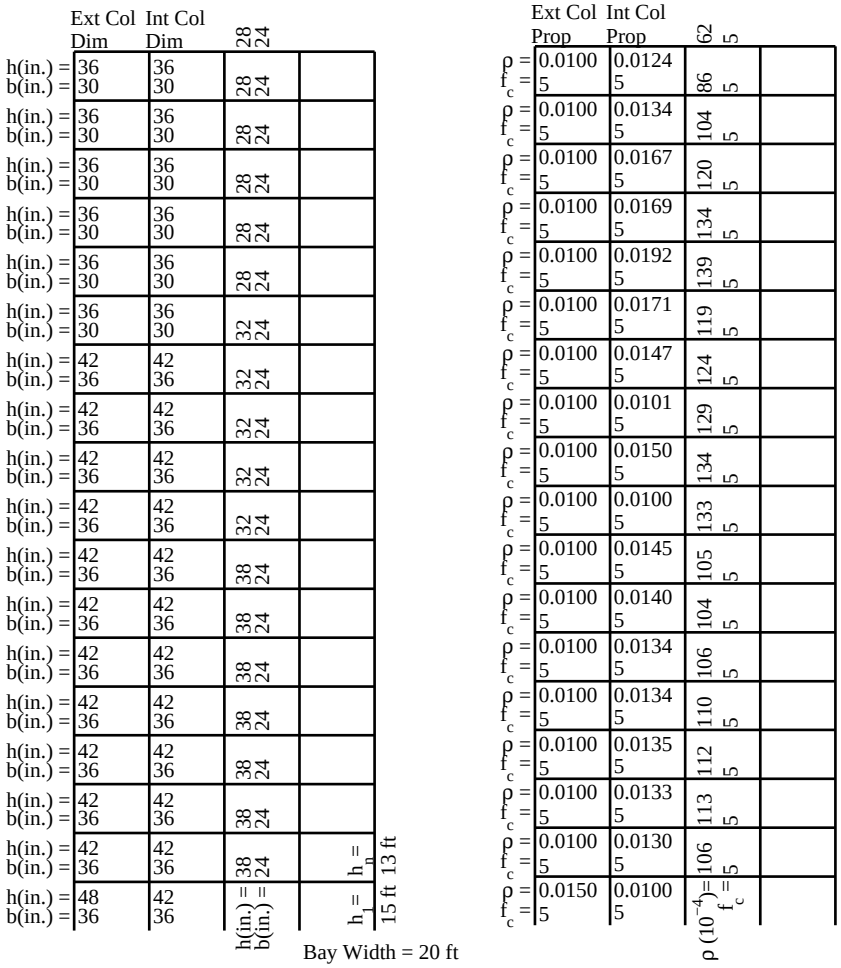

(a) Dimensions (b) Properties

Figure 4.10: Dimensions and Properties of the 18-Story, 1.2 SCWB ratio Structure

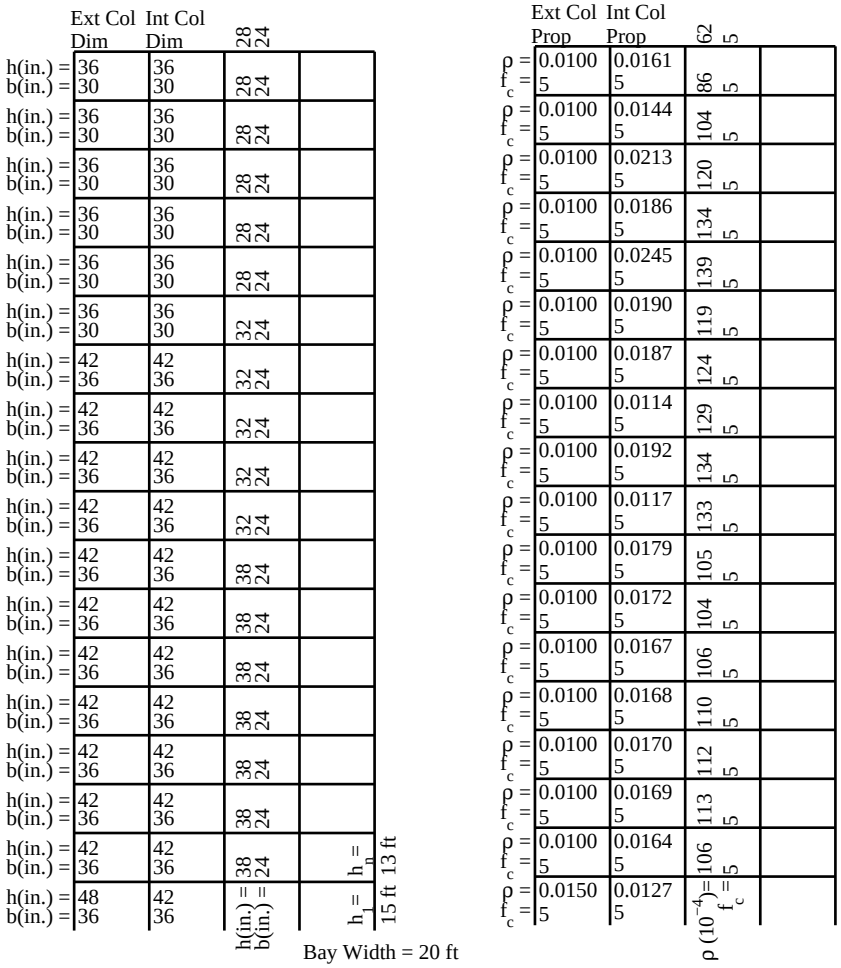

(a) Dimensions (b) Properties

Figure 4.11: Dimensions and Properties of the 18-Story, 1.4 SCWB ratio Structure

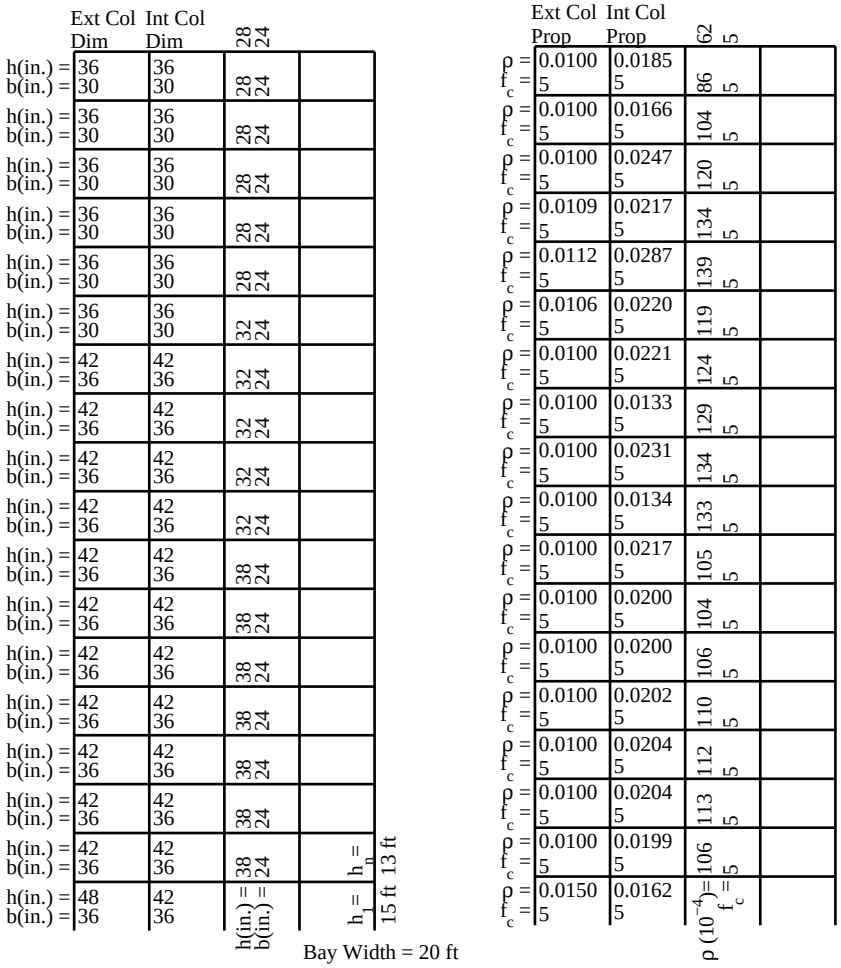

(a) Dimensions (b) Properties

Figure 4.12: Dimensions and Properties of the 18-Story, 1.6 SCWB ratio Structure

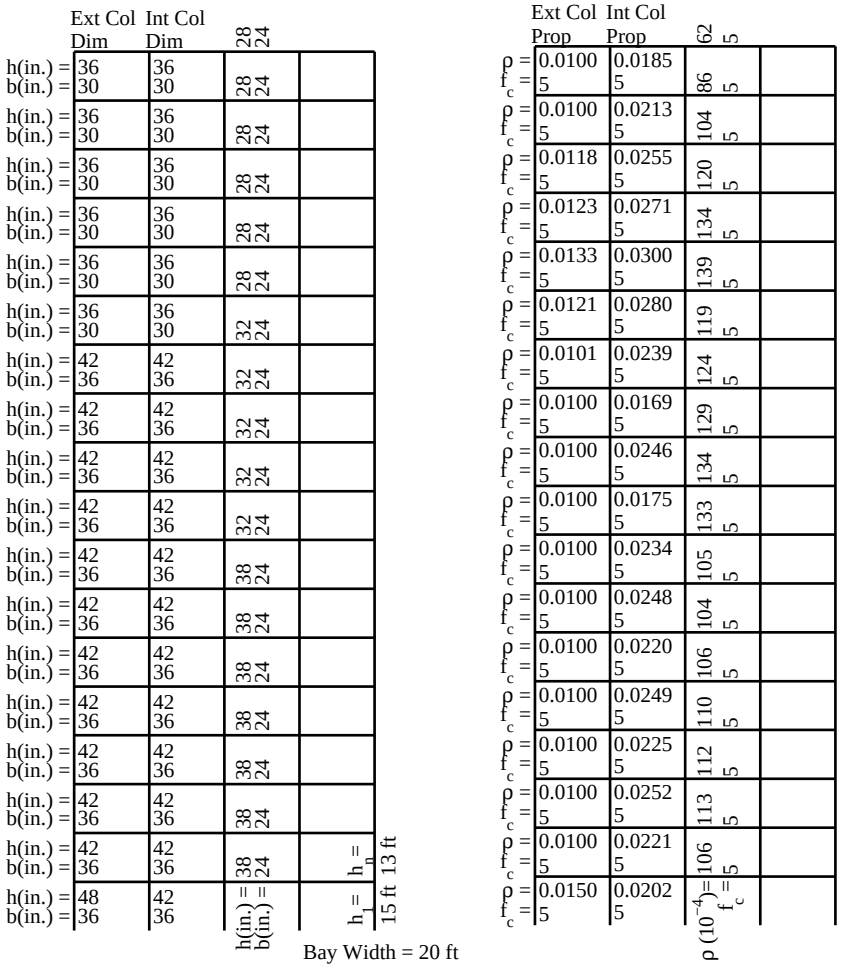

(a) Dimensions (b) Properties

Figure 4.13: Dimensions and Properties of the 18-Story, 1.8 SCWB ratio Structure

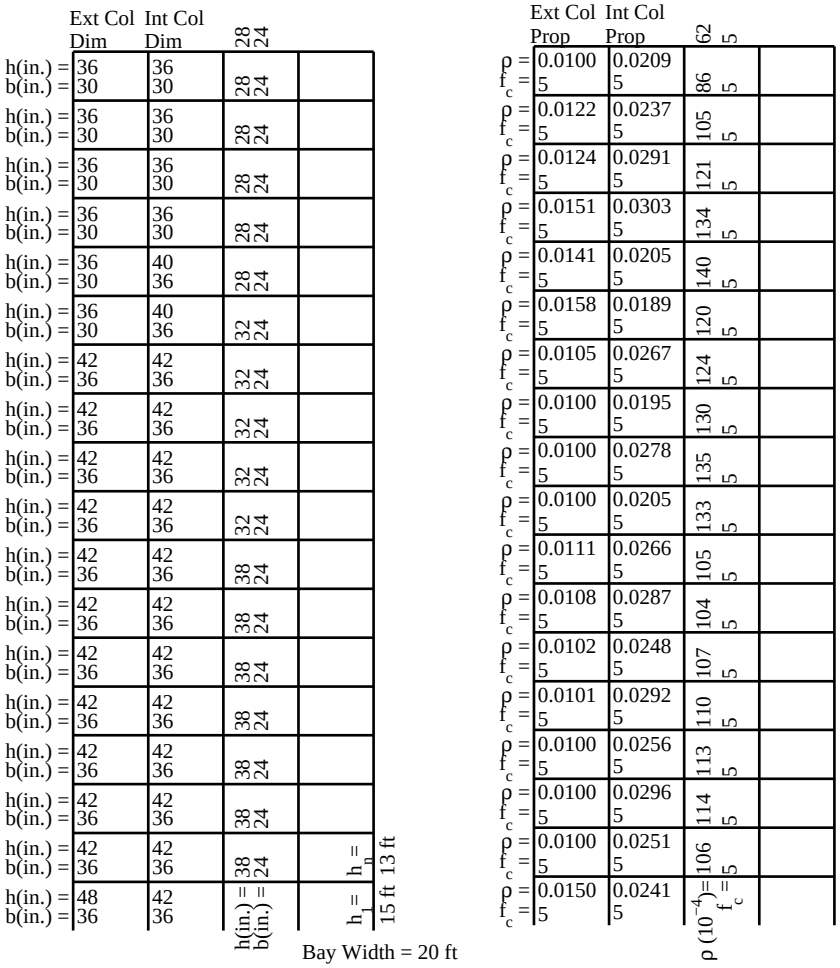

(a) Dimensions (b) Properties

Figure 4.14: Dimensions and Properties of the 18-Story, 2.0 SCWB ratio Structure

4.3 24-Story Structures

The gravity columns for the 24-story structures measure 30 x 30 in. for the first twelve stories, then decrease to 24 x 24 in. for the remaining twelve stories. Figures 4.16 through 4.20 show the dimensions and properties. Similar to the previous buildings, the reinforcement ratios for the exterior columns of the lateral load resisting frames of these buildings are initially controlled by the minimum reinforcement ratio, but only for the 1.2 SCWB ratio. When the SCWB ratio is 1.4 or higher, most of the upper joints are able to meet the target ratio. However, a combination of minimum reinforcement ratios and modal pushover demands still dictate the SCWB ratios in the lower half of the structure. The fundamental period of the 24-story structure is 4.79 sec, only decreasing slightly as the lateral load resisting columns increase to accommodate the greater reinforcement ratios needed for the larger SCWB ratios. Figure 4.15 shows the SCWB ratios at each joint, as well as the mean SCWB ratio of each floor, and the SCWB ratio calculated according to the alternate method.

					μ	Alternate Method
1.04	0.68	0.68	0.68	1.04	0.82	0.77
1.59	1.20	1.20	1.20	1.59	1.35	0.73
1.41	1.20	1.20	1.20	1.41	1.28	0.64
1.31	1.20	1.20	1.20	1.31	1.25	0.67
1.26	1.20	1.20	1.20	1.26	1.22	0.60
1.26	1.21	1.21	1.21	1.26	1.23	0.65
1.20	1.20	1.20	1.20	1.20	1.20	0.64
1.21	1.20	1.20	1.20	1.21	1.21	0.58
1.20	1.21	1.21	1.21	1.20	1.21	0.65
1.21	1.20	1.20	1.20	1.21	1.20	0.57
1.27	1.21	1.21	1.21	1.27	1.23	0.64
1.43	1.20	1.20	1.20	1.43	1.29	0.69
1.75	1.20	1.20	1.20	1.75	1.42	0.65
1.77	1.20	1.20	1.20	1.77	1.43	0.71
1.77	1.20	1.20	1.20	1.77	1.43	0.66
2.11	1.20	1.20	1.20	2.11	1.56	0.78
2.44	1.20	1.20	1.20	2.44	1.70	0.75
2.47	1.20	1.20	1.20	2.47	1.71	0.79
2.44	1.20	1.20	1.20	2.44	1.70	0.75
2.75	1.20	1.20	1.20	2.75	1.82	0.84
2.96	1.20	1.20	1.20	2.96	1.91	0.83
3.55	1.24	1.24	1.24	3.55	2.16	0.96
4.46	1.54	1.54	1.54	4.46	2.71	1.28
5.26	2.12	2.12	2.12	5.26	3.38	1.43

(a) 1.2 SCWB ratio

					μ	Alternate Method
1.04	0.75	0.75	0.75	1.04	0.87	0.82
1.59	1.40	1.40	1.40	1.59	1.47	0.84
1.41	1.40	1.40	1.40	1.41	1.40	0.70
1.40	1.40	1.40	1.40	1.40	1.40	0.78
1.40	1.40	1.40	1.40	1.40	1.40	0.68
1.44	1.40	1.40	1.40	1.44	1.42	0.76
1.40	1.40	1.40	1.40	1.40	1.40	0.74
1.41	1.40	1.40	1.40	1.41	1.40	0.68
1.40	1.41	1.41	1.41	1.40	1.40	0.76
1.40	1.40	1.40	1.40	1.40	1.40	0.67
1.40	1.41	1.41	1.41	1.40	1.41	0.72
1.48	1.40	1.40	1.40	1.48	1.43	0.77
1.75	1.40	1.40	1.40	1.75	1.54	0.71
1.77	1.41	1.41	1.41	1.77	1.55	0.80
1.77	1.40	1.40	1.40	1.77	1.55	0.72
2.11	1.40	1.40	1.40	2.11	1.69	0.88
2.44	1.40	1.40	1.40	2.44	1.82	0.80
2.47	1.41	1.41	1.41	2.47	1.83	0.88
2.44	1.40	1.40	1.40	2.44	1.82	0.81
2.75	1.40	1.40	1.40	2.75	1.94	0.93
2.96	1.40	1.40	1.40	2.96	2.02	0.89
3.55	1.40	1.40	1.40	3.55	2.26	1.03
4.46	1.62	1.62	1.62	4.46	2.76	1.28
5.26	2.12	2.12	2.12	5.26	3.38	1.43

(b) 1.4 SCWB ratio

					μ	Alternate Method
1.04	0.96	0.96	0.96	1.04	0.99	0.98
1.65	1.60	1.60	1.60	1.65	1.62	0.89
1.60	1.60	1.60	1.60	1.60	1.60	0.85
1.65	1.60	1.60	1.60	1.65	1.62	0.86
1.60	1.60	1.60	1.60	1.60	1.60	0.81
1.65	1.60	1.60	1.60	1.65	1.62	0.84
1.60	1.60	1.60	1.60	1.60	1.60	0.88
1.61	1.60	1.60	1.60	1.61	1.60	0.75
1.60	1.60	1.60	1.60	1.60	1.60	0.89
1.60	1.60	1.60	1.60	1.60	1.60	0.74
1.60	1.61	1.61	1.61	1.60	1.61	0.85
1.60	1.60	1.60	1.60	1.60	1.60	0.84
1.80	1.60	1.60	1.60	1.80	1.68	0.80
1.77	1.64	1.64	1.64	1.77	1.69	0.88
1.77	1.60	1.60	1.60	1.77	1.67	0.79
2.11	1.61	1.61	1.61	2.11	1.81	0.96
2.44	1.60	1.60	1.60	2.44	1.94	0.87
2.47	1.60	1.60	1.60	2.47	1.95	0.96
2.44	1.60	1.60	1.60	2.44	1.93	0.88
2.75	1.60	1.60	1.60	2.75	2.06	1.02
2.96	1.60	1.60	1.60	2.96	2.14	0.96
3.55	1.60	1.60	1.60	3.55	2.38	1.10
4.46	1.73	1.73	1.73	4.46	2.82	1.28
5.26	2.12	2.12	2.12	5.26	3.38	1.43

(c) 1.6 SCWB ratio

					μ	Alternate Method
1.01	1.03	1.03	1.03	1.01	1.02	1.02
1.84	1.80	1.80	1.80	1.84	1.82	1.06
1.80	1.80	1.80	1.80	1.80	1.80	0.92
1.81	1.80	1.80	1.80	1.81	1.80	1.00
1.80	1.80	1.80	1.80	1.80	1.80	0.89
1.82	1.80	1.80	1.80	1.82	1.81	0.96
1.80	1.80	1.80	1.80	1.80	1.80	0.97
1.82	1.80	1.80	1.80	1.82	1.81	0.86
1.80	1.80	1.80	1.80	1.80	1.80	0.98
1.80	1.80	1.80	1.80	1.80	1.80	0.86
1.80	1.80	1.80	1.80	1.80	1.80	0.93
1.80	1.80	1.80	1.80	1.80	1.80	0.97
1.84	1.80	1.80	1.80	1.84	1.81	0.85
1.80	1.80	1.80	1.80	1.80	1.80	0.97
1.80	1.80	1.80	1.80	1.80	1.80	0.84
1.94	1.80	1.80	1.80	1.94	1.86	1.01
2.26	1.80	1.80	1.80	2.26	1.98	0.92
2.27	1.80	1.80	1.80	2.27	1.99	1.02
2.29	1.80	1.80	1.80	2.29	2.00	0.92
2.61	1.80	1.80	1.80	2.61	2.12	1.08
2.79	1.80	1.80	1.80	2.79	2.20	1.02
3.36	1.80	1.80	1.80	3.36	2.43	1.14
4.23	1.81	1.81	1.81	4.23	2.78	1.24
5.00	2.11	2.11	2.11	5.00	3.27	1.39

(d) 1.8 SCWB ratio

					μ	Alternate Method
1.12	1.10	1.10	1.10	1.12	1.11	1.11
2.00	2.02	2.02	2.02	2.00	2.01	1.19
2.00	2.00	2.00	2.00	2.00	2.00	1.00
2.02	2.02	2.02	2.02	2.02	2.02	1.15
2.00	2.00	2.00	2.00	2.00	2.00	0.96
2.02	2.02	2.02	2.02	2.02	2.02	1.11
2.00	2.00	2.00	2.00	2.00	2.00	1.05
2.00	2.00	2.00	2.00	2.00	2.00	0.98
2.00	2.05	2.05	2.05	2.00	2.03	1.10
2.00	2.00	2.00	2.00	2.00	2.00	0.94
2.01	2.06	2.06	2.06	2.01	2.04	1.09
2.00	2.00	2.00	2.00	2.00	2.00	1.03
2.00	2.01	2.01	2.01	2.00	2.00	0.99
2.02	1.99	1.99	1.99	2.02	2.00	1.03
2.00	2.00	2.00	2.00	2.00	2.00	0.98
2.01	2.00	2.00	2.00	2.01	2.00	1.04
2.26	2.00	2.00	2.00	2.26	2.10	1.04
2.27	2.00	2.00	2.00	2.27	2.11	1.06
2.29	2.01	2.01	2.01	2.29	2.12	1.04
2.61	2.04	2.04	2.04	2.61	2.27	1.13
2.79	1.99	1.99	1.99	2.79	2.31	1.10
3.36	2.02	2.02	2.02	3.36	2.56	1.22
4.23	2.00	2.00	2.00	4.23	2.89	1.30
5.00	2.20	2.20	2.20	5.00	3.32	1.39

(e) 2.0 SCWB ratio

Figure 4.15: SCWB Ratios calculated using an alternate method, calculated at each joint and averaged over each floor of the 24-Story Structure

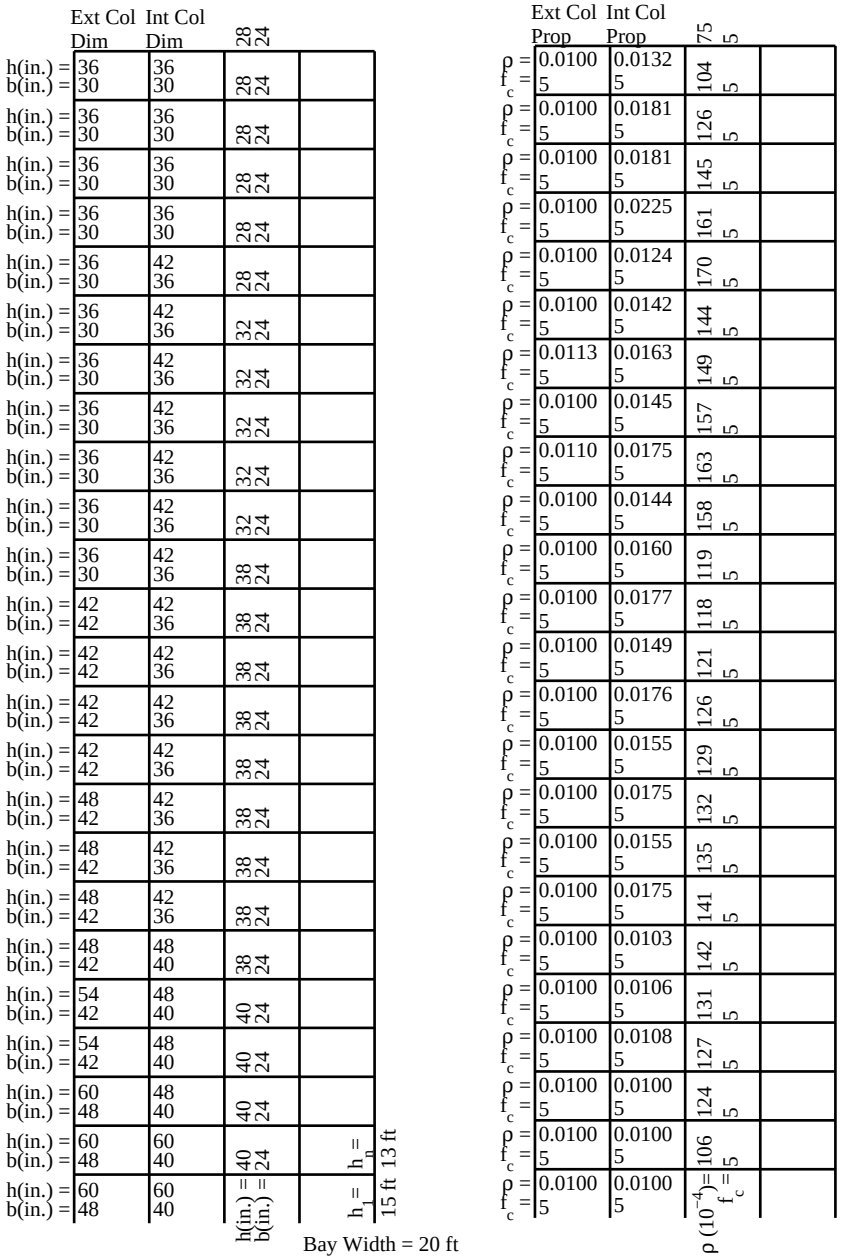

(a) Dimensions (b) Properties

Figure 4.16: Dimensions and Properties of the 24-Story, 1.2 SCWB ratio Structure

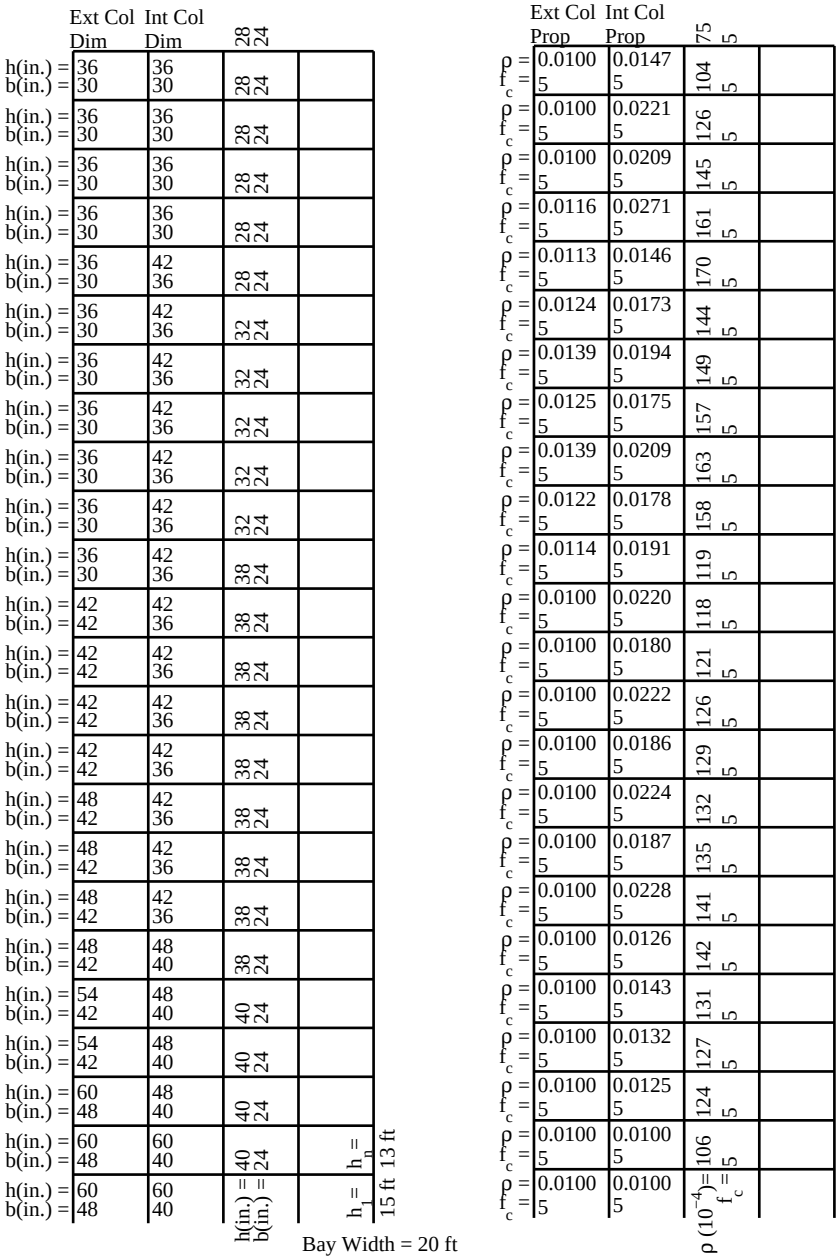

(a) Dimensions (b) Properties

Figure 4.17: Dimensions and Properties of the 24-Story, 1.4 SCWB ratio Structure

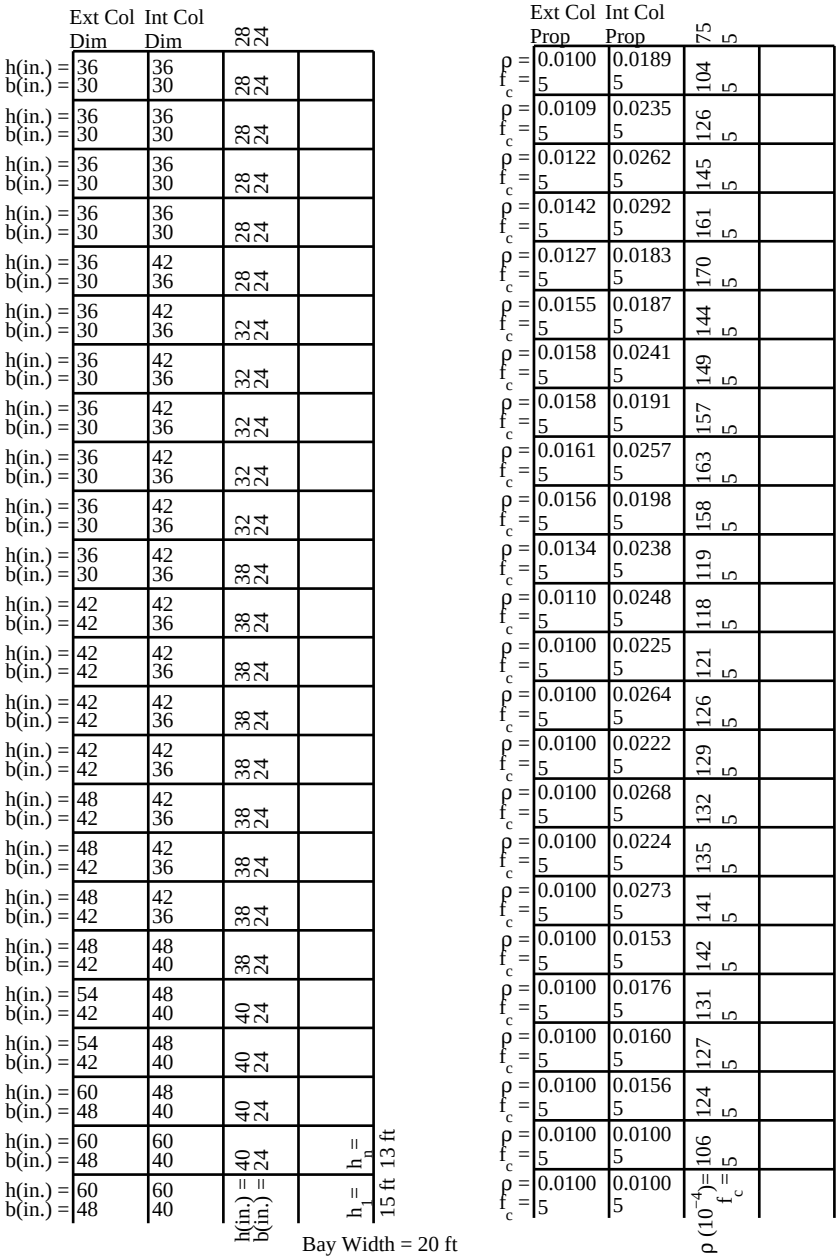

(a) Dimensions (b) Properties

Figure 4.18: Dimensions and Properties of the 24-Story, 1.6 SCWB ratio Structure

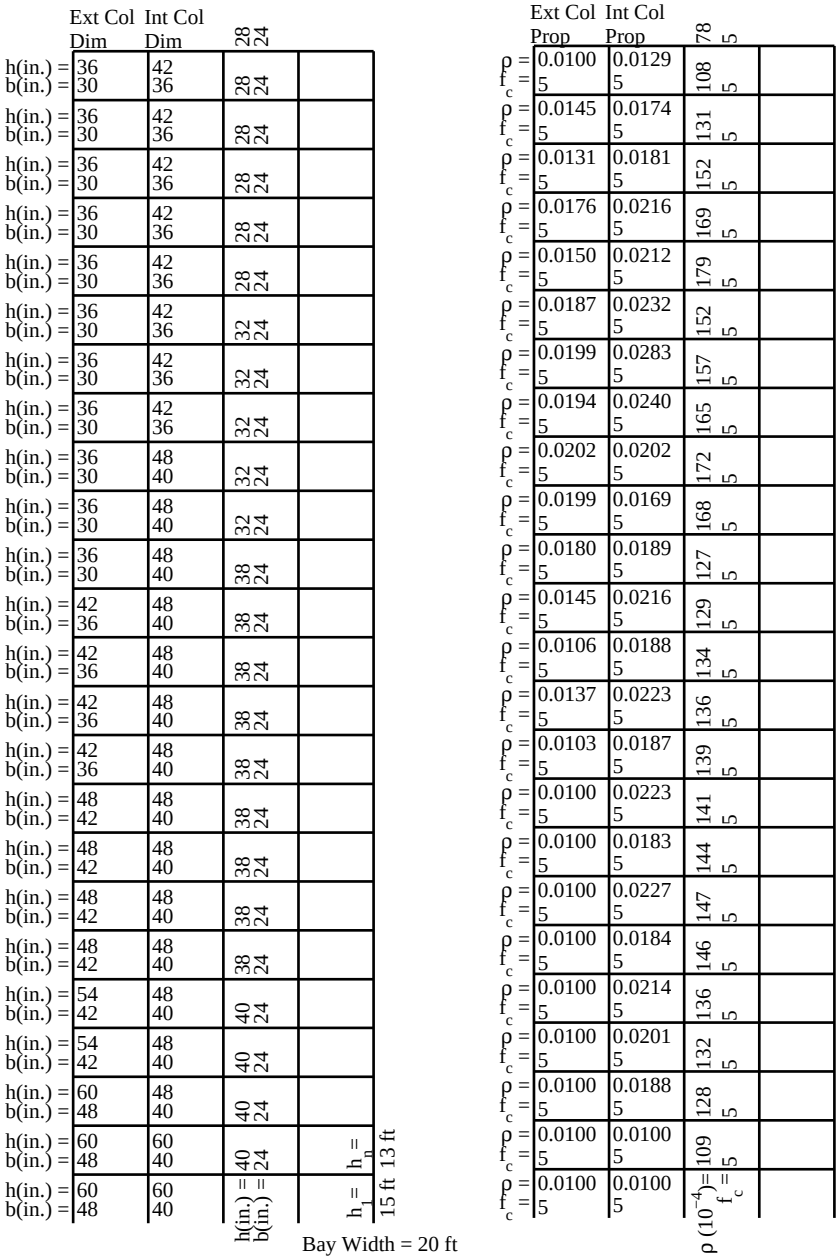

(a) Dimensions (b) Properties

Figure 4.19: Dimensions and Properties of the 24-Story, 1.8 SCWB ratio Structure

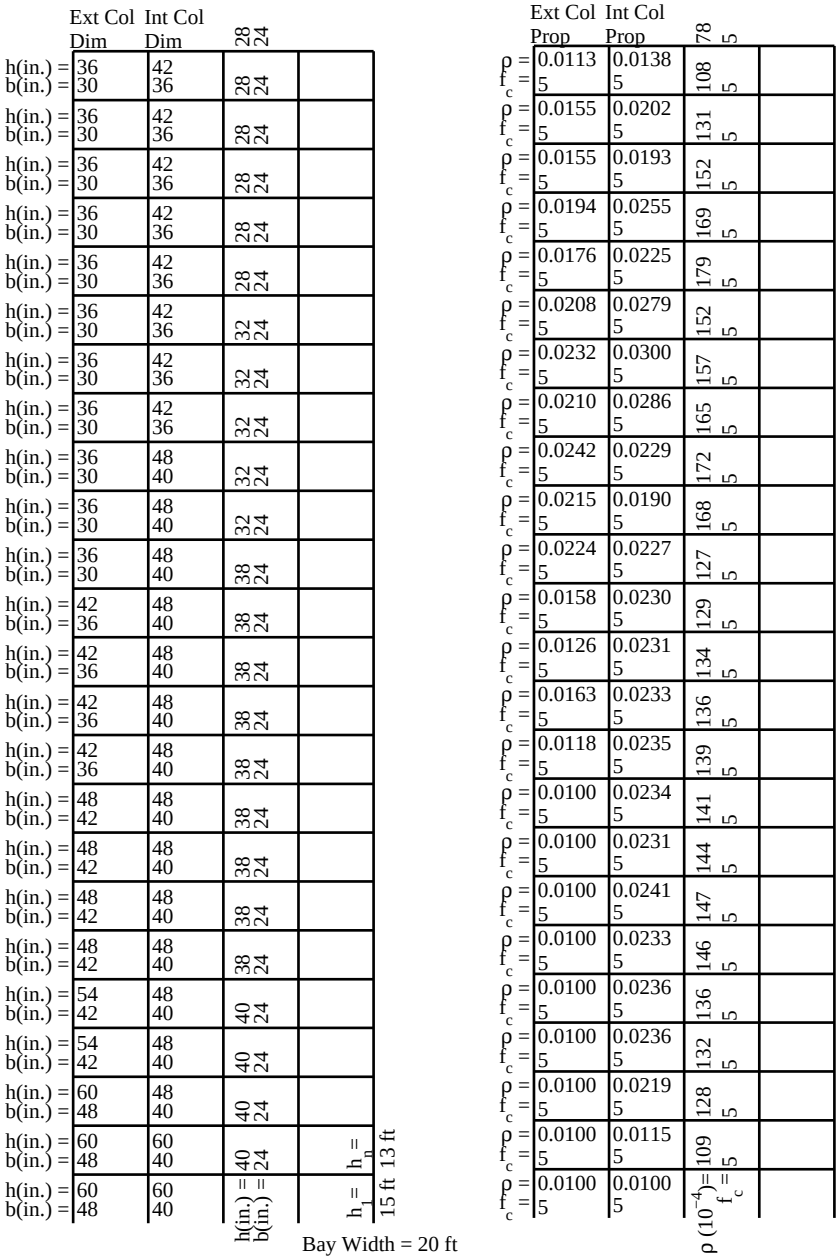

(a) Dimensions (b) Properties

Figure 4.20: Dimensions and Properties of the 24-Story, 2.0 SCWB ratio Structure

Chapter 5

Results

Pushover analyses using an inverted triangular load are performed on all structures to obtain various values needed for the computation of the probability of collapse and adjustment factors. IDA analyses were performed to obtain the Sa at which collapse occurred and construct the fragility curves. Select results from one of the time histories that compose the IDA analyses are shown in section 5.2. Results and discussion of each structure will follow.

5.1 Typical Results from a Pushover Analysis

Figure 5.2 depicts the formation of hinges in the 12-story, 1.8 SCWB ratio structure at increasing displacements of the nonlinear static pushover analysis. Neglecting the lateral resistance provided by the gravity framing results in pushover curves with strongly negative post-yielding stiffness, as can be seen in figure 5.1.

5.2 Typical Results from an Incremental Dynamic Analysis

Figures 5.3, 5.4 and 5.5 depict typical results from a time history analysis. The results presented in these figures come from the 12-story, 1.8 SCWB ratio structure excited by ground motion 1900003. Figure 5.6 shows the results of the complete incremental dynamic analysis utilizing all ground motions for the same 12-story, 1.8 SCWB ratio structure.

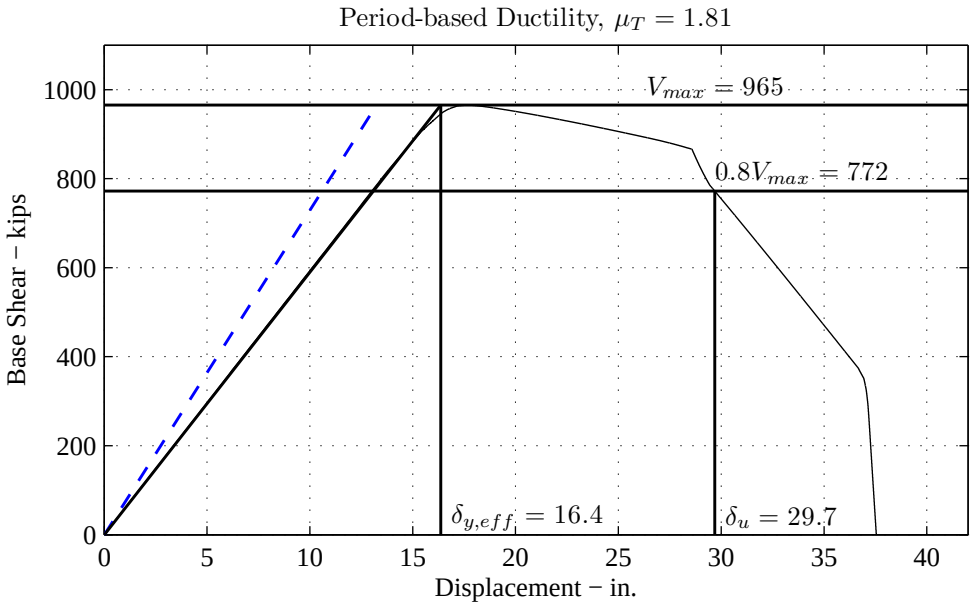

Figure 5.1: Nonlinear Static Pushover 12-Story, 1.8 SCWB Ratio

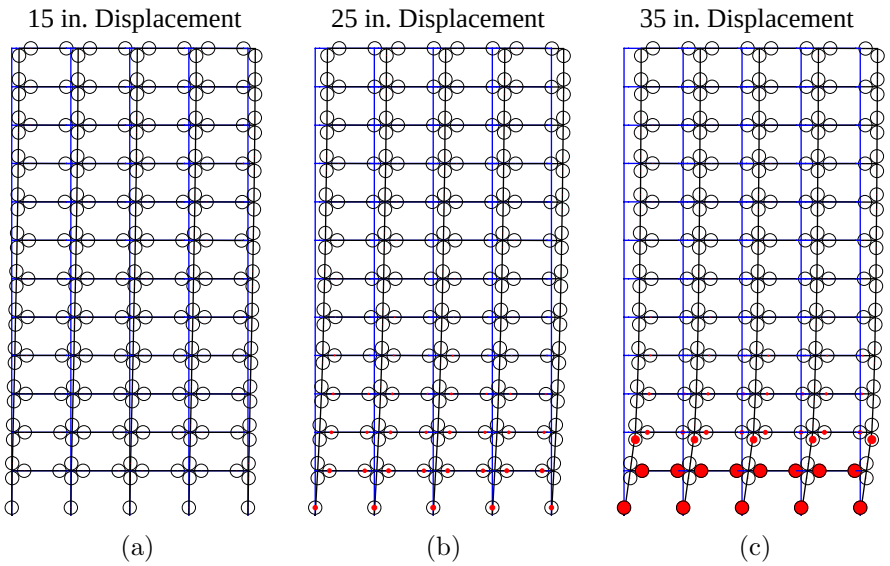

Figure 5.2: Hinge Formation at Various Levels of Displacement for the 12-Story, 1.8 SCWB Ratio Pushover

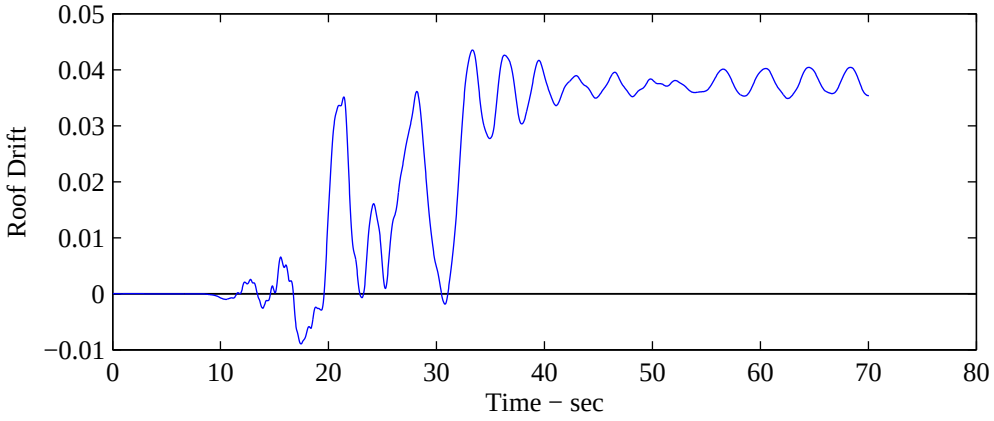

(a)

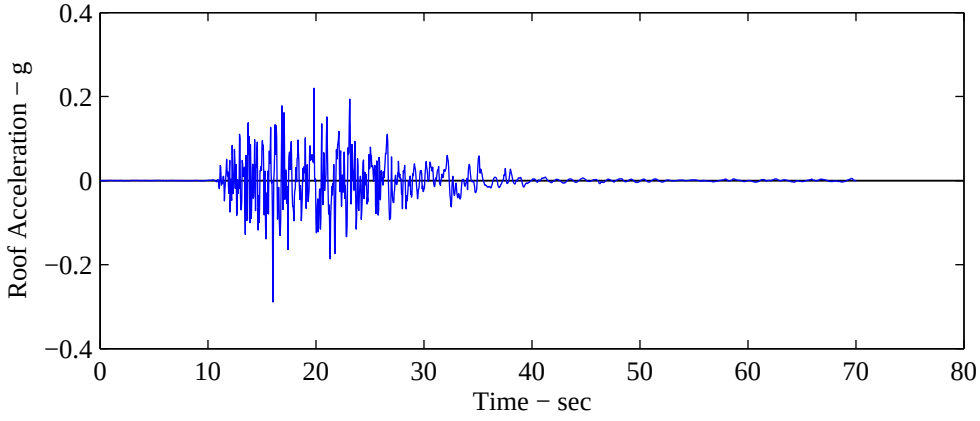

(b)

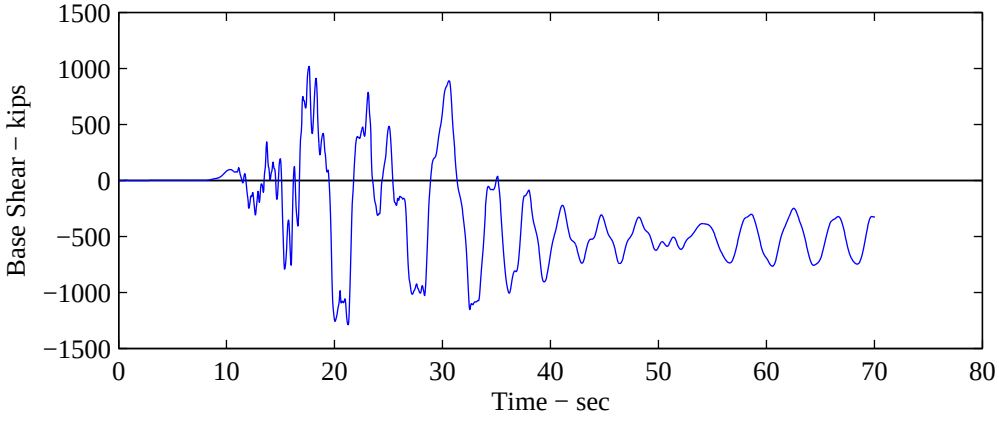

(c)

Figure 5.3: Ground Motion 1900003 Response Histories for the 12-Story, 1.8 SCWB Ratio Structure

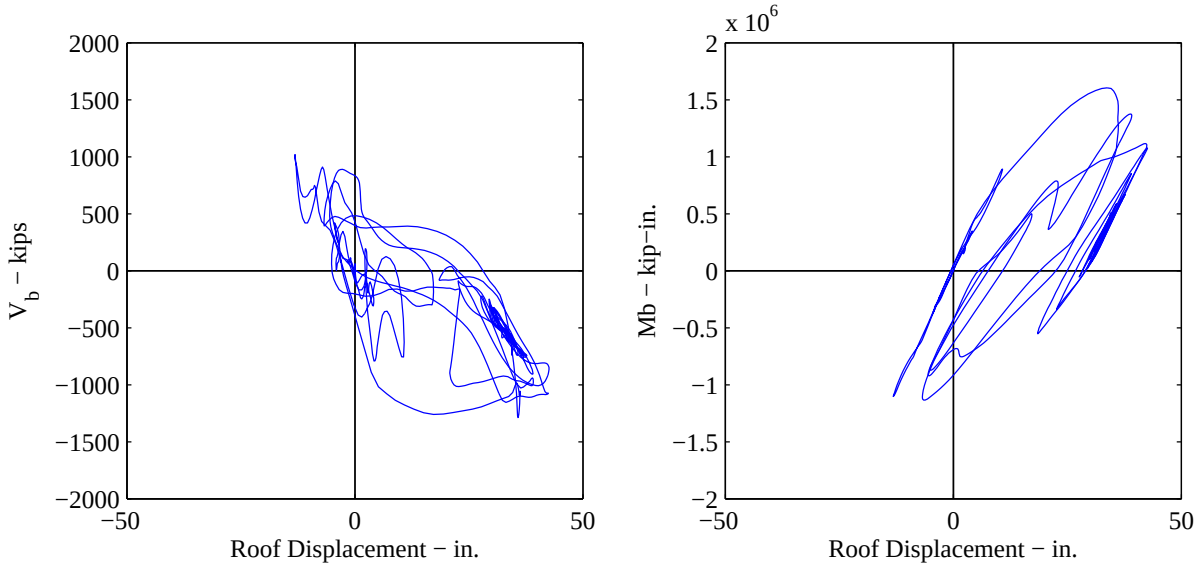

(a) Base Shear (b) Base Moment

Figure 5.4: Ground Motion 1900003 Base Shear and Moment versus Roof Displacement for the 12-Story, 1.8 SCWB Ratio Structure

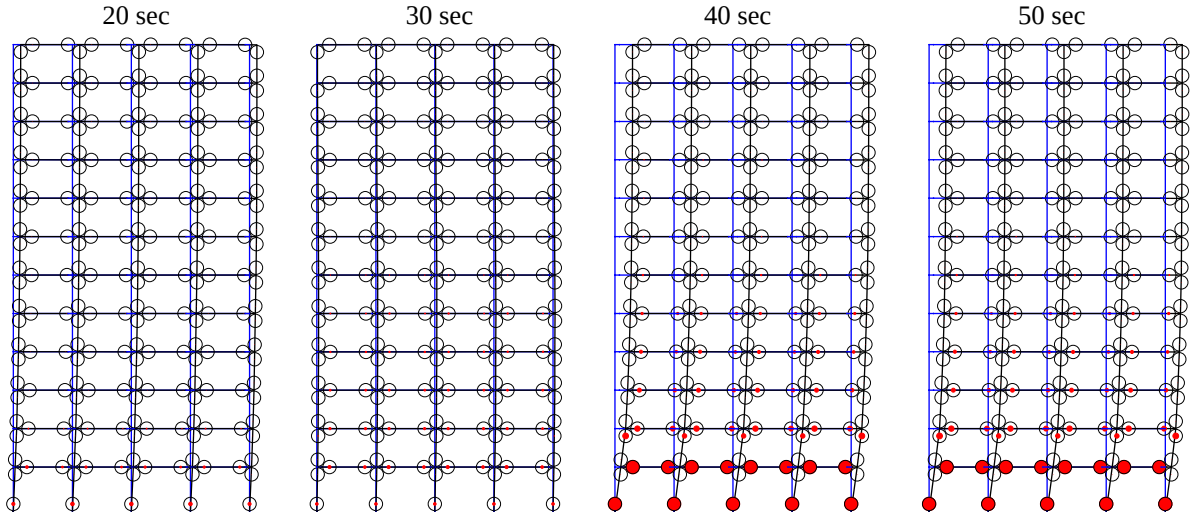

(a) (b) (c) (d)

Figure 5.5: Ground Motion 1900003 Frame and Hinges at 20, 30, 40, and 50 sec for the 12-Story, 1.8 SCWB Ratio Structure

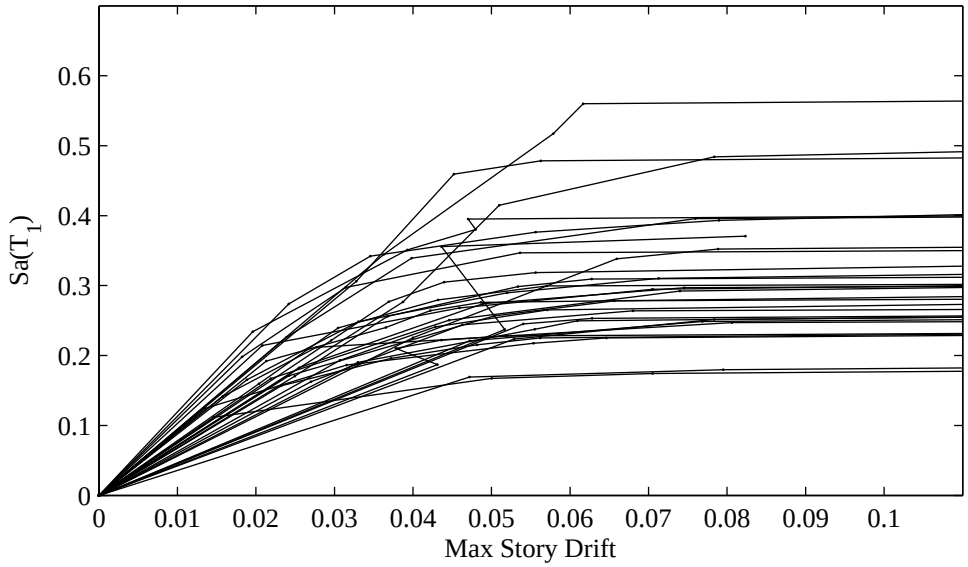

Figure 5.6: Incremental Dynamic Analysis Results for the 12-Story, 1.8 SCWB Ratio Structure

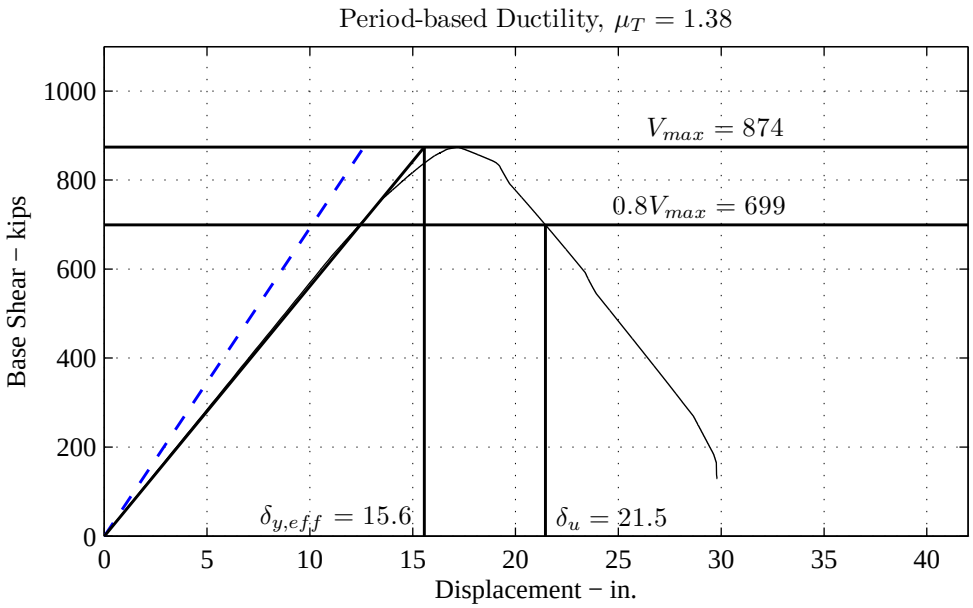

Figure 5.7: Nonlinear Static Pushover 12-Story, 1.2 SCWB Ratio

5.3 12-Story Structures

Figures 5.7 to 5.11 depict the curves obtained from the nonlinear static pushover analyses of the 12-story structures. The maximum base shear increases as the SCWB ratio increases, starting with $V_{max} = 874$ kips for the 1.2 SCWB ratio and increasing to $V_{max} = 985$ kips for the 2.0 SCWB ratio. It should be noted that the design base shear was 605 kips, evidence of the overstrength built into design process for these structures. The period based ductilities increase from $\mu_T = 1.38$ for the 1.2 SCWB ratio to $\mu_T = 2.07$ for the 2.0 SCWB ratio. As discussed in the methodology chapter, the dashed blue line in these figures depicts the fundamental period as defined by FEMA P695; because this overestimates the stiffness of the structures, for the purpose of this study, the yield displacement is instead obtained by passing a line through the plot at $0.7V_{max}$ and defining δ_y as the point at which the line intersects V_{max}. Figure 5.12 shows the mechanisms formed from the pushover analysis. The failure mechanism does not spread beyond the first two stories even though the SCWB ratio is nearly doubled.

Figures 5.13 to 5.17 show the fragility curves developed from the 30 ground motion incremental dynamic analyses. The probabilities of collapse given a maximum considered earthquake are $P(C|MCE) = 38\%$, 24%, 17%, 9.5%, and 7.2% for SCWB ratios 1.2, 1.4, 1.6, 1.8, and 2.0 respectively. Adjusting for spectral shape, these probabilities become $P(C|MCE) = 29\%$, 17%, 9.9%, 4.8%, and 3.2%, respectively. As expected, increasing the SCWB ratio decreases the probability of collapse (Figure 5.18). An increase from 1.2 to 1.4 results in a 41% decrease in the probability of collapse. An increase from 1.4 to 1.6 results in a 42% decrease; increasing to from 1.6 to 1.8 results in a 52% decreases; and increasing to from 1.8 to 2.0 results in another 33% decrease. The median spectral acceleration of

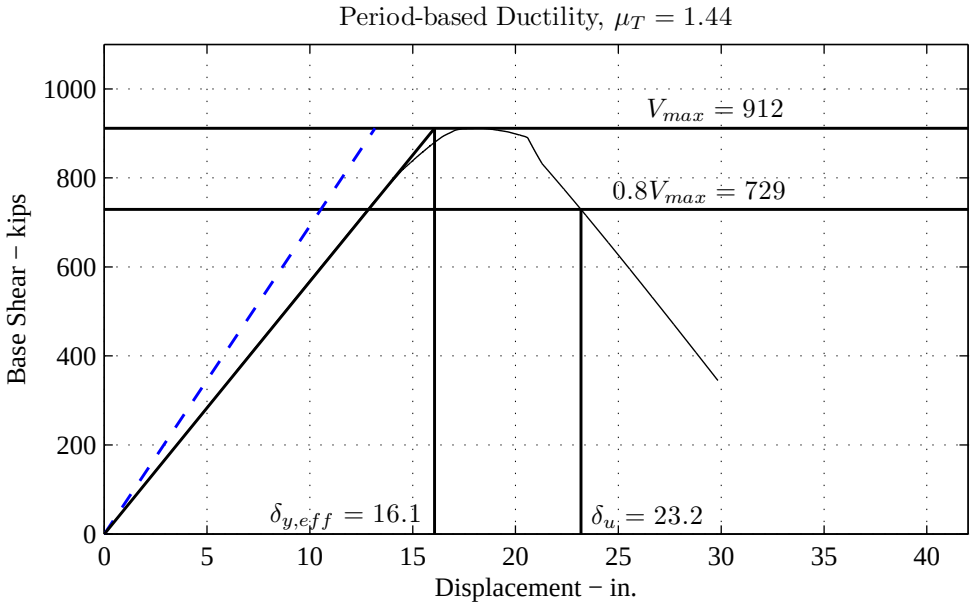

Figure 5.8: Nonlinear Static Pushover 12-Story, 1.4 SCWB Ratio

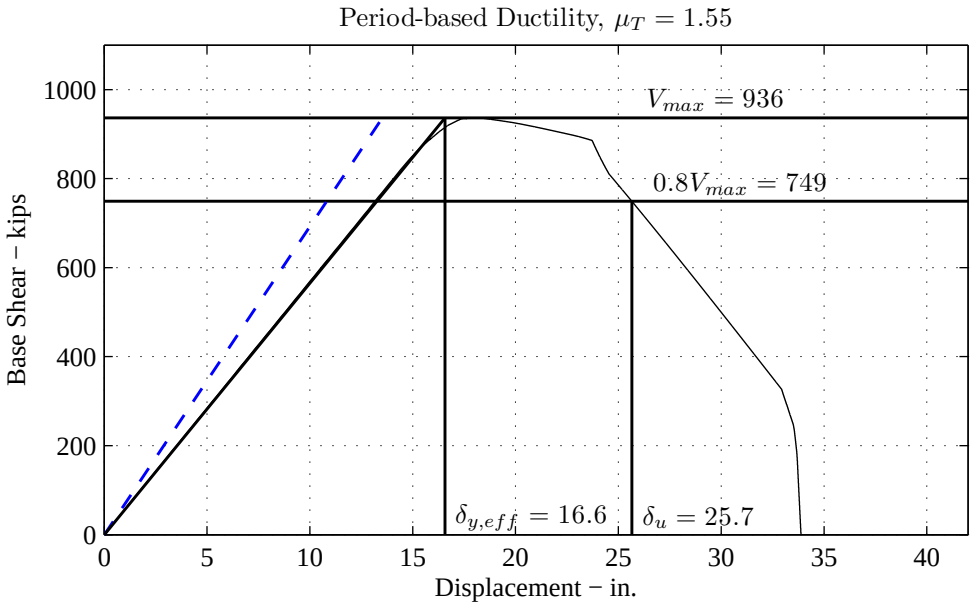

Figure 5.9: Nonlinear Static Pushover 12-Story, 1.6 SCWB Ratio

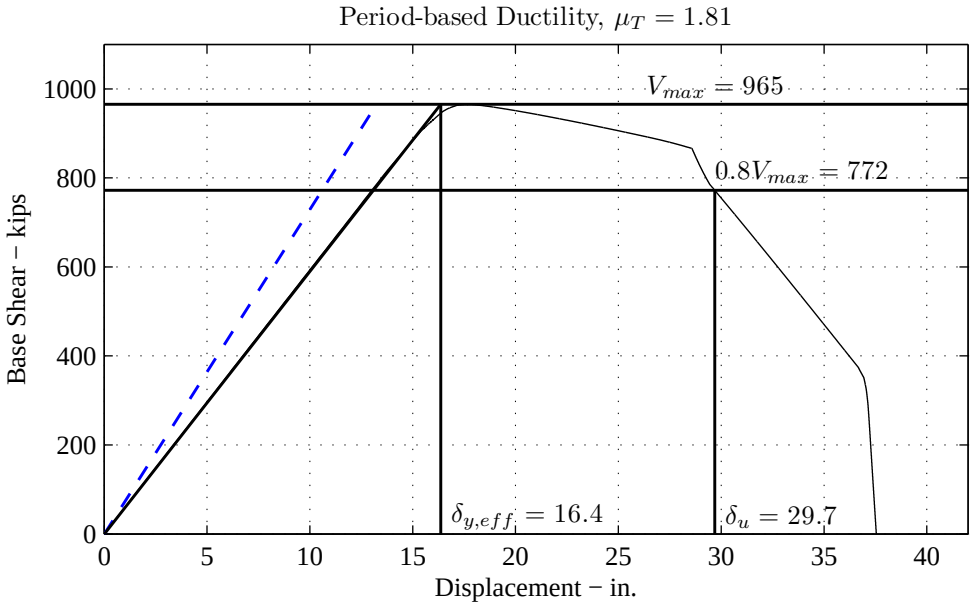

Figure 5.10: Nonlinear Static Pushover 12-Story, 1.8 SCWB Ratio

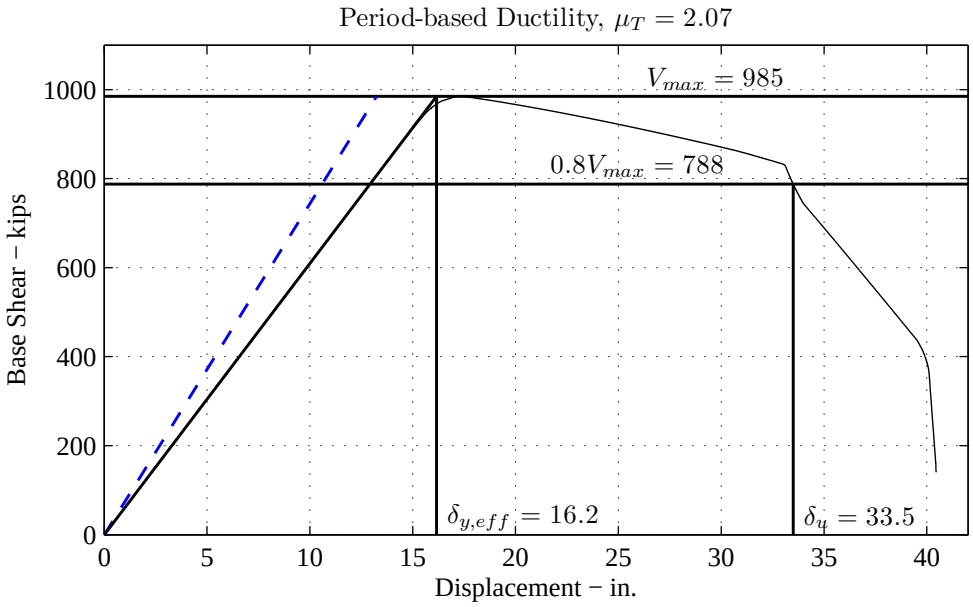

Figure 5.11: Nonlinear Static Pushover 12-Story, 2.0 SCWB Ratio

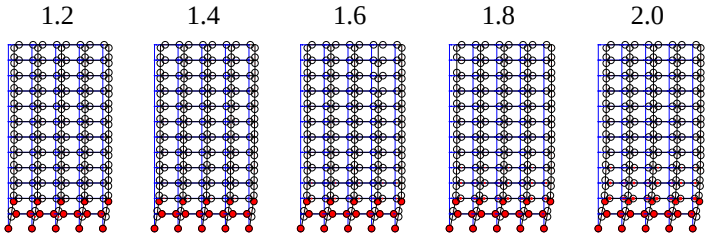

Figure 5.12: Failure Mechanisms from Nonlinear Static Pushover Analyses - 12-Story Structure

collapse for each SCWB ratio are $0.20g$, $0.23g$, $0.25g$, $0.3g$, and $0.33g$, also increasing as the SCWB ratio increases. The adjusted collapse margin ratio (ACMR) also increases as SCWB ratios increase. For the 12-story structure, the ACMR are 1.21, 1.39, 1.55, 1.83, and 1.97 for SCWB ratios 1.2, 1.4, 1.6, 1.8, and 2.0 respectively. The ACMR increases 15% as the SCWB increases from 1.2 to 1.4, 12% from 1.4 to 1.6, 18% from 1.6 to 1.8, and 7.7% from 1.8 to 2.0.

The failure mechanisms from the incremental dynamic analyses are shown in full in Appendix A.1. Table 5.1 summarizes the results. The 1.2 SCWB ratio structure develops a failure mechanism involving only the first story for 87% of the ground motions. The remainder develop a mechanism incorporating the first two stories. The 1.4 SCWB ratio structure develops a failure mechanism involving the first two stories for 63% of the ground motion, with the remainder involving only the first story. With a 1.6 SCWB ratio, the structure develops a failure mechanism incorporating the first two floors for 93% (or all but two) of the ground motions. The 1.8 and 2.0 SCWB ratio structures develop a two-story mechanism for all the ground motions. The mechanism never spreads beyond the first two stories; even a SCWB ratio of 2.0 does not prevent a partial collapse story mechanism from occurring.

Increasing the SCWB ratio from a 1.2 to 1.4 incorporates an additional story into the mechanism in 50% of the ground motions; increasing from 1.4 to 1.6 incorporates an additional story in only 30% of the ground motions. The remaining two ground motions develop the two-story mechanism when the SCWB ratio is 1.8. No further benefit is gained from increasing the SCWB ratio to 2.0 with regard to the spread of the failure mechanism.

5.4 18-Story Structures

Figures 5.19 to 5.23 depict the nonlinear static pushover curves of the 18-story structures. The maximum base shear increases from $V_{max} = 1259$ kips for the 1.2 SCWB ratio to $V_{max} = 1265$ kips for the 2.0 SCWB ratio. The design base shear was 830 kips, evidence of the overstrength built into design process for these structures. The period based ductility increases from $\mu_T = 1.38$ for the 1.2 SCWB ratio to $\mu_T = 2.07$ for the 2.0 SCWB ratio. The failure mechanisms from these analyses, shown in Figure 5.24, show no significant spread over the height of the structure, incorporating only the first three stories for SCWB ratios

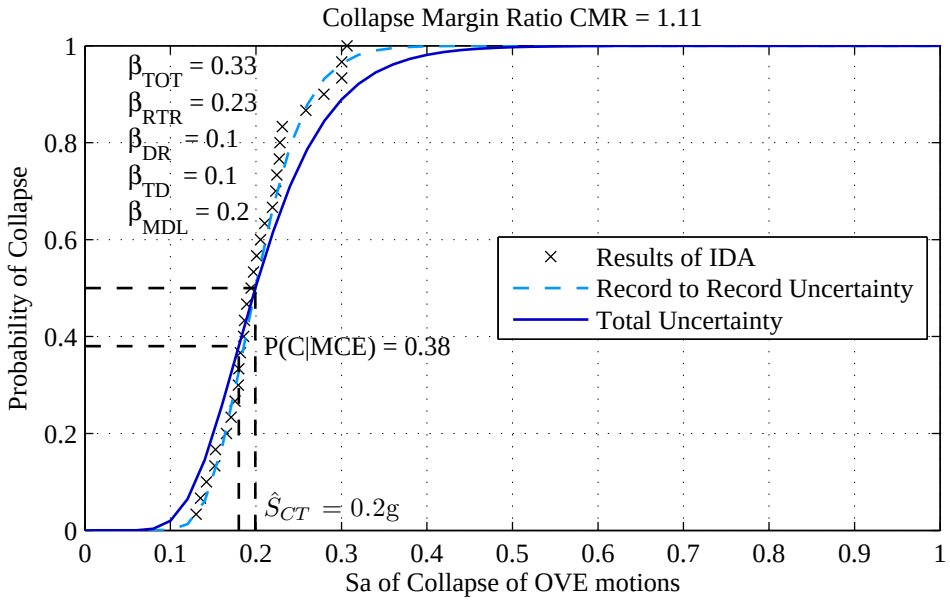

(a) No Adjustment

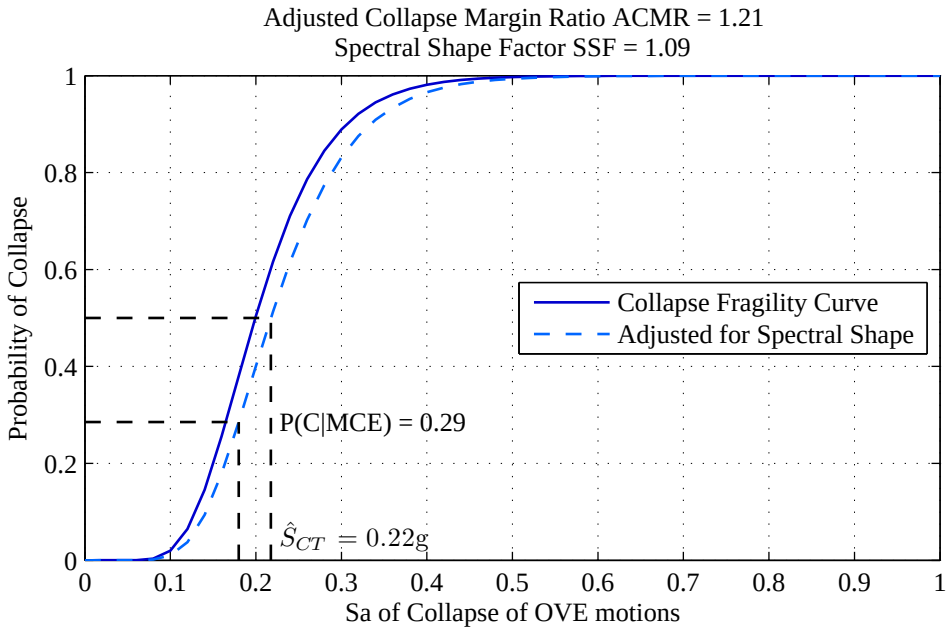

(b) Adjusted for Spectral Shape

Figure 5.13: Fragility Curves for 12-Story, 1.2 SCWB ratio

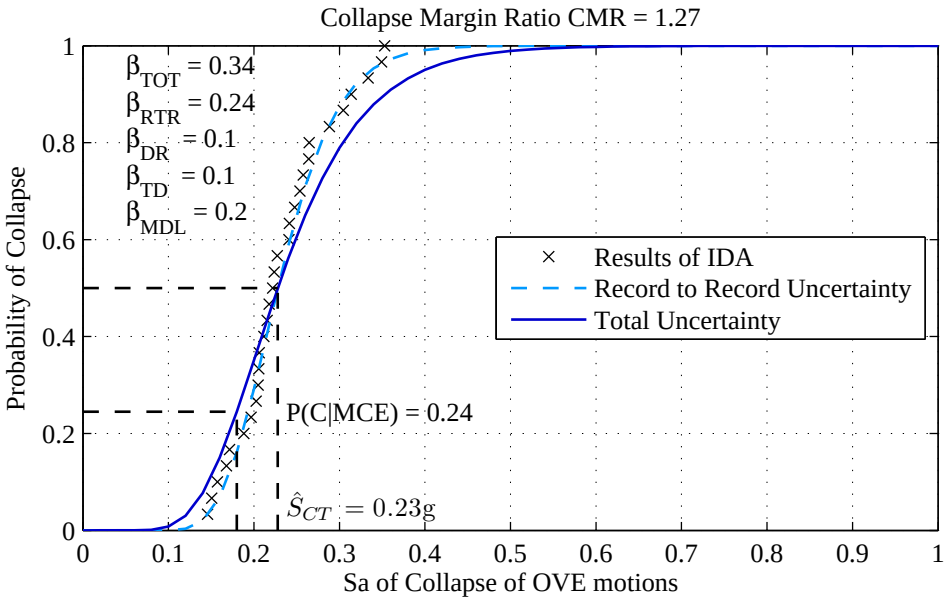

(a) No Adjustment

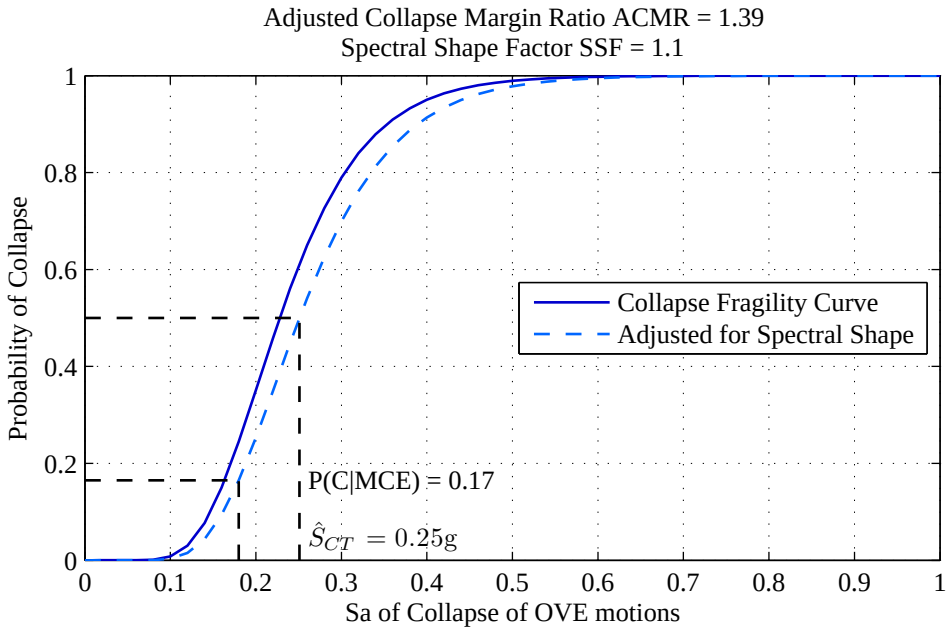

(b) Adjusted for Spectral Shape

Figure 5.14: Fragility Curves for 12-Story, 1.4 SCWB ratio

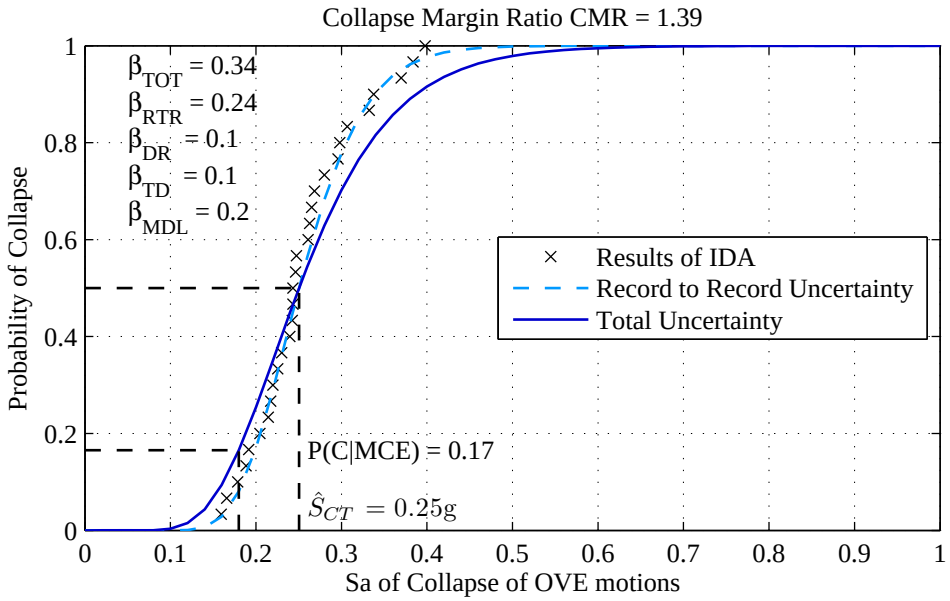

(a) No Adjustment

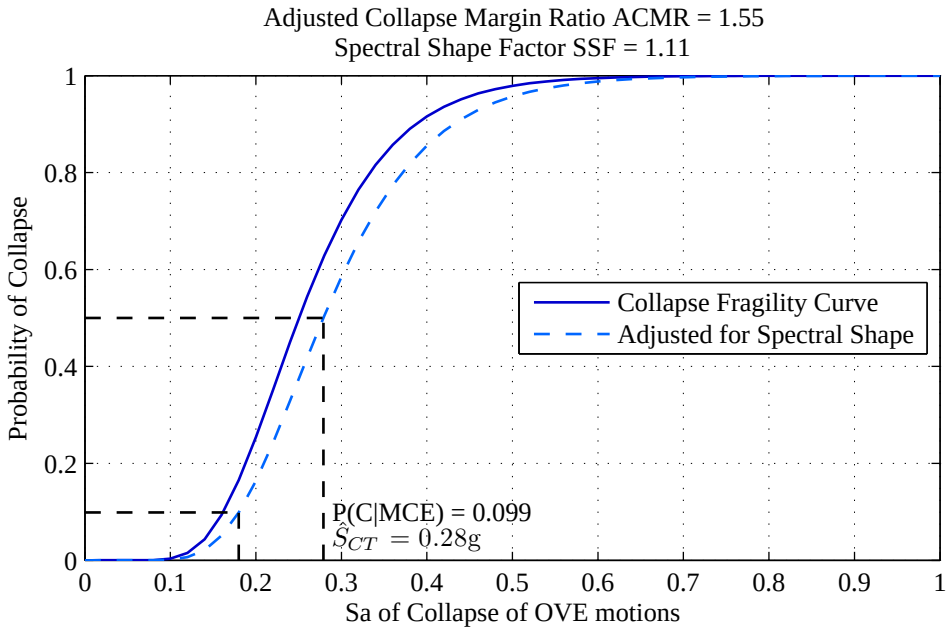

(b) Adjusted for Spectral Shape

Figure 5.15: Fragility Curves for 12-Story, 1.6 SCWB ratio

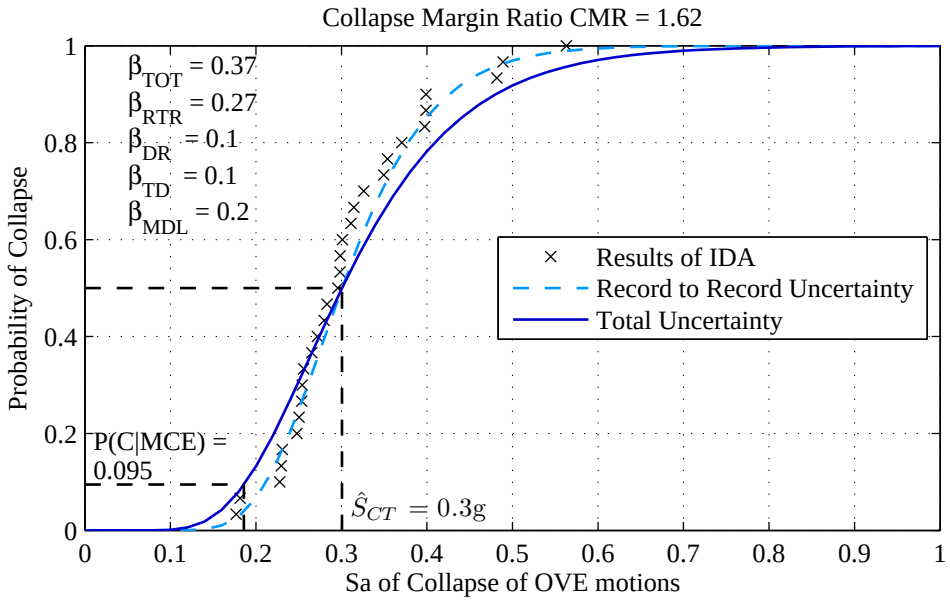

(a) No Adjustment

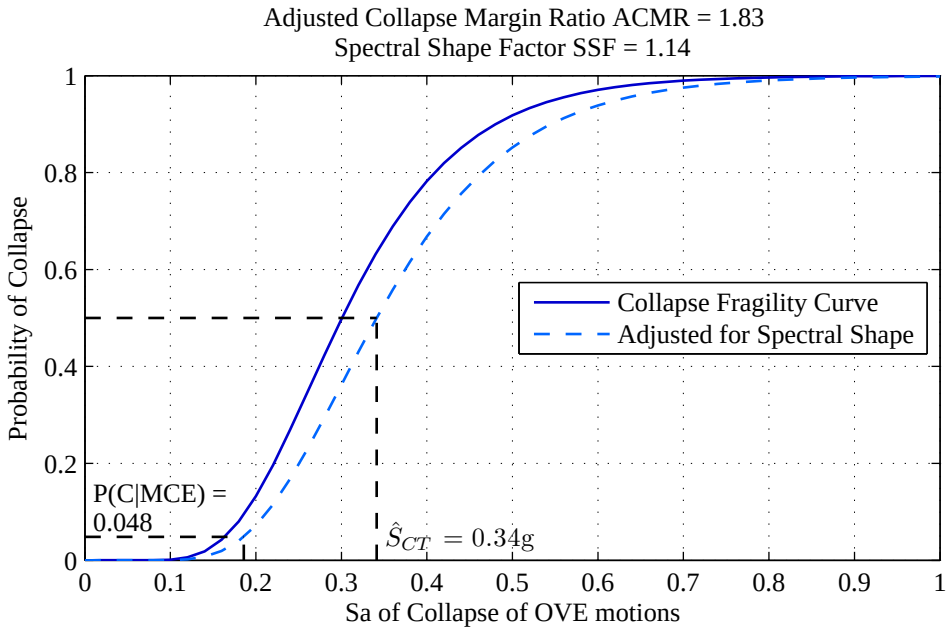

(b) Adjusted for Spectral Shape

Figure 5.16: Fragility Curves for 12-Story, 1.8 SCWB ratio

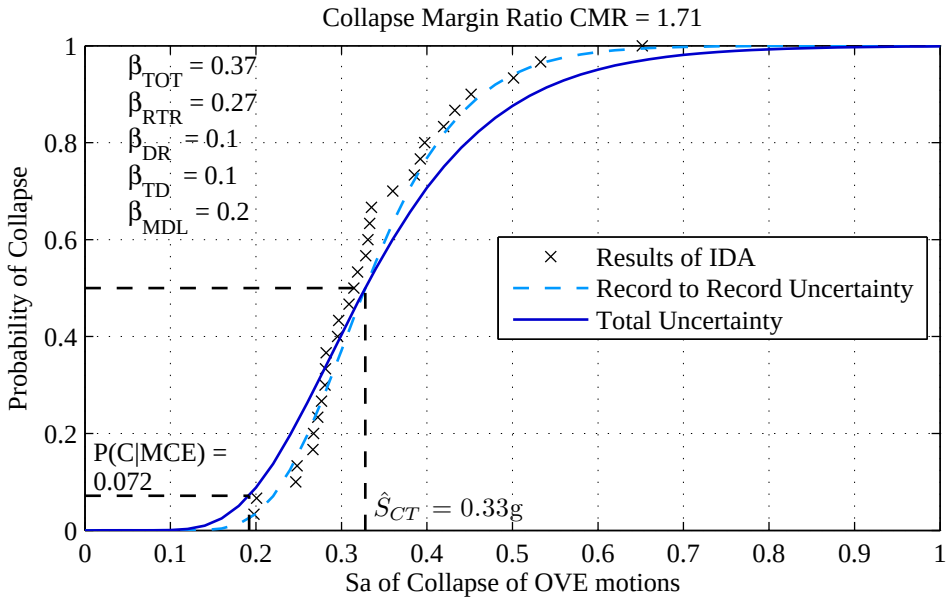

(a) No Adjustment

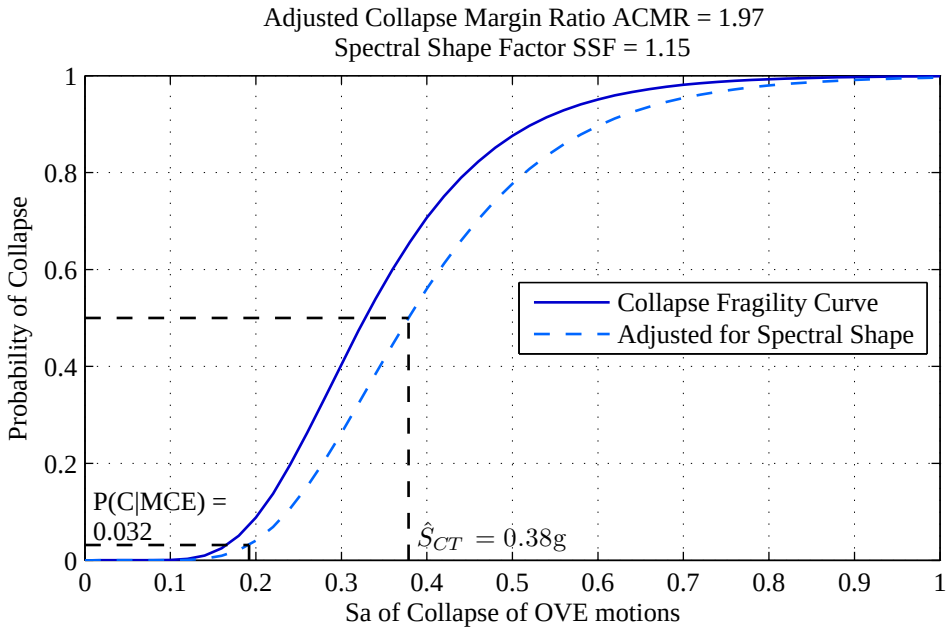

(b) Adjusted for Spectral Shape

Figure 5.17: Fragility Curves for 12-Story, 2.0 SCWB ratio

Table 5.1: Number of Floors Involved in Failure Mechanism - 12-Story Structure

	SCWB Ratio				
Ground Motion	1.2	1.4	1.6	1.8	2.0
1100838	2	2	2	2	2
1100900	1	1	2	2	2
1101155	2	2	2	2	2
1101163	1	2	2	2	2
1101515	1	2	2	2	2
1101546	1	2	2	2	2
1101792	1	2	2	2	2
1102114	2	2	2	2	2
1900001	1	1	2	2	2
1900002	1	1	2	2	2
1900003	1	2	2	2	2
1900004	1	1	2	2	2
1900005	1	1	2	2	2
1900006	1	1	2	2	2
1900007	1	2	2	2	2
2100838	1	2	2	2	2
2100900	1	1	2	2	2
2101155	1	2	2	2	2
2101163	1	2	2	2	2
2101515	1	2	2	2	2
2101546	1	1	1	2	2
2101792	1	2	2	2	2
2102114	1	1	1	2	2
2900001	1	2	2	2	2
2900002	2	2	2	2	2
2900003	1	1	2	2	2
2900004	1	1	2	2	2
2900005	1	2	2	2	2
2900006	1	2	2	2	2
2900007	1	2	2	2	2

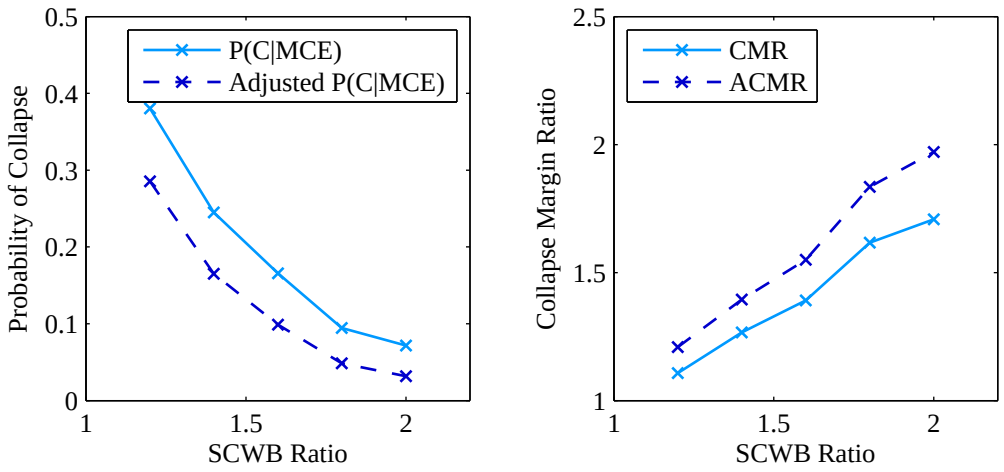

Figure 5.18: Probability of Collapes of 12-Story Structure

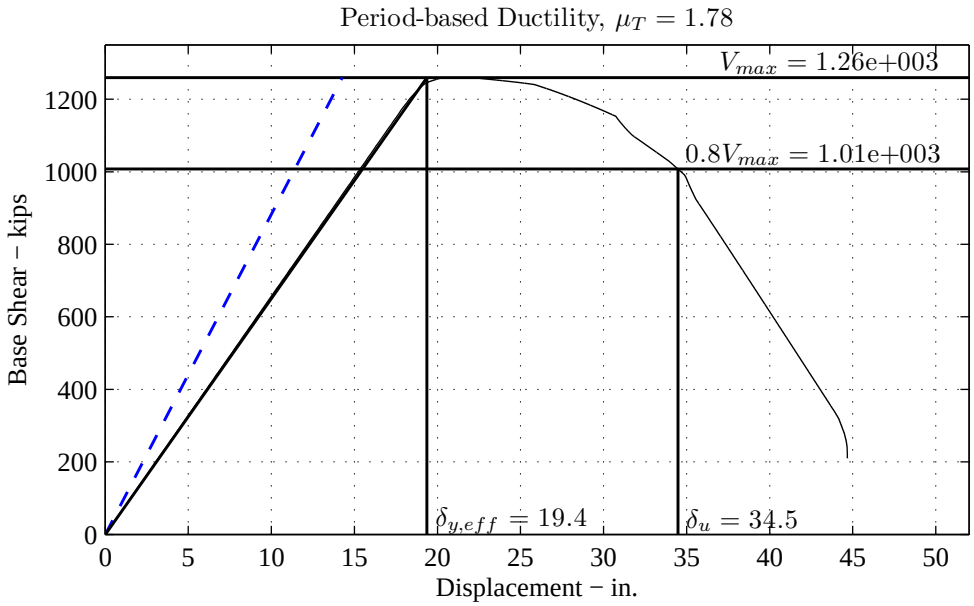

Figure 5.19: Nonlinear Static Pushover 18-Story, 1.2 SCWB Ratio

1.2 to 1.6. Only when the SCWB ratio reaches 1.8 does the mechanism increase by one story. With a SCWB ratio 2.0 the mechanism is not as well defined but appears to develop over five stories.

Figures 5.25 to 5.29 show the fragility curves for the 18-story structure developed from the 30 ground motion incremental dynamic analyses. The probabilities of collapse given a maximum considered earthquake are $P(C|MCE) = 19\%$, 14%, 10%, 7.0%, and 5.2% for SCWB ratios 1.2, 1.4, 1.6, 1.8, and 2.0 respectively. Adjusting for spectral shape, these probabilities become $P(C|MCE) = 11\%$, 6.9%, 4.4%, 2.5%, and 1.6%, respectively. As expected,

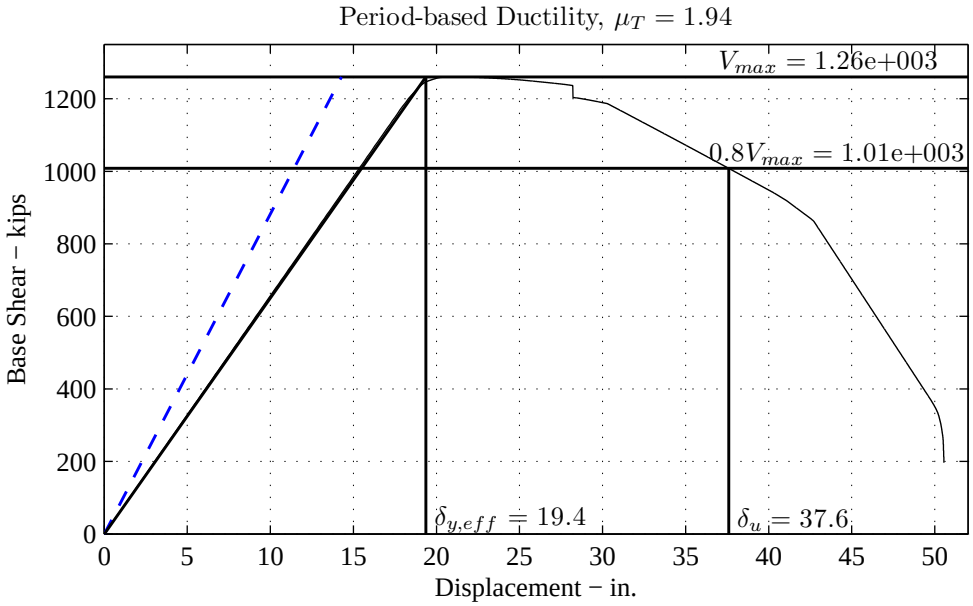

Figure 5.20: Nonlinear Static Pushover 18-Story, 1.4 SCWB Ratio

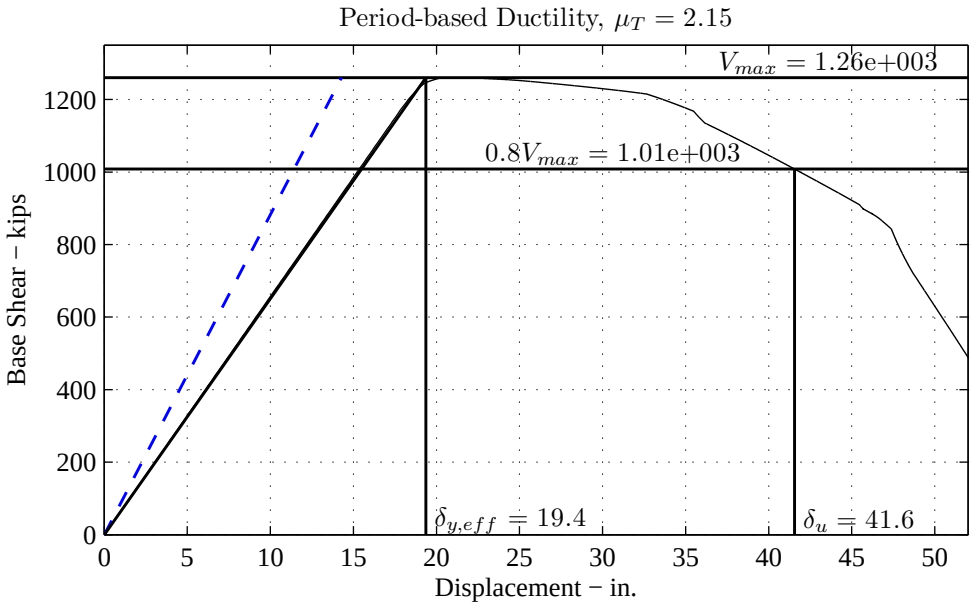

Figure 5.21: Nonlinear Static Pushover 18-Story, 1.6 SCWB Ratio

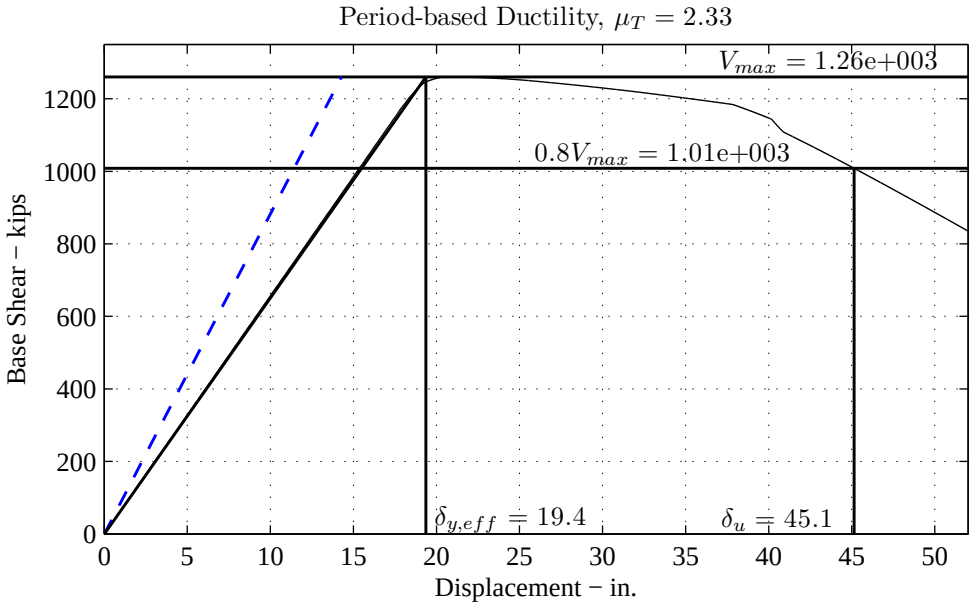

Figure 5.22: Nonlinear Static Pushover 18-Story, 1.8 SCWB Ratio

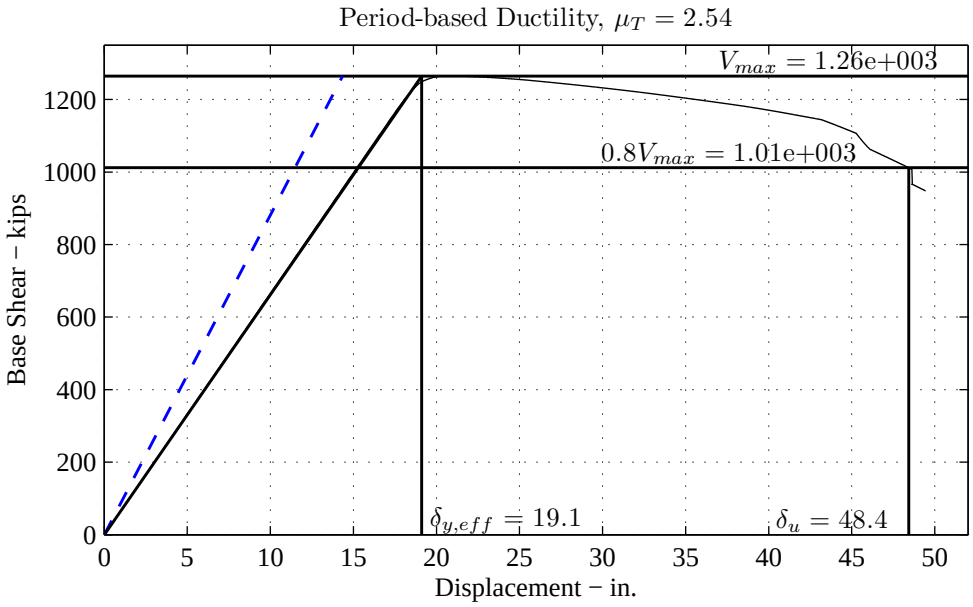

Figure 5.23: Nonlinear Static Pushover 18-Story, 2.0 SCWB Ratio

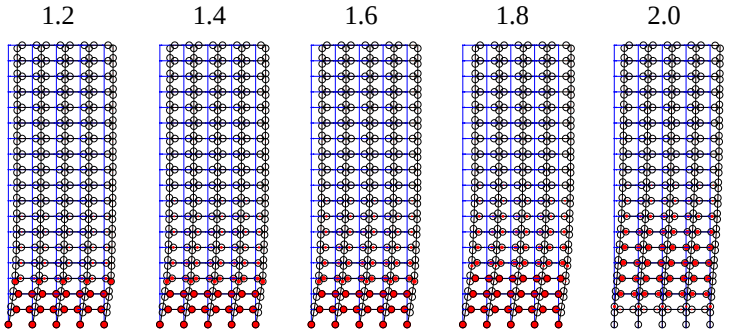

Figure 5.24: Failure Mechanisms from Nonlinear Static Pushover Analyses - 18-Story Structure

increasing the SCWB ratio decreases probability of collapse (Figure 5.30). Increasing the SCWB ratio from 1.2 to 1.4 decreases the probability of collapse by 26%; increasing from 1.4 to 1.6 decreases it by 29%;, increasing from 1.6 to 1.8 decreases it by 30%; and increasing from 1.8 to 2.0 decreases it by 26%. The median spectral acceleration of collapse for each SCWB ratio are $0.23g$, $0.25g$, $0.26g$, $0.28g$, and $0.29g$ for SCWB ratios 1.2, 1.4, 1.6, 1.8, and 2.0 respectively, increasing as the SCWB ratio increases. The adjusted collapse margin ratio (ACMR) also increases as SCWB ratios increase. For the 12-story structure, the ACMR are 1.53, 1.65, 1.77, 1.90, and 2.01 for SCWB ratios 1.2, 1.4, 1.6, 1.8, and 2.0 respectively. The ACMR increases only 7.8% (compared to 15% for the 12-story structure) as the SCWB increases from 1.2 to 1.4, 7.3% from 1.4 to 1.6, 7.3% from 1.6 to 1.8, and 5.8% from 1.8 to 2.0.

Table 5.2 summarizes the results of the failure mechanisms for the 18-story structure. In all but one case the first two stories develop the story failure mechanism for the 1.2 and 1.4 SCWB ratio structures. With a 1.6 SCWB ratio, 17% of the ground motions create a story mechanism that spreads to include the third story; the rest remain at two stories. As the failure mechanism spreads to the third floor, the story mechanism is no longer clearly defined in that an upper column mechanism does not form, though the plastic-hinged beams do not spread to the top of the structure. These ill-defined mechanisms are denoted by the prime in the table. For the 1.8 SCWB ratio structure, 53% of the ground motions produce mechanisms that have spread to incorporate the first three stories. Only 17% of the ground motions produce mechanisms that do not spread, remaining as two-story mechanisms for the 2.0 SCWB ratio structure. As with the 12-story structure, this structure does not prevent partial collapse mechanisms even when the columns are twice as strong as the beams.

With regard to increasing the spread of the mechanism over the height of the structure, no benefit is gained from increasing the SCWB ratio from 1.2 to 1.4. Increasing from 1.4 to 1.6 incorporates an additional story in only 17% of the ground motions. Forty percent of the ground motions develop a mechanism with an additional story when the SCWB ratio is increased from 1.6 to 1.8. Increasing to 2.0 gains an additional story in 27% of the ground motions.

There is one interesting case in this analysis, as denoted by the asterisks in the table, that

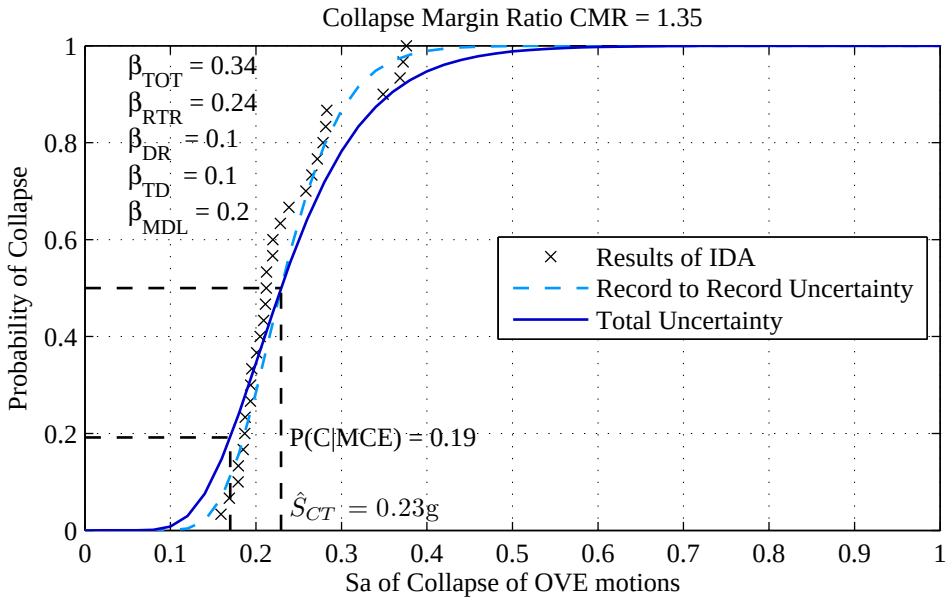

(a) No Adjustment

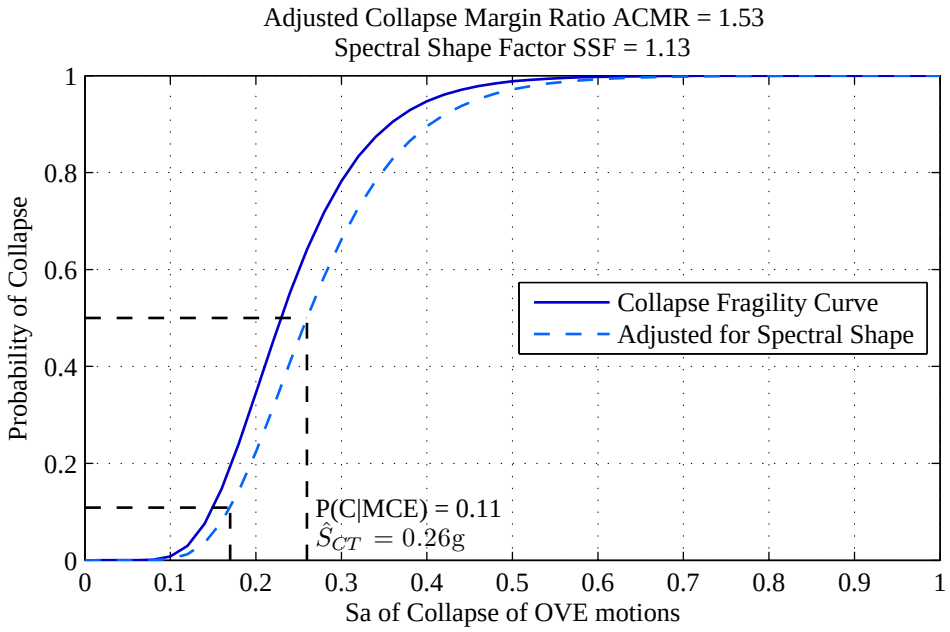

(b) Adjusted for Spectral Shape

Figure 5.25: Fragility Curves for 18-Story, 1.2 SCWB ratio

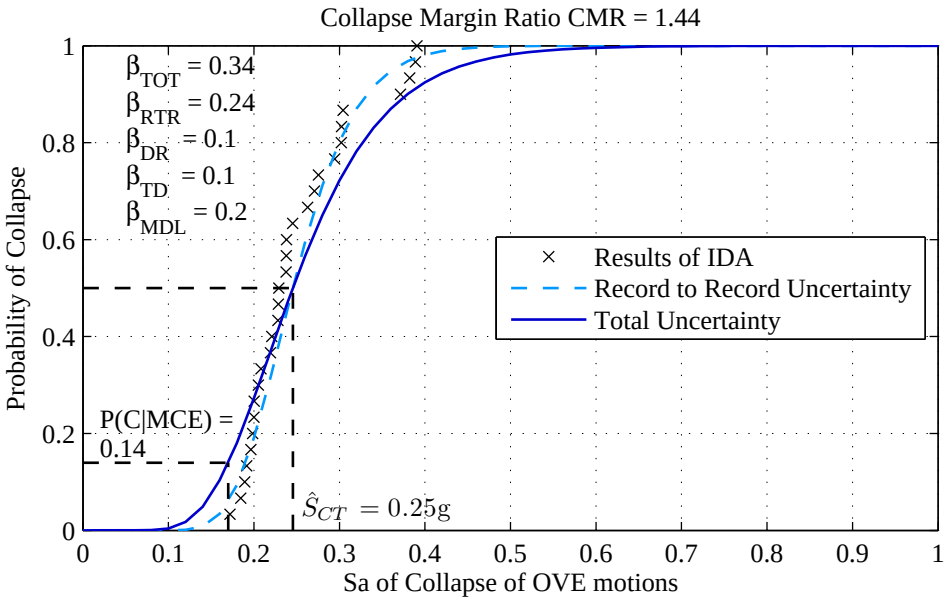

(a) No Adjustment

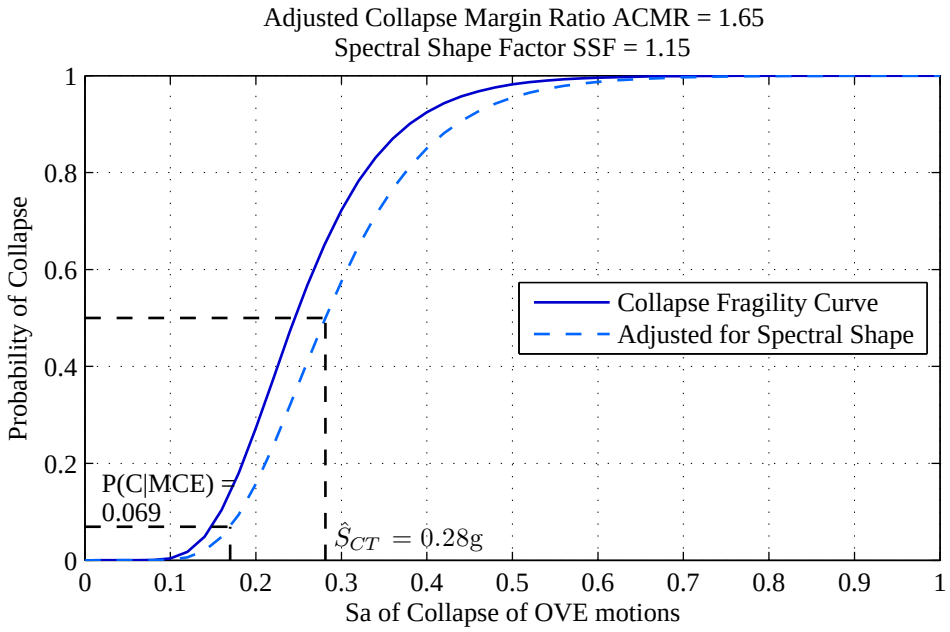

(b) Adjusted for Spectral Shape

Figure 5.26: Fragility Curves for 18-Story, 1.4 SCWB ratio

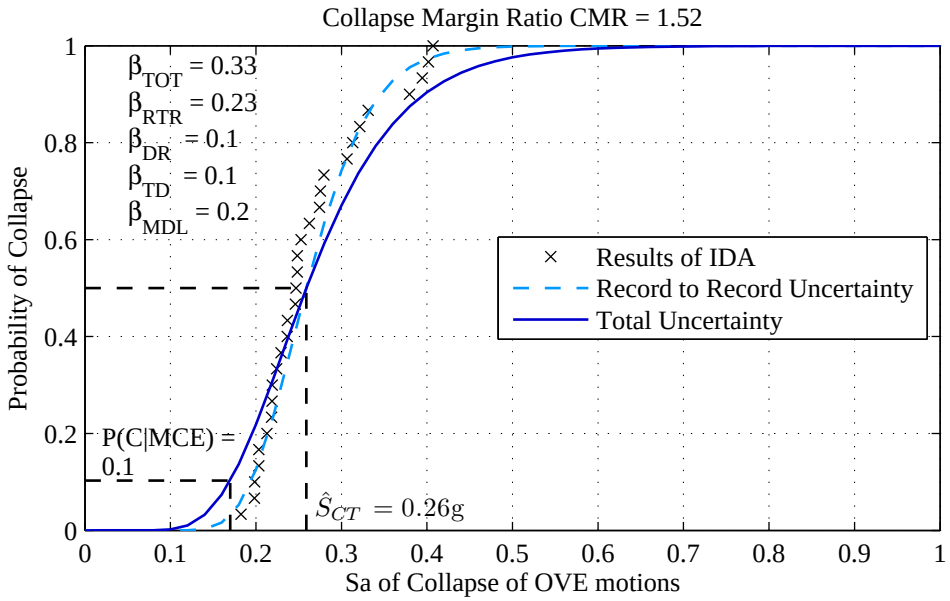

(a) No Adjustment

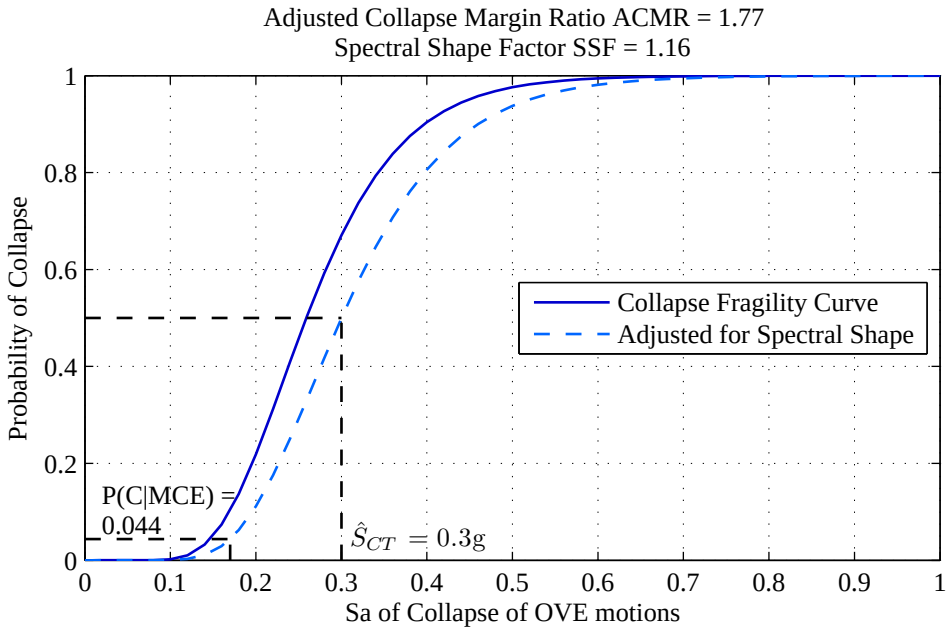

(b) Adjusted for Spectral Shape

Figure 5.27: Fragility Curves for 18-Story, 1.6 SCWB ratio

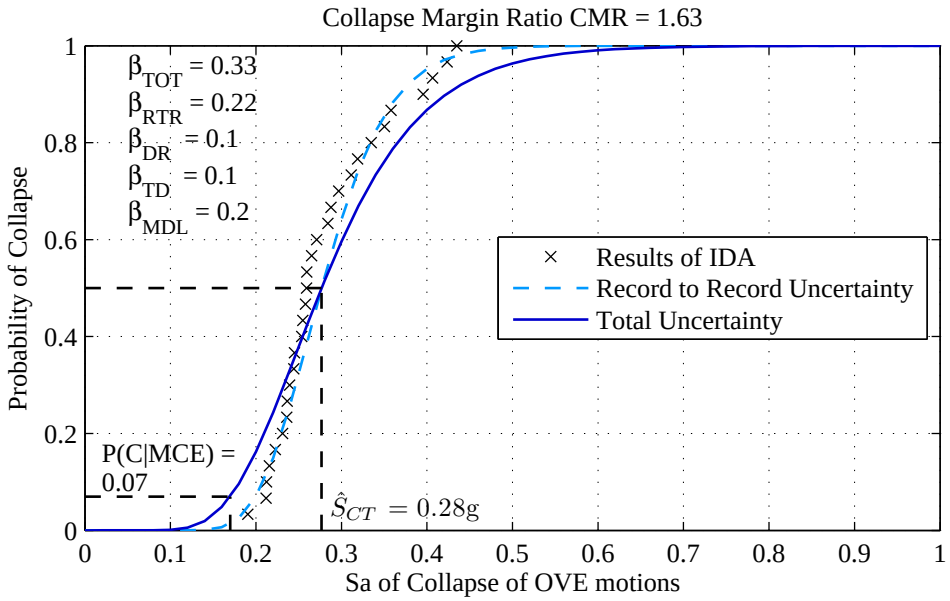

(a) No Adjustment

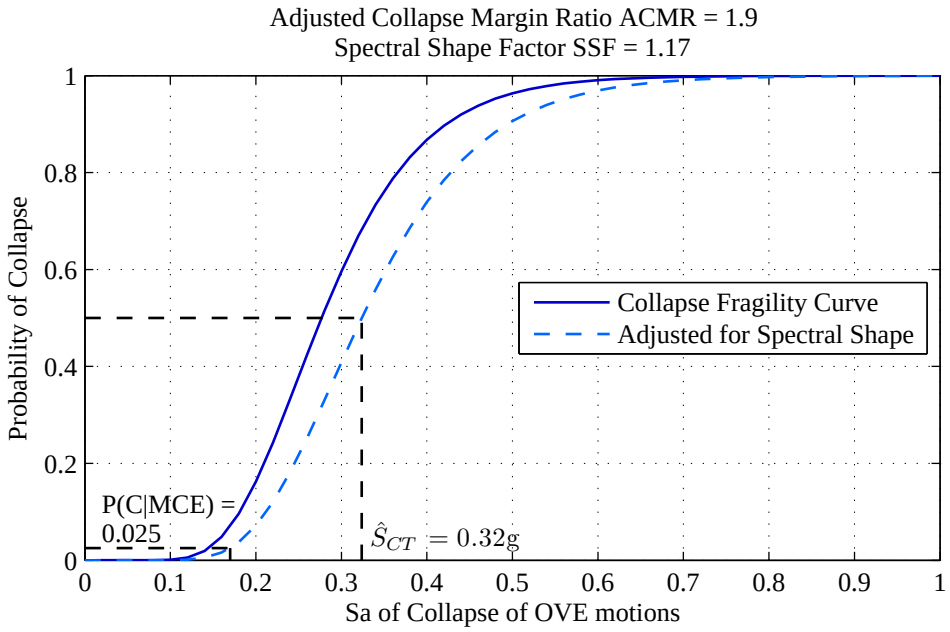

(b) Adjusted for Spectral Shape

Figure 5.28: Fragility Curves for 18-Story, 1.8 SCWB ratio

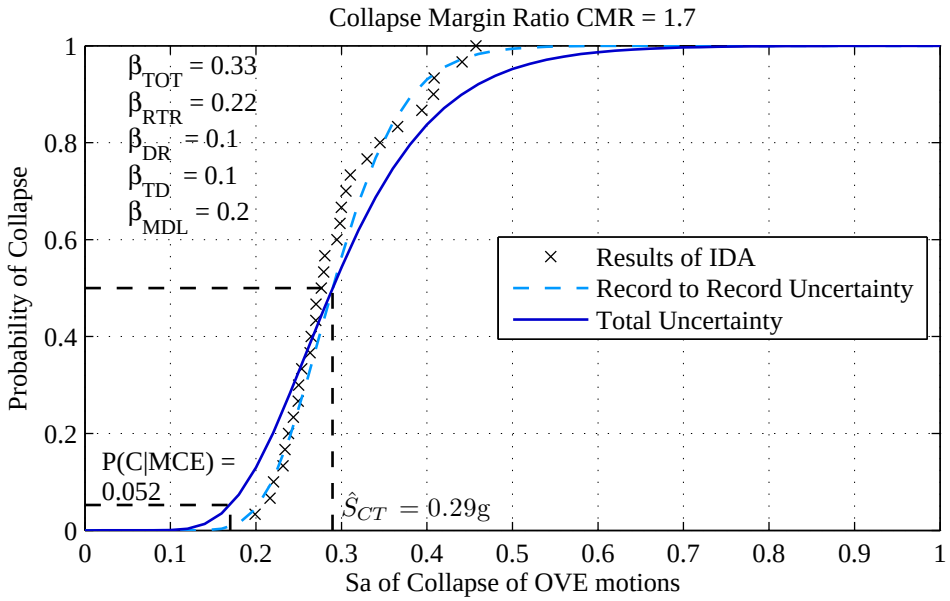

(a) No Adjustment

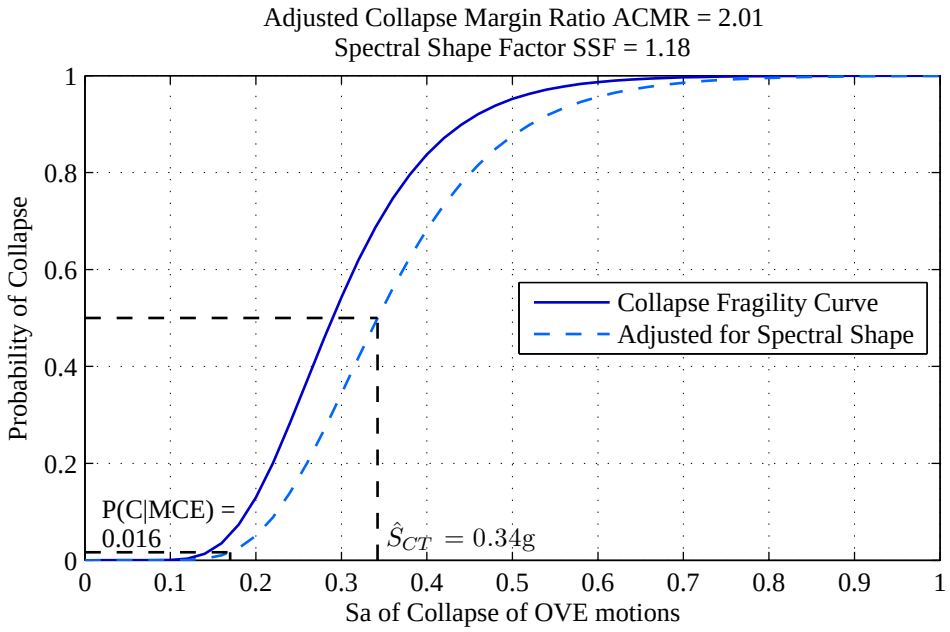

(b) Adjusted for Spectral Shape

Figure 5.29: Fragility Curves for 18-Story, 2.0 SCWB ratio

Table 5.2: Number of Floors Involved in Failure Mechanism - 18-Story Structure

	SCWB Ratio				
Ground Motion	1.2	1.4	1.6	1.8	2.0
1100838	2	2	2	2	2
1100900	2	2	2	3’	3’
1101155	2	2	2	3’	3’
1101163	2	2	2	2	3’
1101515	2	2	2’	3’	3’
1101546	2	2	2	2	3’
1101792	2	2	2	3’	3’
1102114	2	2	2	2	2
1900001	2	2	2	2	3’
1900002	2	2	2	3’	3’
1900003	2	2	2	3’	3’
1900004	2	2	3’	3’	3’
1900005	2	2	2	3’	3’
1900006	2	2	2	2	3’
1900007	2	2	2	2	2
2100838	2	2	2	2	3’
2100900	2	2	2	3’	3’
2101155	2	2	2	2	3’
2101163	2	2	2	3’	3’
2101515	2	2	2	3’	3’
2101546	2	2	2	2	2
2101792	1*	1*	3*	-	8*
2102114	2	2	2	3’	3’
2900001	2	2	2	2	3’
2900002	2	2	3’	3’	3’
2900003	2	2	3’	3’	3’
2900004	2	2	2	2	3’
2900005	2	2	2	2	2
2900006	2	2	3’	3’	3’
2900007	2	2	2	3’	3’

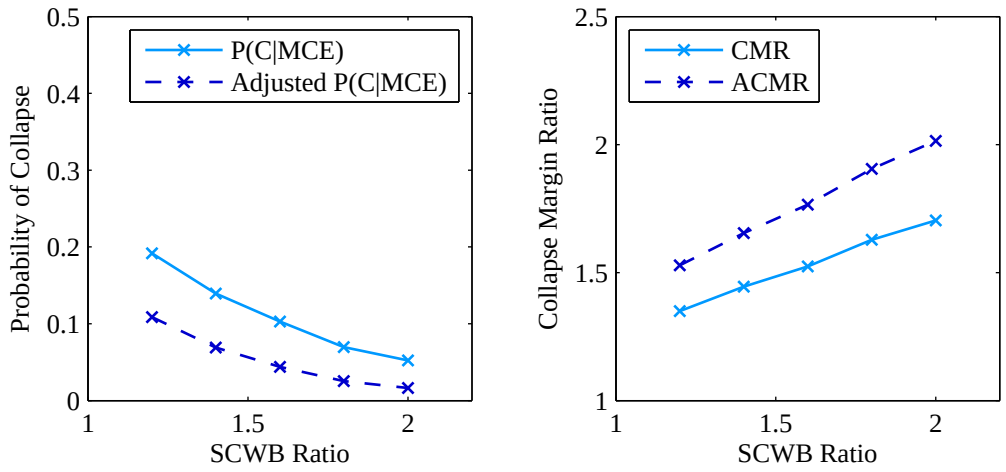

Figure 5.30: Probability of Collapse of 18-Story Structure

does not behave like the others; for this ground motion, the failure mechanisms develop at about two-thirds up the height of the structure, clearly indicating higher modes are influential in this failure.

5.5 24-Story Structures

Figures 5.31 to 5.35 depict the nonlinear static pushover curves of the 24-story structures. The maximum base shear increases from $V_{max} = 1636$ kips for the 1.2 SCWB ratio to $V_{max} = 1750$ kips for the 2.0 SCWB ratio. The design base shear was 1160 kips, again evidence of the overstrength built into design process for these structures. The period based ductility increases from $\mu_T = 1.76$ for the 1.2 SCWB ratio to $\mu_T = 2.34$ for the 2.0 SCWB ratio. The failure mechanisms from these analyses, shown in Figure 5.36, do not occur at the base of the structure, but rather about a third of the way up the structure. This is likely due to the higher SCWB ratios in the lower third of the structure compared to those of the 12- and 18- story structures. One can examine the mean values for a quick comparison. The failure mechanisms for the 1.2, 1.4 and 1.6 SCWB ratios are well defined, incorporating stories eight through twelve, for a total of five stories participating in the mechanism. For the 1.8 SCWB ratio structure, the failure mechanism moves down two floors to incorporate stories six through ten, still only utilizing five stories. The failure mechanism for the 2.0 SCWB structure is similar to that of the 1.8 SCWB structure, but not as well defined.

Figures 5.37 to 5.41 show the fragility curves for the 24-story structure developed from the 30 ground motion incremental dynamic analyses. The probabilities of collapse given a maximum considered earthquake are $P(C|MCE) = 11\%$, 9.7%, 9.1%, 8.6%, and 7.7% for SCWB ratios 1.2, 1.4, 1.6, 1.8, and 2.0 respectively. Adjusting for spectral shape, these probabilities become $P(C|MCE) = 6.0\%$, 4.9%, 4.3%, 3.8%, and 3.2%, respectively. As expected, increasing the SCWB ratio decreases the probability of collapse (Figure 5.42). Increasing the SCWB ratio from 1.2 to 1.4 decreases the probability of collapse by 12%;

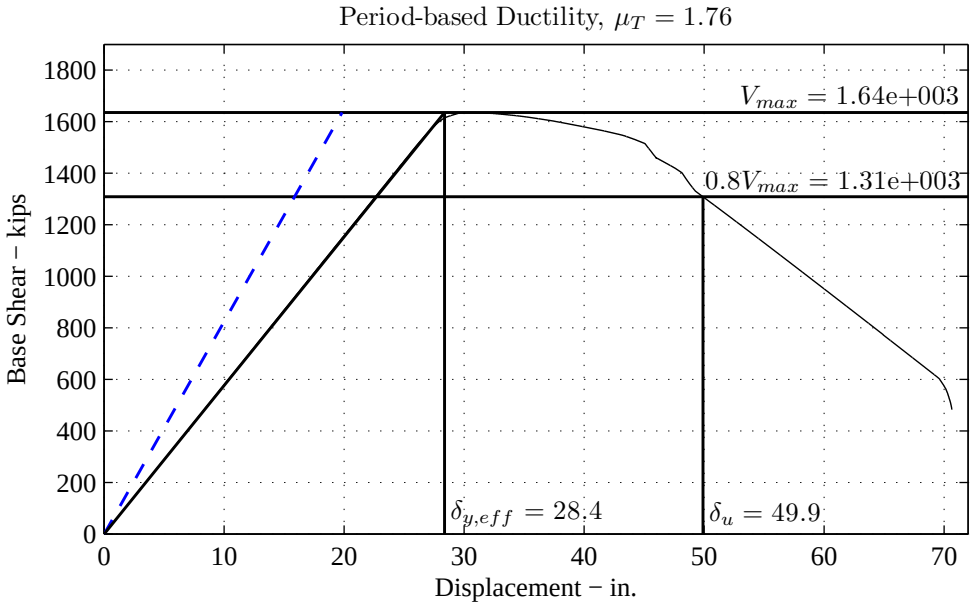

Figure 5.31: Nonlinear Static Pushover 24-Story, 1.2 SCWB Ratio

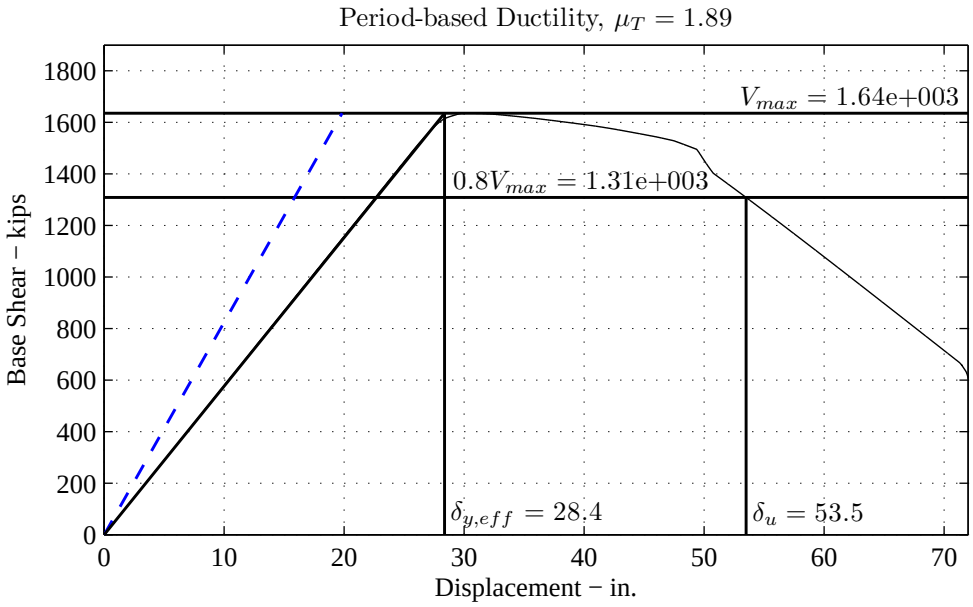

Figure 5.32: Nonlinear Static Pushover 24-Story, 1.4 SCWB Ratio

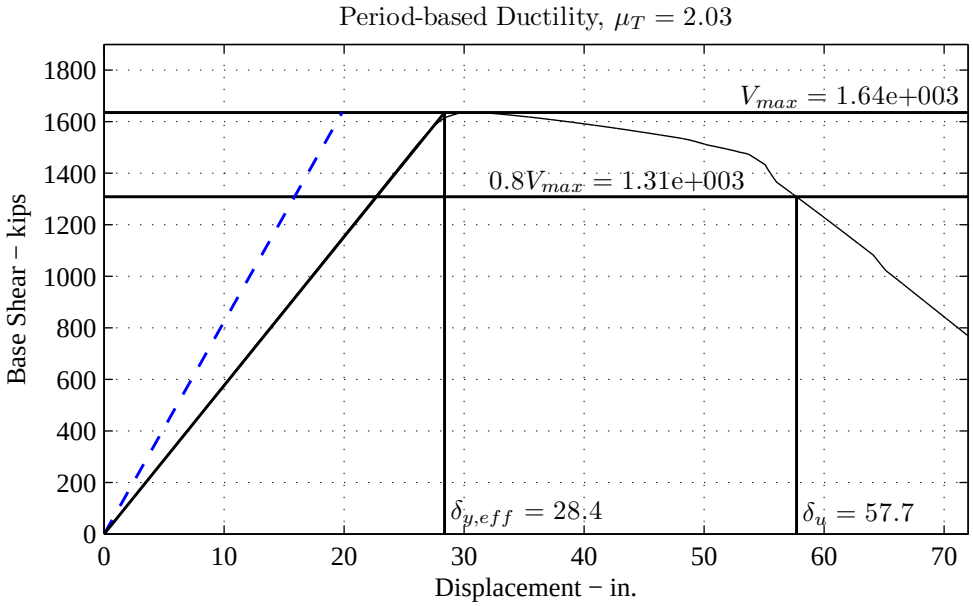

Figure 5.33: Nonlinear Static Pushover 24-Story, 1.6 SCWB Ratio

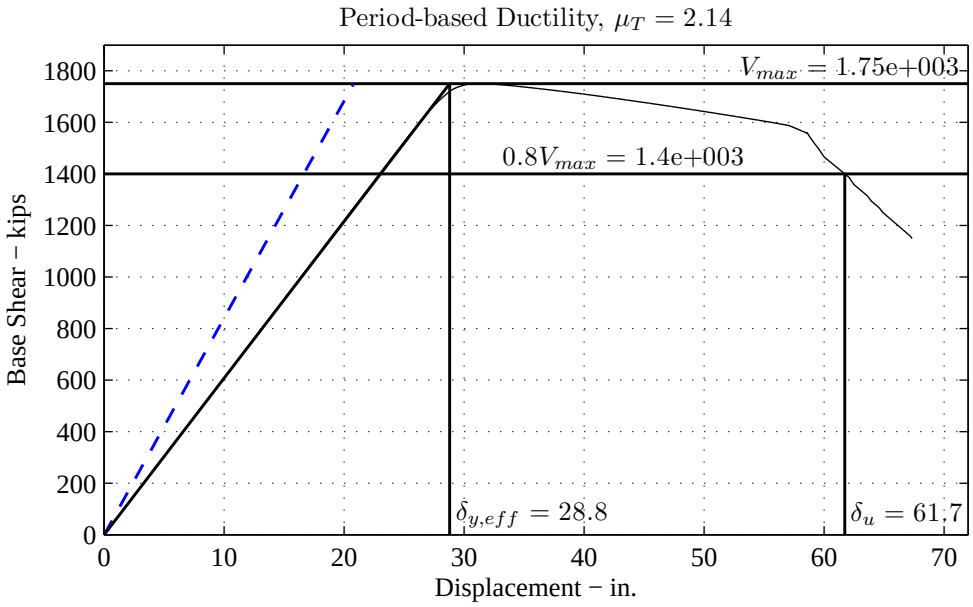

Figure 5.34: Nonlinear Static Pushover 24-Story, 1.8 SCWB Ratio

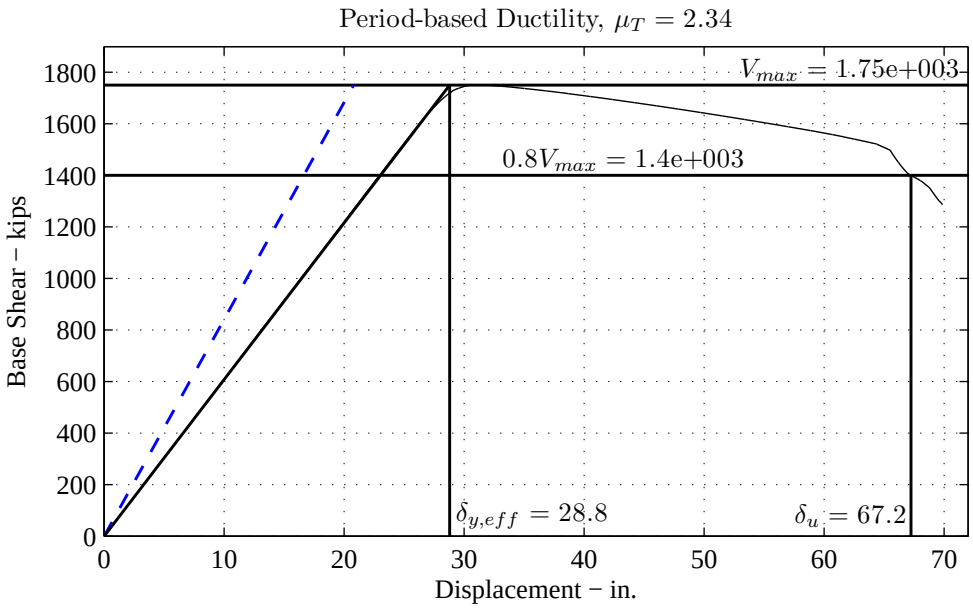

Figure 5.35: Nonlinear Static Pushover 24-Story, 2.0 SCWB Ratio

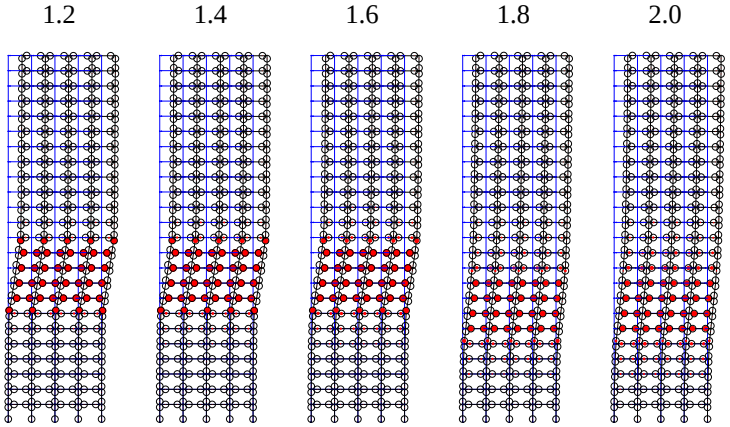

Figure 5.36: Failure Mechanisms from Nonlinear Static Pushover Analyses - 24-Story Structure

increasing from 1.4 to 1.6 decreases it by 6%;, increasing from 1.6 to 1.8 decreases it by 5%; and increasing from 1.8 to 2.0 decreases it by 10%. Compared to the 12-story structure, the 24-story structure does not benefit nearly as much from an increase in SCWB ratios. The median spectral acceleration of collapse for each SCWB ratio are $0.23g$, $0.23g$, $0.24g$, $0.24g$, and $0.25g$, increasing as the SCWB ratio increases, though not as significantly as the previous 18- and 12- story structures. The adjusted collapse margin ratio (ACMR) also increases as SCWB ratios increase. For the 12-story structure, the ACMR are 1.79, 1.84,

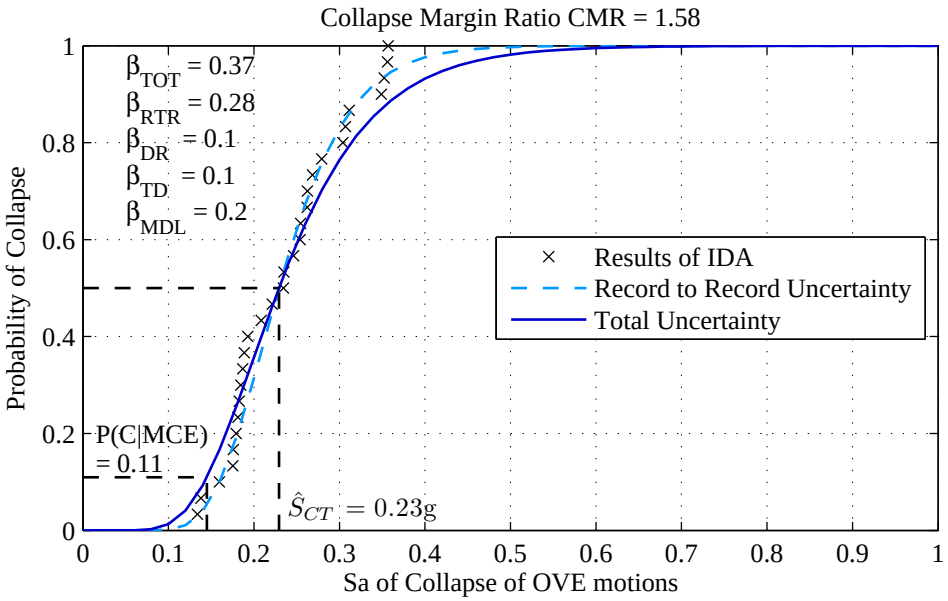

(a) No Adjustment

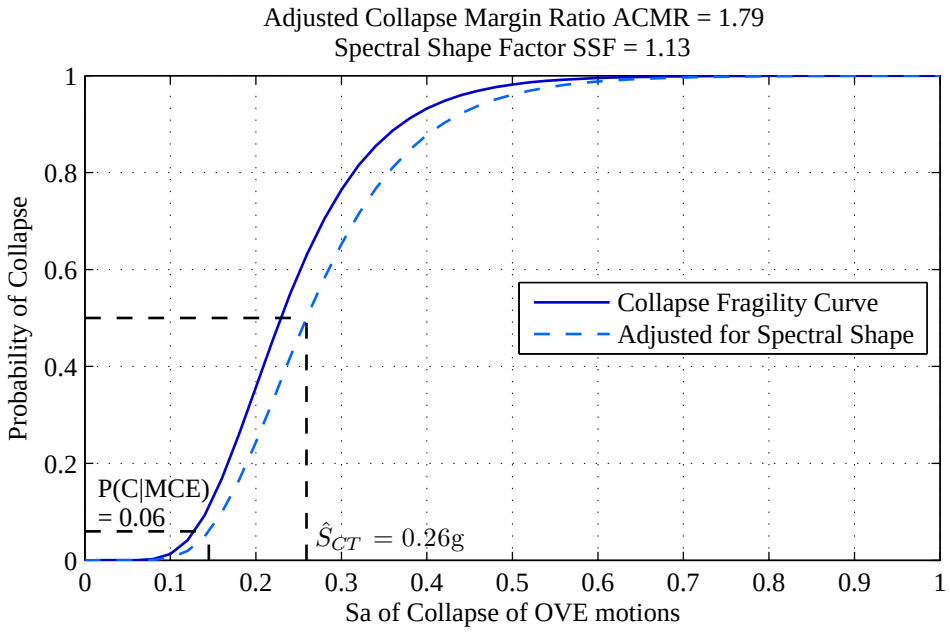

(b) Adjusted for Spectral Shape

Figure 5.37: Fragility Curves for 24-Story, 1.2 SCWB ratio

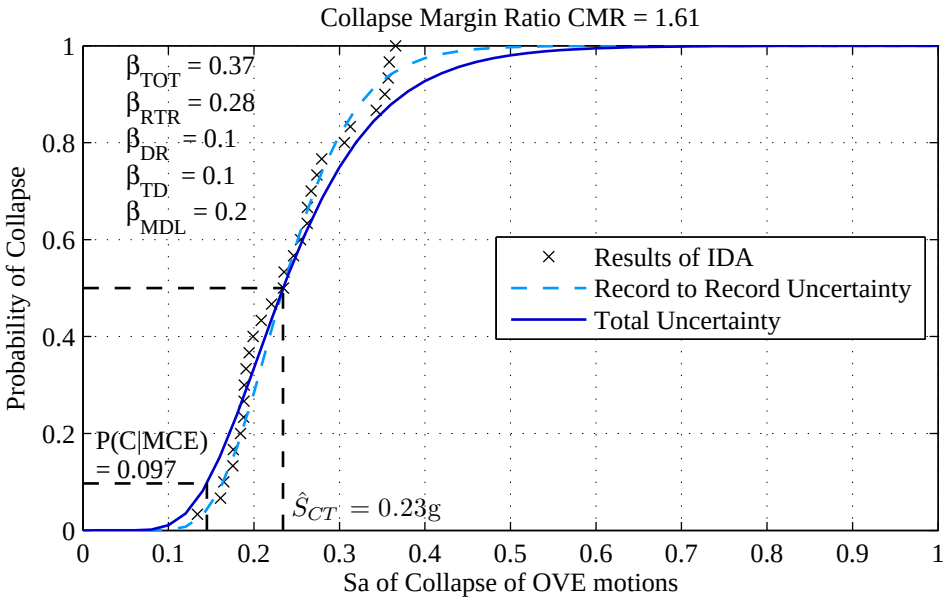

(a) No Adjustment

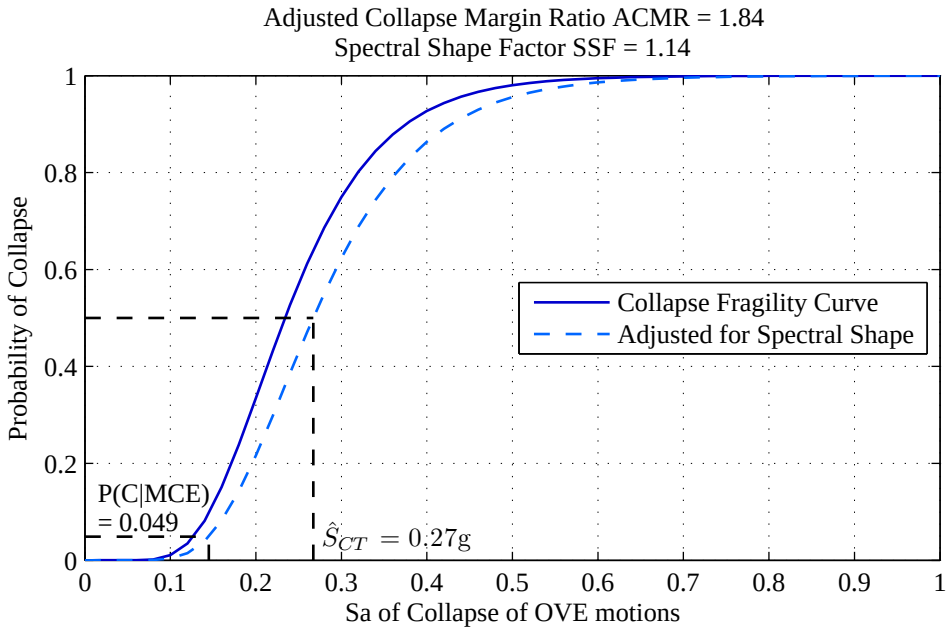

(b) Adjusted for Spectral Shape

Figure 5.38: Fragility Curves for 24-Story, 1.4 SCWB ratio

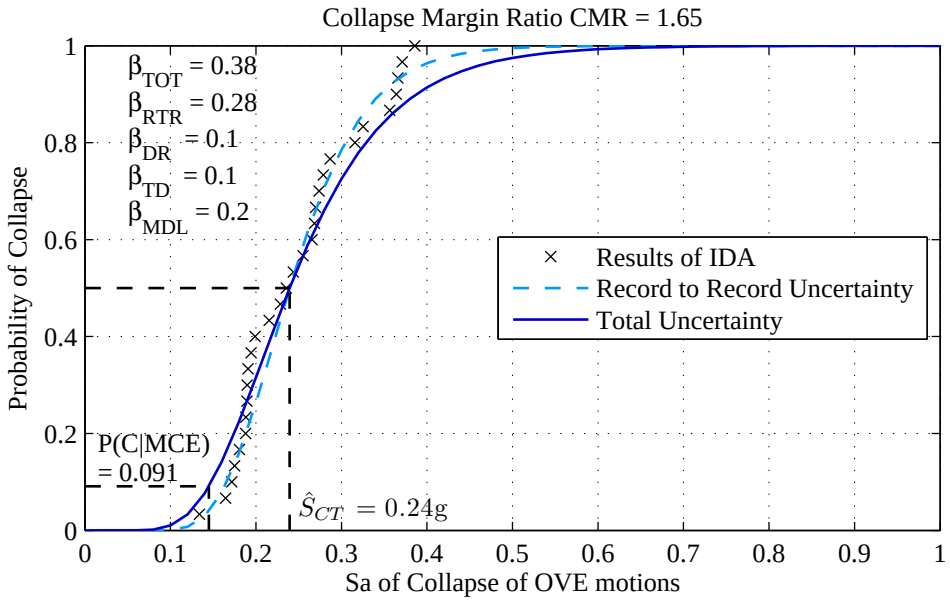

(a) No Adjustment

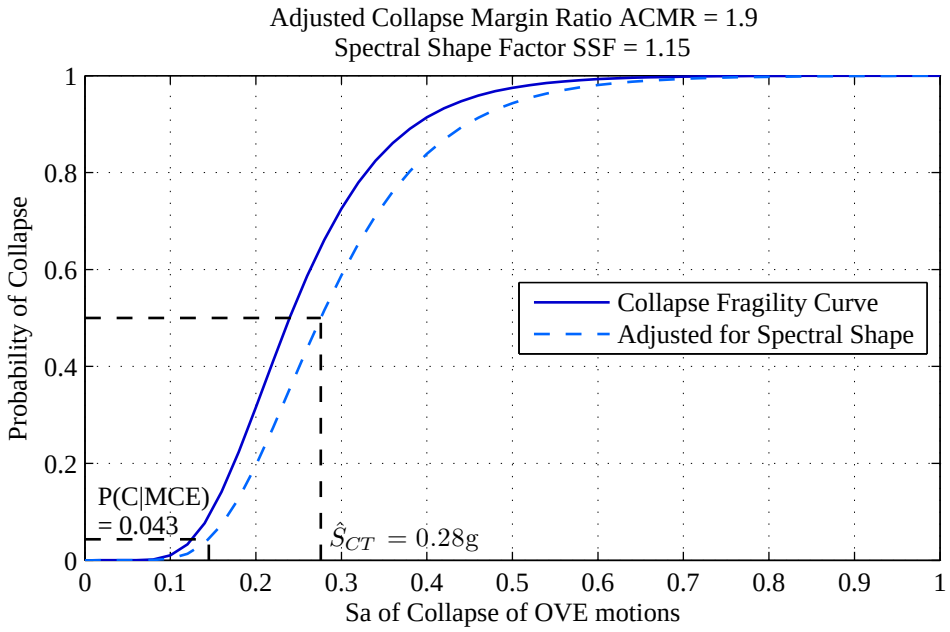

(b) Adjusted for Spectral Shape

Figure 5.39: Fragility Curves for 24-Story, 1.6 SCWB ratio

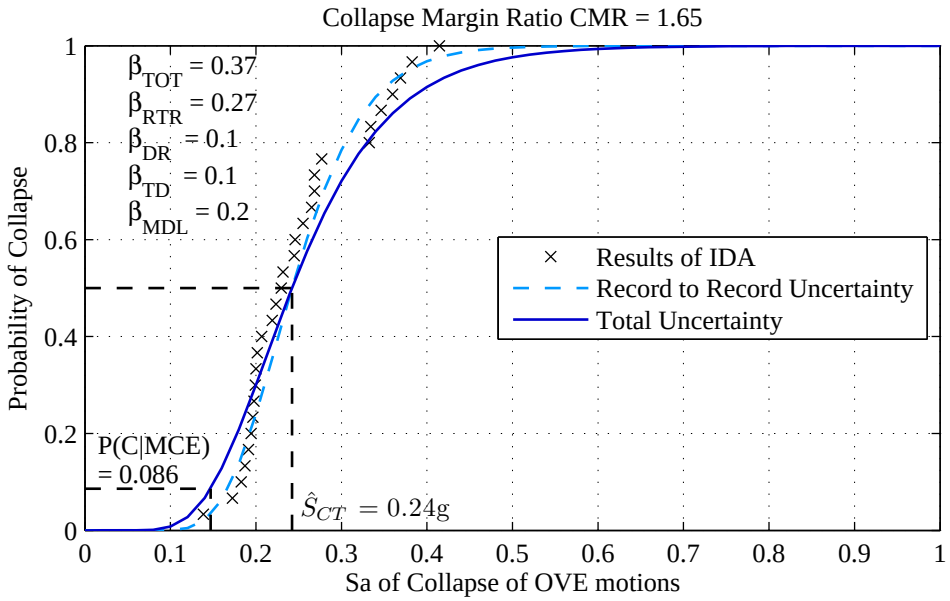

(a) No Adjustment

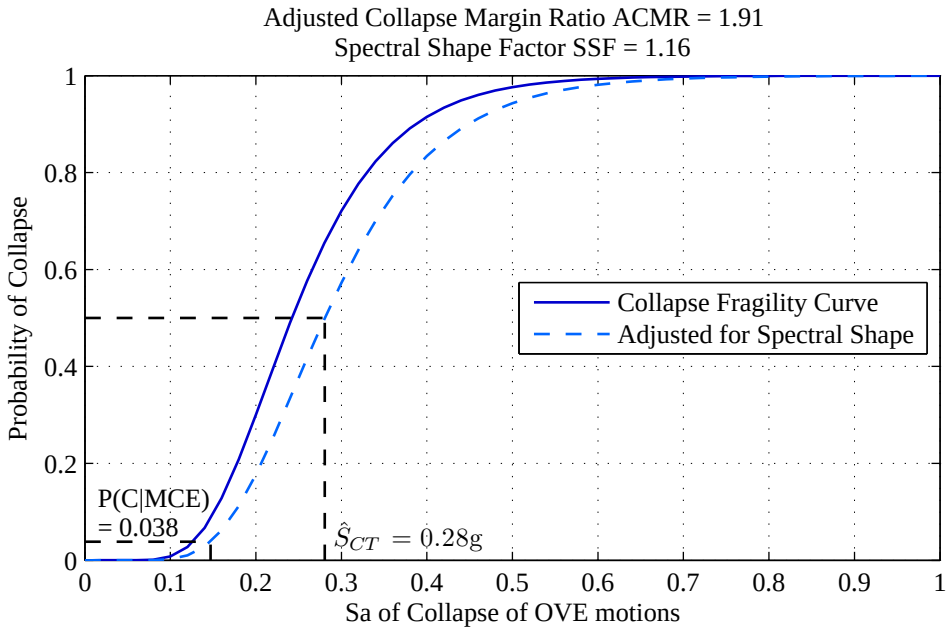

(b) Adjusted for Spectral Shape

Figure 5.40: Fragility Curves for 24-Story, 1.8 SCWB ratio

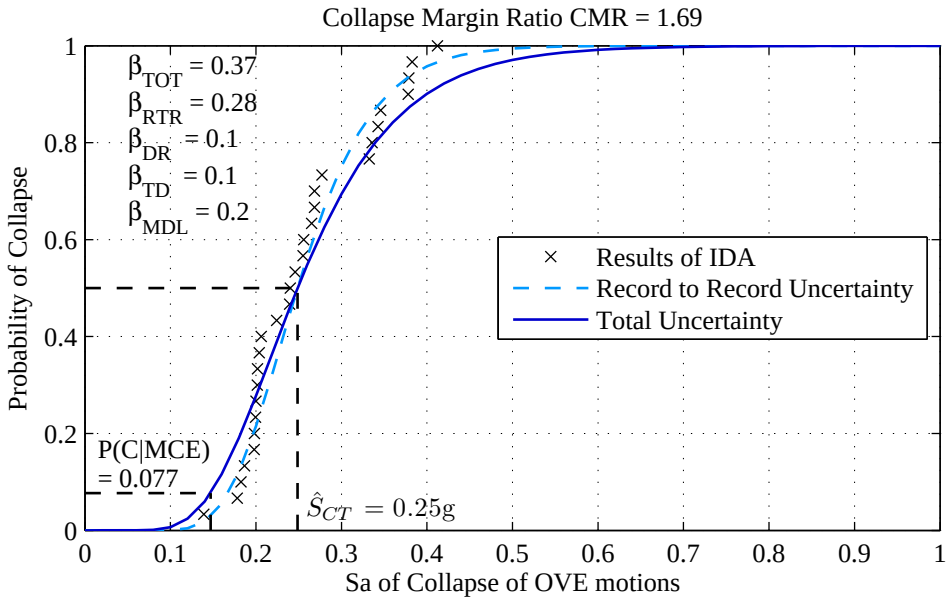

(a) No Adjustment

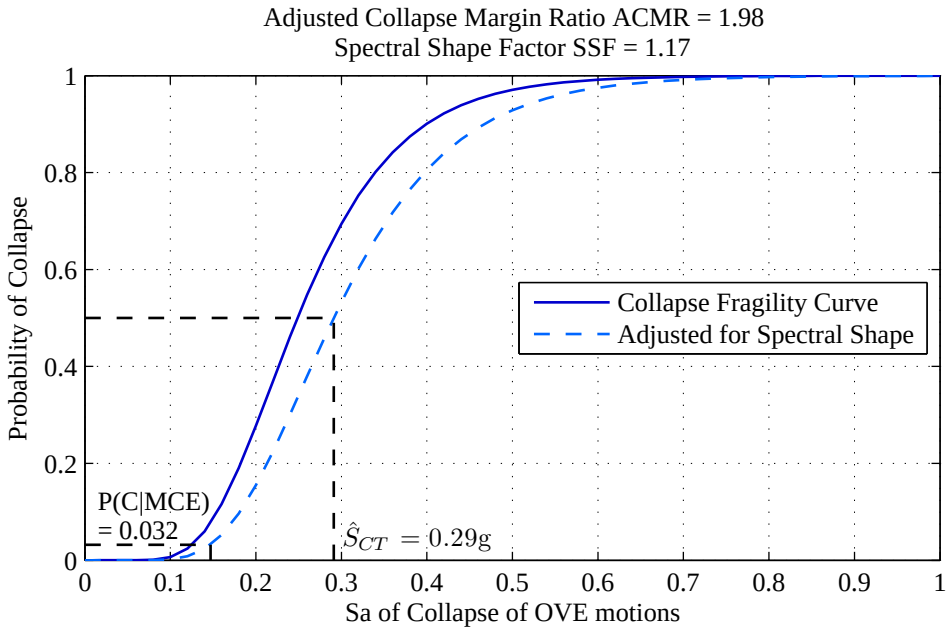

(b) Adjusted for Spectral Shape

Figure 5.41: Fragility Curves for 24-Story, 2.0 SCWB ratio

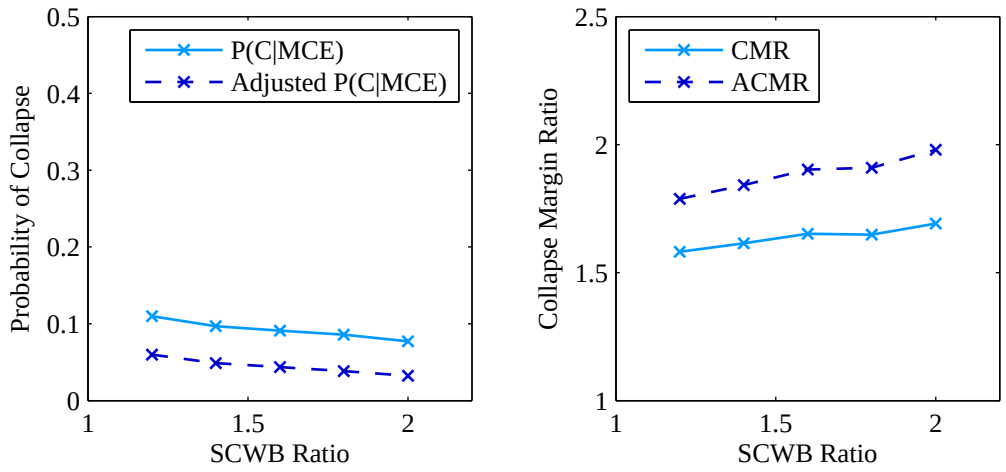

Figure 5.42: Probability of Collapse of 24-Story Structure

1.90, 1.91, and 1.98 for SCWB ratios 1.2, 1.4, 1.6, 1.8, and 2.0 respectively. The ACMR increases only 2.8% (compared to 7.8% for the 18-story structure and 15% for the 12-story structure) as the SCWB increases from 1.2 to 1.4, 3.3% from 1.4 to 1.6, 0.53% from 1.6 to 1.8, and 3.7% from 1.8 to 2.0.

Table 5.3 summarizes the results of the failure mechanisms for the 24-story structure. Most of the mechanisms are not clearly defined and there is no spread of the story mechanism as the SCWB ratio increases. The entries in the table with asterisks are story mechanisms that did not form at the base of the structure: for ground motion 1101546, the mechanisms formed about one-quarter up the height of the structure; for ground motion, 2101792, they occurred about three-quarters up the height of the structure; and for ground motion 2900003, they occurred about two-thirds up the height. This structure indicates there is little gain toward achieving a whole building mechanism by increasing the SCWB ratio.

5.6 Summary of IDA Results

The effects of SCWB ratios on tall structures have been evaluated from two vantage points: from the perspective of the statistical probability of collapse and that of story-mechanism-spread over the height of the structure. Figures 5.43 and 5.44 show the increase in collapse margin ratios and the decrease in the probabilities of collapse given an increase in SCWB ratios for all structures. As the structures increase in height, the benefit gained from increased SCWB ratios decreases. (For the SCWB ratio increase from 1.2 to 1.4 the ACMR increased 15% for the 12-story structure, 7.8% for the 18-story structure and 2.8% for the 24-story structure, and the P(C|MCE) decreased by 41%, 26% and 12% for the 12-, 18- and 24-story structures, respectively.) This may be due in part to the minimum steel reinforcement ratios required by the columns of the taller structures. The columns sizes were determined by the axial load, not the moment demand, so many of the SCWB ratios in the lower columns are greater than the intended SCWB target. With larger than intended SCWB ratios at

Table 5.3: Number of Floors Involved in Failure Mechanism - 24-Story Structure

	SCWB Ratio				
Ground Motion	1.2	1.4	1.6	1.8	2.0
1100838	4	4	4	4	4
1100900	6	6	6	6	6
1101155	4	4	4	4	4
1101163	5	5	5	5	5
1101515	4	4	4	4	4
1101546	3*	4*	4*	6	6
1101792	4	4	4	4	4
1102114	4	4	4	4	4
1900001	5	5	5	5	5
1900002	4	4	4	4	4
1900003	4	4	4	4	4
1900004	4	4	4	4	4
1900005	4	4	4	4	4
1900006	4	4	4	4	4
1900007	6	6	6	6	6
2100838	5	5	5	5	5
2100900	4	4	4	5	5
2101155	4	4	4	4	4
2101163	4	4	4	4	4
2101515	4	4	4	4	4
2101546	4	4	4	4	4
2101792	2*	2*	3*	4	4
2102114	4	4	4	4	4
2900001	5	5	5	5	5
2900002	4	4	4	4	4
2900003	2*	4	4	4	4
2900004	4	4	4	4	4
2900005	4	4	4	4	4
2900006	4	4	4	4	4
2900007	4	4	4	2	4

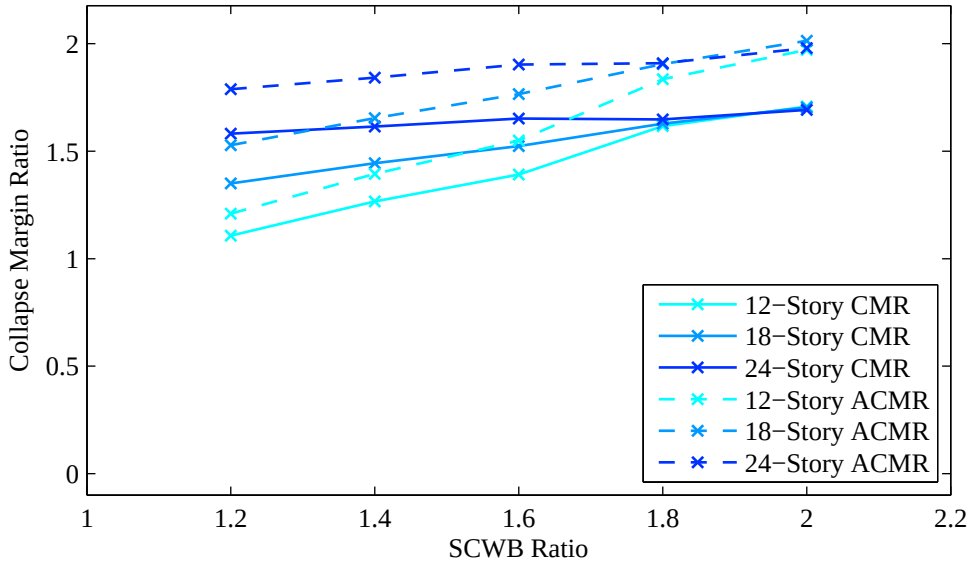

Figure 5.43: Increase in collapse margin ratios (CMR) as SCWB ratios increase

the onset of the design, the moment capacities do not need to be increased to meet the subsequent SCWB ratios, thus the increase in overall capacity is not as significant for those stories, leading to a less significant increase in CMR and decrease in P(C|MCE). Not only does increasing SCWB ratios have less effect on the collapse capacities of taller structures, it has little effect on the failure mechanism that forms. The increase in performance could be attributed to the increase in overall column strength more than an increase in the number of stories (and thus the amount of dissipated energy) involved in the mechanism. If one were to choose an acceptable adjusted P(C|MCE) to be 10% or less, then the 12-story structure would require a 1.6 SCWB ratio, the 18-story structure would require a 1.4 SCWB ratio, and the 24-story structure would require a 1.2 SCWB ratio. It may be that the SCWB ratio should be dependent upon the height of the structure. These conclusions are subject to the assumption, among others, that the gravity framing contributes inertial mass and gravity loads but does not provide any lateral force resistance.

Although increasing SCWB ratios in the taller structures in this study did not have a significant impact on the performance of the structures, the taller structures have lower collapse capacities than the 12-story structure from the outset. For a given SCWB ratio as the height of the structures increase from 12 stories, P(C|MCE) decreases. This is consistent with the findings of Haselton et al. (2011) and suggests that higher SCWB ratios and full building mechanisms may not be necessary for the satisfactory performance of tall structures. This increase in performance may be due in part to the reinforcement ratios needed to meet the minimum requirements as well as the minimum base shear code requirements that the taller structures must meet. The design of the 12-story structure was not controlled by the minimum base shear, whereas the two taller structures were.

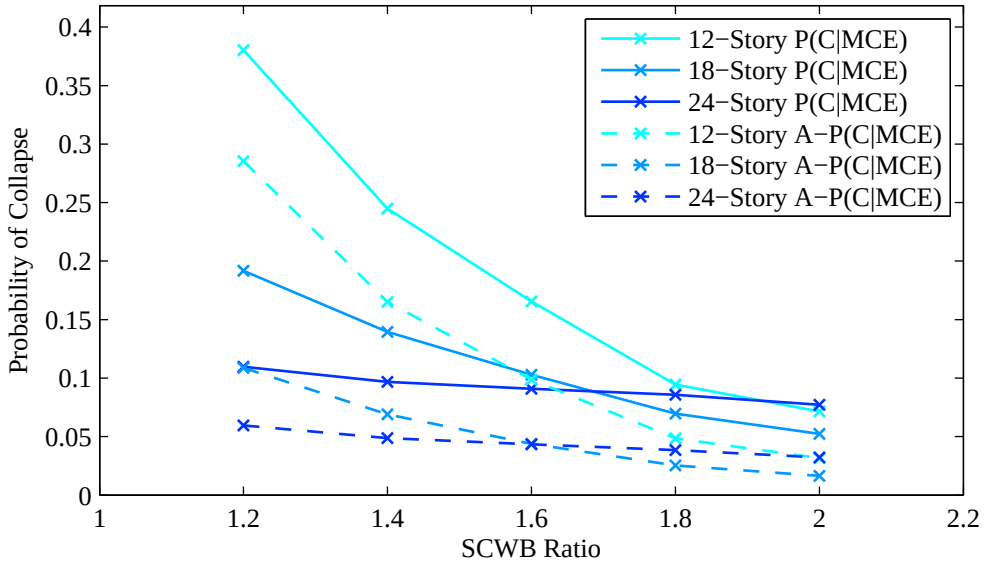

Figure 5.44: Decrease in probablity of collapse, $P(C|MCE)$, as SCWB ratios increase

5.7 Rigid Plastic Analysis of the 12- and 18-Story Structures

The ability of the two definitions of the SCWB ratio presented in this study to measure the performance of a structure are evaluated though rigid plastic analyses of three variations of the 12-story, 1.2 SCWB ratio structure. All three variations of the structure have identical SCWB ratios as calculated by the alternate method. The moments in the columns, however, are adjusted such that SCWB ratios as defined at each joint vary from one structure to the next. These moments are assumed to be plastic moment capacities. Each building is then analyzed using the upper bound theorem of plastic analysis. A collapse mechanism is assumed to have formed from the base of the structure to the n^{th} floor. A collapse load factor (λ_{cn}) for an inverted triangular load over the height of the structure is obtained from the principal of virtual work given the assumed collapse mechanism and the moment capacities of each member. The load factors for each assumed collapse mechanism are shown in figure 5.45, 5.46 and 5.47. The load factors are displayed on the floors that correspond to the highest floor involved in the associated mechanism. Though the SCWB ratios as defined by the code at each joint varies from one building to the next, the collapse load factors, λ_{cn}, do not. That the load factor, λ_{cn} does not change implies that the collapse mechanism remains the same from one variation of the building to the next. The alternate method of calculating the SCWB ratios appears to be a better measure of performance as it remains stable and consistent with the collapse mechanism.

The rigid plastic analysis is also used in an attempt to predict the number of stories in a partial collapse mechanism. Figure 5.48 shows an example of a frame set-up with N stories for use in the plastic analysis. An inverted triangular load is applied to the frame; a story mechanism, and the corresponding plastic hinging, is assumed to have formed consisting

Ext Col	Int Col	Beam	λ_c
7055	7410	5203	12697
7602	9489	7000	12367
8148	10485	8325	12081
8695	12108	9460	11882
9242	13076	10489	11720
9788	14469	11434	11623
10335	15082	12305	11541
10881	16442	13159	11520
11428	17121	13977	11484
11974	18148	14651	11481
12521	17963	14990	11431
19545	14819	13697	12854

(a) Moments amd Collapse Load Factors

Calculated Per ACI 318					Alternate Method
1.36	0.71	0.71	0.71	1.36	0.87
2.09	1.21	1.21	1.21	2.09	0.78
1.89	1.20	1.20	1.20	1.89	0.72
1.78	1.19	1.19	1.19	1.78	0.71
1.71	1.20	1.20	1.20	1.71	0.69
1.66	1.20	1.20	1.20	1.66	0.69
1.64	1.20	1.20	1.20	1.64	0.67
1.61	1.20	1.20	1.20	1.61	0.68
1.60	1.20	1.20	1.20	1.60	0.66
1.60	1.20	1.20	1.20	1.60	0.67
1.63	1.20	1.20	1.20	1.63	0.66
2.34	1.20	1.20	1.20	2.34	0.76

(b) SCWB Ratios

Figure 5.45: Moments, collapse load factors (λ_c) and SCWB ratios for a variation of the 12-story, 1.2 SCWB ratio structure

of stories one to n; an initial displacement at the onset of the formation of the collapse mechanism is also assumed. The leaning column contributes the $P-\Delta$ forces that the frame is required to resist, $H_i = \frac{P_i * \Delta}{\sum_0^i h}$. The force at level n is given as:

$$H_n = \frac{\sum_n^N P_i * \Delta}{\sum_0^n h} \tag{5.1}$$

These forces are a function of the displacement and require integration over the displacement δ to obtain the virtual work. The external and internal work are then calculated to solve for the collapse factor, λ_c. The external work is composed of the virtual work done by the external forces, λF, and the resisting forces, H_i, through an additional small horizontal displacement, δ. The internal work is the virtual work done by the moments through the

Ext Col	Int Col	Beam	λ_c
8467	6469	5203	12697
9122	8476	7000	12367
9778	9398	8325	12081
10434	10948	9460	11882
11090	11844	10489	11720
11746	13164	11434	11623
12401	13704	12305	11541
13057	14991	13159	11520
13713	15597	13977	11484
14369	16551	14651	11481
15025	16293	14990	11431
23454	12213	13697	12854

(a) Moments amd Collapse Load Factors

Calculated Per ACI 318					Alternate Method
1.63	0.62	0.62	0.62	1.63	0.87
2.51	1.07	1.07	1.07	2.51	0.78
2.27	1.07	1.07	1.07	2.27	0.72
2.14	1.08	1.08	1.08	2.14	0.71
2.05	1.09	1.09	1.09	2.05	0.69
2.00	1.09	1.09	1.09	2.00	0.69
1.96	1.09	1.09	1.09	1.96	0.67
1.93	1.09	1.09	1.09	1.93	0.68
1.92	1.09	1.09	1.09	1.92	0.66
1.92	1.10	1.10	1.10	1.92	0.67
1.96	1.10	1.10	1.10	1.96	0.66
2.81	1.04	1.04	1.04	2.81	0.76

(b) SCWB Ratios

Figure 5.46: Moments, collapse load factors (λ_c) and SCWB ratios for a variation of the 12-story, 1.2 SCWB ratio structure

additional rotations of the hinges as a result of δ. The assumed number of stories involved, n, is varied from 1 to N, and the smallest collapse load factor, λ, obtained should then indicate the collapse mechanism of the structure.

The above analysis is performed on the 12- and 18-story structures. The analysis predicts that the 12-story structure will form a one-story mechanism for all SCWB ratios examined in this study. From the nonlinear static pushover analysis, the 12-story structure is shown to develop a collapse mechanism consisting of the first two floors for all five SCWB ratios. The plastic analysis predicts that the 18-story structure will form a two-story mechanism for all SCWB ratios. From the pushover analysis, the 18-story structure is shown to develop a three-story mechanism for SCWB ratios 1.2, 1.4 and 1.6, a four-story mechanism for SCWB ratio 1.8 and possibly a five-story mechanism for the SCWB ratio 2.0. The rigid plastic analysis is not able to predict the mechanism because the structures are only forming partial collapse mechanisms. This results in a substantial portion of the structure remaining indeterminate and requiring assumptions about displacements at the onset of the collapse mechanism.

Ext Col	Int Col	Beam	λ_c
5644	8351	5203	12697
6082	10503	7000	12367
6519	11571	8325	12081
6956	13267	9460	11882
7393	14308	10489	11720
7830	15774	11434	11623
8268	16460	12305	11541
8705	17893	13159	11520
9142	18645	13977	11484
9579	19745	14651	11481
10016	19632	14990	11431
15636	17425	13697	12854

(a) Moments amd Collapse Load Factors

Calculated Per ACI 318					Alternate Method
1.08	0.80	0.80	0.80	1.08	0.87
1.68	1.35	1.35	1.35	1.68	0.78
1.51	1.33	1.33	1.33	1.51	0.72
1.42	1.31	1.31	1.31	1.42	0.71
1.37	1.31	1.31	1.31	1.37	0.69
1.33	1.32	1.32	1.32	1.33	0.69
1.31	1.31	1.31	1.31	1.31	0.67
1.29	1.31	1.31	1.31	1.29	0.68
1.28	1.31	1.31	1.31	1.28	0.66
1.28	1.31	1.31	1.31	1.28	0.67
1.31	1.31	1.31	1.31	1.31	0.66
1.87	1.35	1.35	1.35	1.87	0.76

(b) SCWB Ratios

Figure 5.47: Moments, collapse load factors (λ_c) and SCWB ratios for a variation of the 12-story, 1.2 SCWB ratio structure

The rigid plastic analysis assumes no deformations in the floors above the mechanism, but in reality there would be varying levels of elastic and inelastic deformations increasing the $P-\Delta$ effect. This analysis also does not account for strain-hardening that is accounted for in the nonlinear static pushover analysis. For these reasons, it is expected that the rigid plastic analysis would not be able to predict the collapse mechanism. The rigid plastic analysis does, however, support the finding that increasing the SCWB ratios does little to increase the number of stories involved in the mechanism.

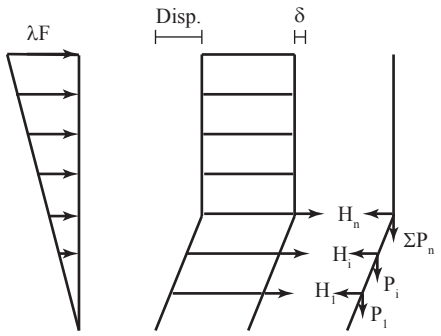

Figure 5.48: A sketch of a plastic analysis set-up

Chapter 6

Conclusion

6.1 Summary

The goal of this study was to examine the effects of strong-column, weak-beam ratios on tall reinforced concrete special moment frame structures. Fifteen structures were modelled in Opensees: three heights (12, 18 and 24 stories) each at five SCWB ratios (1.2, 1.4, 1.6, 1.8, and 2.0). These structures were developed from a single floor plan: a perimeter reinforced concrete moment-resisting-frame structure with two four-bay frames in each direction. Any lateral resistance provided by the gravity framing was neglected. This design was selected so that this study could build on work done by Haselton and Deierlein (2008). The moment-rotation relationship was defined for zero-length springs at the ends of the columns and beams by employing the ModIMKPeakOreinted material developed by Fardis and Haselton, (Fardis & Biskinis, 2003; Haselton, Liel, et al., 2008). Having done so, the peak rotations at the ends of the elements could then be recorded. A nonlinear static analysis as well as an incremental dynamic analysis using 30 ground motions were performed on each structure. From the results of the IDA, fragility curves were obtained using the maximum likelihood method. Thus the probability of collapse given a maximum credible event, P(C|MCE), of each structure was obtained.

These conclusions are subject to the assumption, among others, that the gravity framing contributes inertial mass and gravity loads but does not provide any lateral force resistance. For all structures P(C|MCE) decreased as SCWB ratios increased. The 12-story structure saw the most dramatic decrease; as the structures increased in height, the benefit of increasing the SCWB ratios decreased. For a given SCWB ratio, however, the taller structures have a lower probability of collapse. This is consistent with the findings of Haselton et al. (2011) and suggests that higher SCWB ratios and full building mechanisms may not be necessary for the satisfactory performance of tall structures. Plots of the story mechanisms formed by each ground motion show the ineffectiveness of increasing SCWB ratios. Though some mechanisms spread by a story or two as SCWB ratios increase, none come close to creating a complete building mechanism. The required SCWB ratios needed for full building mechanisms would not be practical for the project sponsor.

An evaluation of the effectiveness of SCWB ratio definitions through rigid plastic analyses leads to a conclusion that the alternate method as defined in this study provides a more stable

and consistent measure of performance of a given structures.

6.2 Future Research Possibilities

Several assumptions and simplifications were made to reduce the complexity of the model, thus allowing for it to run within a reasonable time. As access to and capabilities of super computers improve, the complexity of the numerical model of the structure could be increased. Among the changes that could be made: modelling the structure in three dimensions as opposed to the current two-dimensional model with a leaning column, implementing a more complex joint model, modelling the change in axial forces in the columns, and modelling distributed loads on the beams. Another option might be to change the column reinforcement ratios at the mid-point of the column, which would be a more realistic representation of current building codes. This was not done in this study so as to reduce the number of required elements, thus increasing the efficiency of the analyses. Though not related to the efficiency of the model, but rather the efficiency of the design process, a more precise design of the structure utilizing the complete moment-axial diagram could be done.

The model for the reinforced concrete moment-rotation relationship was calibrated conservatively, due to the small number of monotonic tests and small deformation levels reached; increasing the database of such tests could improve the model (Haselton & Deierlein, 2008). The material model used to implement the moment-rotation relationship, ModIMKPeakOriented, has been updated since the onset of this study. Using the most recent version, or updating it further if needed, could improve the efficiency and stability of the analyses.

It may also be beneficial to study variations on the buildings. This study looked at a specific site in Los Angeles, specifically one classified as far-field, soil class C. Other types of soil class sites could be studied as well as near-field sites. Only one floor plan was considered in this study; it would be interesting to study taller buildings with wider bases to reduce the influence the axial forces have on the column reinforcement ratios and thus the SCWB ratios. As has been suggested by a few sources (NZS:3101, 2006; Haselton et al., 2011), varying the SCWB ratio over the height of the structure could be an area of further investigation.

As mentioned previously, this study agrees with others (Haselton et al., 2011) that P(C|MCE) appears to peak in structures around 12 stories tall. Further research could focus on structures eight to 16 stories tall to examine this critical height, possibly determining if SCWB ratios should be height or period dependent.

Lastly, one could explore the discrepancy between the code-defined fundamental period and the fundamental period obtained from the numerical model.

References

ACI Committee 318. (2008). *Building Code Requirements for Structural Concrete (318-08) and Commentary.* American Concrete Institute, Farmington Hills, MI.

ACI Committee 318. (2014). *Building Code Requirements for Structural Concrete (318-14).* American Concrete Institute, Farmington Hills, MI.

Altoontash, A. (2004). *Simulation and Damage Models for Performance Assessment of Reinforced Concrete Beam-Column Joints.* Unpublished doctoral dissertation, Stanford University.

American Society of Civil Engineers. (2006). *Minimum Design Loads for Buildings and Other Structures.*

Ang, A. H., & Tang, W. H. (1973). *Probability Concepts in Engineering Planning and Design* (Vol. 1). New York: John Wiley and Sons.

Applied Technology Council. (2009). *Quantification of Building Seismic Performance Factors - FEMA P695.* 201 Redwood Shores Parkway, Suite 240, Redwood City, CA 94065.

Baker, J. W., & Cornell, C. A. (2006). Spectral shape, epsilon and record selection. *Earthquake Engineering and Structural Dynamics*, *35*, 1077–1095.

Building Seismic Safety Council of the National Institute of Building Sciences. (2009). *Research Needs Identified During Development of the 2009 NEHRP Recommended Seismic Provisions for New Buildings and Other Structures.*

Canadian Standards Association. (2004). *Design of Concrete Structures.* 5060 Spectrum Way, Suite 100, Mississauga, Ontario, Canada L4W 5N6.

Concrete Design Committee P 3101. (2006). *New Zealand Standard - Concrete Structures Standard.* Standards New Zealand, Private Bag 2439, Wellington 6140: Standards New Zealand.

Dooley, K. L., & Bracci, J. M. (2001, November – December). Seismic Evaluation of Column-to-Beam Strength Ratios in Reinforced Concrete Frames. *ACI Structural Journal*, *98*(6), 843–851.

Durrani, A. J., & Wight, J. K. (1985, May–June). Behavior of Interior Beam-to-Column Connections Under Earthquake-Type Loading. *ACI Journal*(82-30), 343–349.

Elwood, K. J., & Eberhard, M. O. (2009, July-August). Effective Stiffness of Reinforced Concrete Columns. *ACI Structural Journal*, *106*(4).

Elwood, K. J., Matamoros, A. B., Wallace, J. W., Lehman, D. E., Heintz, J. A., Mitchell, A. D., et al. (2007, August). Update to ASCE/SEI 41 Concrete Provisions. *Earthquake Spectra*, *23*(3), 493-523.

European Committee for Standardization. (2004). *Eurocode 8: Design of structures for earthquake resistance – Part 1: General rules, seismic actions and rules for buildings.*

Fardis, M. N., & Biskinis, D. E. (2003, September). *Deformation Capacity of RC Members, as Controlled by Flexure or Shear.* International Symposium Honoring Shunsuke Otani.

Fardis, M. N., & Biskinis, D. E. (2010). *Deformations at flexural yielding of members with continuous or lap-spliced bars.* (Unpublished)

Fardis, M. N., & Pinto, P. E. (2007, July). *Guidelines for Displacement-based Design of Buildings and Bridges* (Tech. Rep. No. 2007/05). LESSLOSS.

Federal Emergency Management Agency. (2000). *Prestandard and Commentary for the Seismic Rehabilitation of Buildings*. ASCE, 1801 Alexander Bell Drive, Virginia, 20191.

Haselton, C. B., & Deierlein, G. G. (2008, February). *Assessing Seismic Collapse Safety of Modern Reinforced Concrete Moment-Frame Buildings* (Tech. Rep. No. PEER 2007/08). Pacific Earthquake Engineering Research Center.

Haselton, C. B., Goulet, C. A., Mitrani-Reiser, J., Beck, J. L., Deierlein, G. G., Porter, K. A., et al. (2008, August). *An Assessment to Benchmark the Seismic Performance of a Code-Conforming Reinforced Concrete Moment-Frame Building* (Tech. Rep. No. PEER 2007/12). Pacific Earthquake Engineering Research Center.

Haselton, C. B., Liel, A. B., Deierlein, G. G., Dean, B. S., , & Chou, J. H. (2011, April). Seismic Collapse Safety of Reinforced Concrete Buildings. 1:Assessment of Ductile Moment Frames. *Jouranl of Structural Engineering*, *137*(4), 481–491.

Haselton, C. B., Liel, A. B., Lange, S. T., & Deierlein, G. G. (2008, May). *Beam-Column Element Model Calibrated for Predicting Flexural Response Leading to Global Collapse of RC Frame Buildings* (Tech. Rep. No. PEER 2007/03). Pacific Earthquake Engineering Research Center.

Ibarra, L. F., & Krawinkler, H. (2005, September). *Global Collapse of Frame Structures under Seismic Excitation* (Tech. Rep. No. PEER 2005/06). Pacific Earthquake Engineering Research Center.

Ibarra, L. F., Medina, R. A., & Krawinkler, H. (2005, June). Hysteretic models that incorporate strength and stiffness deterioration. *Earthquake Engineering and Structural Dynamics*, *34*, 1489-1511.

Joint ACI-ASCE Committee 352. (2002). *Recommendations for Design of Beam-Column Connections in Monolithic Reinforced Concrete Structures* (Tech. Rep.). American Concrete Institute, P.O. Box 9094, Farmington Hills, MI 48333-9094: American Concrete Institute.

Kuntz, G. L., & Browning, J. (2003, September – October). Reduction of Column Yielding During Earthquakes for Reinforced Concrete Frames. *ACI Structural Journal*, *100*(5), 573–580.

Lignos, D. G., & Krawinkler, H. (2012, August). Development and Utilization of Structural Component Databases for Performance-Based Earthquake Engineering. *Journal of Structural Engineering*, *doi:10.1061/(ASCE)ST.1943-541X.0000646*.

McKenna, F., Fenves, G. L., Scott, M. H., & Jeremić, B. (2000). *Open System for Earthquake Engineering Simulation.* http://opensees.berkeley.edu/.

Moehle, J., Bozorgnia, Y., Jayaram, N., Jones, P., Rahnama, M., Shome, N., et al. (2011). *Case Studies of the Seismic Performance of Tall Buildings Designed by Alternative Means* (Tech. Rep. No. PEER 2011/05). Pacific Earthquake Engineering Research Center.

Panagiotakos, T. B., & Farids, M. N. (2001, March-April). Deformations of Reinforced Concrete Members at Yielding and Ultimate. *ACI Structural Journal*, *98*(2).

Paulay, T., & Priestley, M. J. N. (1992). *Seismic Design of Reinforced Concrete and Masonry Buildings*. John Wiley and Sons, Inc.

SEAOC Seismology Committee. (2008, September). Reinforced concrete structures [Computer software manual]. Structural Engineers Associaton of California, Sacramento, CA. (Accessible via the world wide web at:

http://www.seaoc.org/bluebook/index.html)

Shome, N. (1999). *Probabilistic Seismic Demand Analysis of Nonlinear Structures*. Unpublished doctoral dissertation, Stanford University.

Vamvatsikos, D., & Cornell, C. A. (2002). Incremental Dynamic Analysis. *Earthquake Engineering and Structural Dynamics*, *31*, 491–514.

Zareian, F., & Medina, R. A. (2010). A practical method for proper modeling of structural damping in inelastic plane structural systems. *Computers and Structures*.

Appendix A

Failure Mechanisms

A.1 12-Story Building

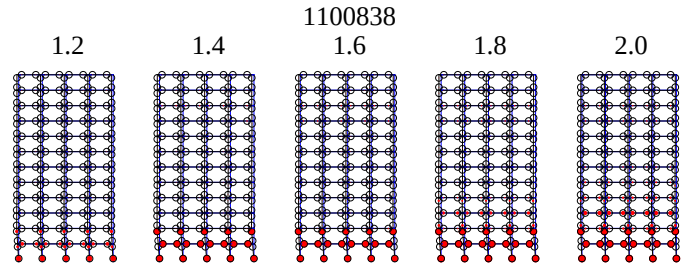

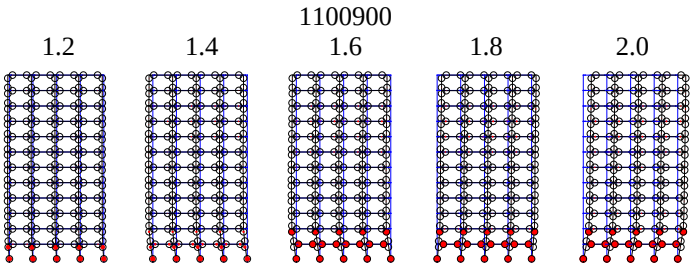

1101155

1.2 1.4 1.6 1.8 2.0

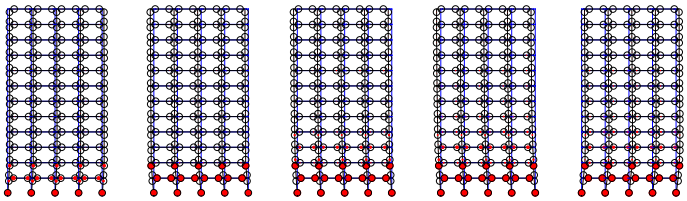

1101163

1.2 1.4 1.6 1.8 2.0

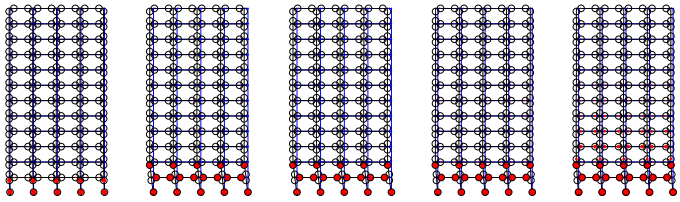

1101515

1.2 1.4 1.6 1.8 2.0

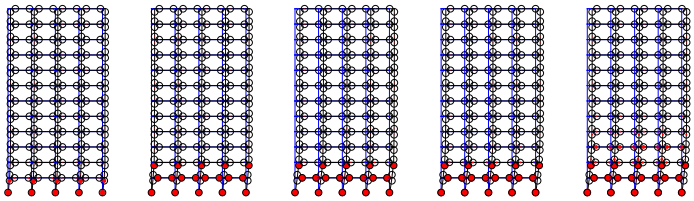

1101546

1.2 1.4 1.6 1.8 2.0

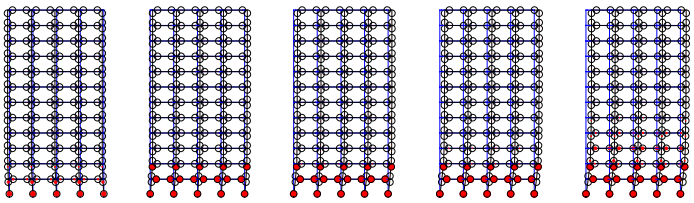

1101792

1.2 1.4 1.6 1.8 2.0

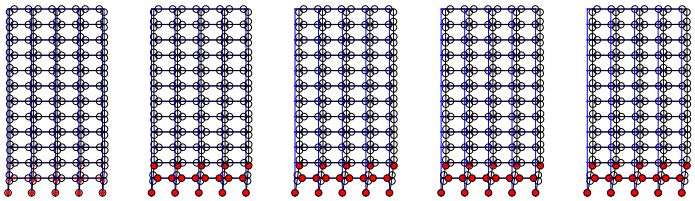

1102114

1.2 1.4 1.6 1.8 2.0

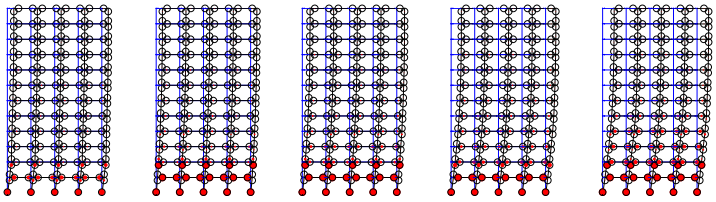

1900001

1.2 1.4 1.6 1.8 2.0

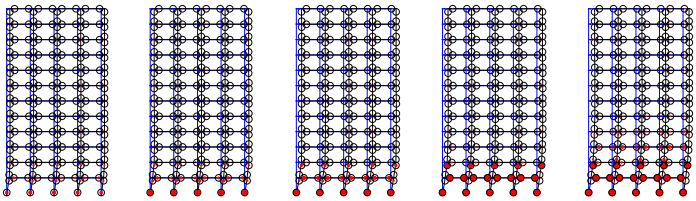

1900002

1.2 1.4 1.6 1.8 2.0

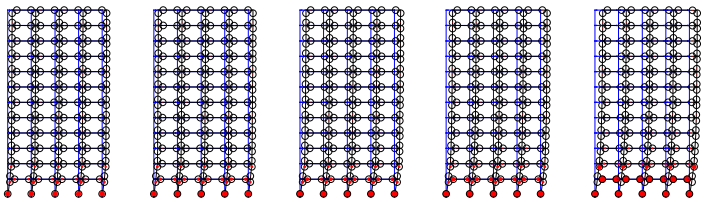

1900003

1.2 1.4 1.6 1.8 2.0

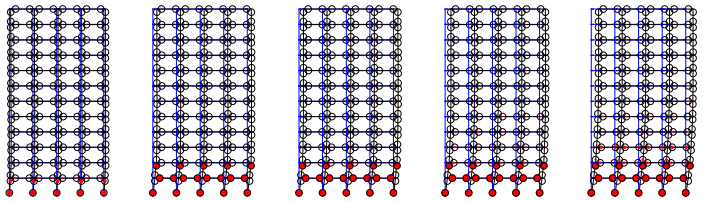

1900004

1.2 1.4 1.6 1.8 2.0

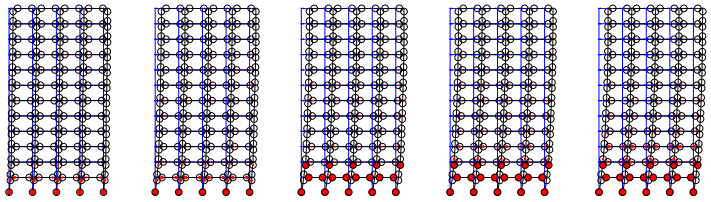

1900005

1.2 1.4 1.6 1.8 2.0

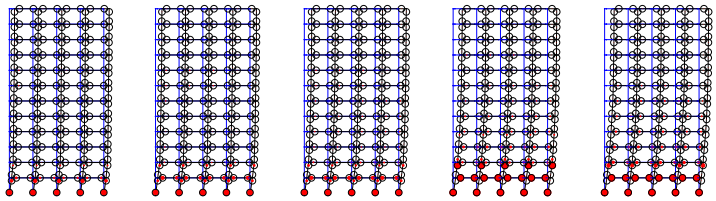

1900006

1.2 1.4 1.6 1.8 2.0

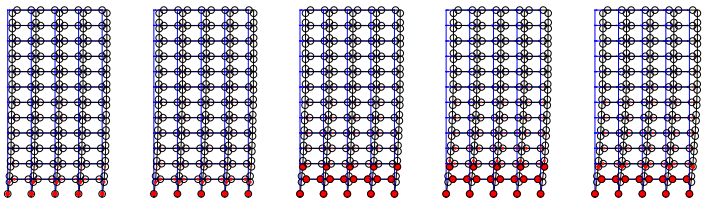

1900007

1.2 1.4 1.6 1.8 2.0

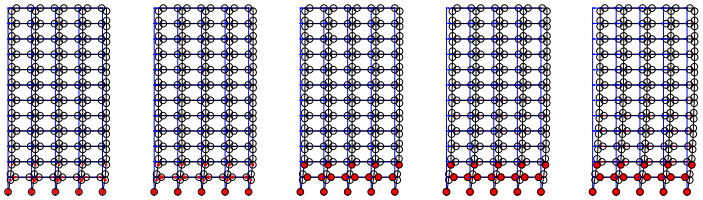

2100838

1.2 1.4 1.6 1.8 2.0

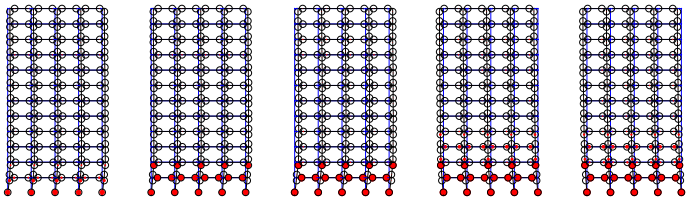

2100900

1.2 1.4 1.6 1.8 2.0

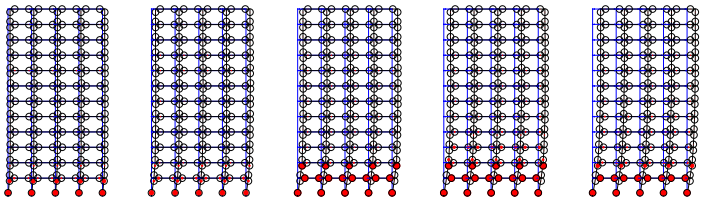

2101155

1.2 1.4 1.6 1.8 2.0

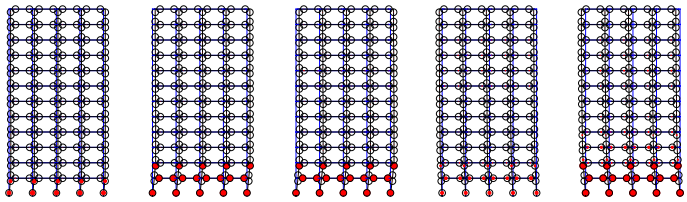

2101163

1.2 1.4 1.6 1.8 2.0

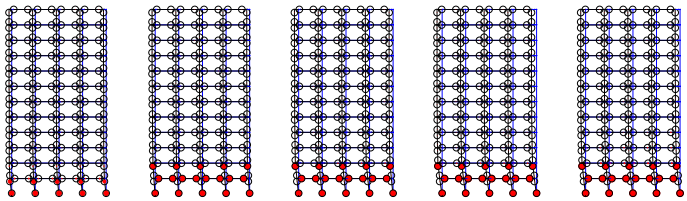

2101515

1.2 1.4 1.6 1.8 2.0

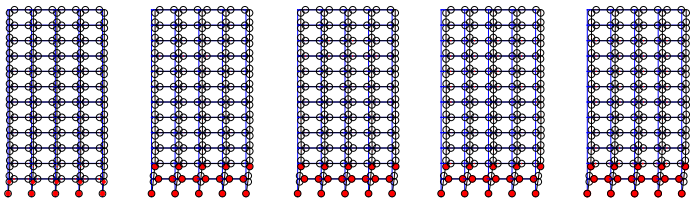

2101546

1.2 1.4 1.6 1.8 2.0

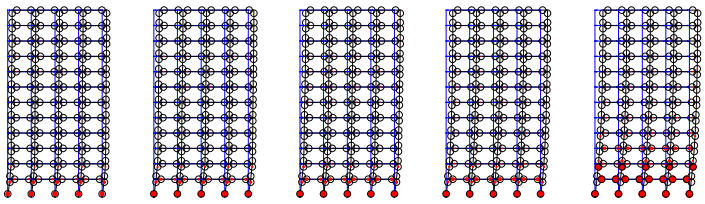

2101792

1.2 1.4 1.6 1.8 2.0

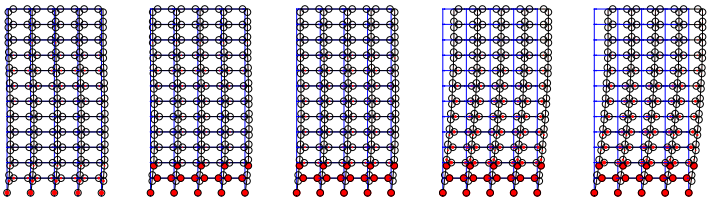

2102114

1.2 1.4 1.6 1.8 2.0

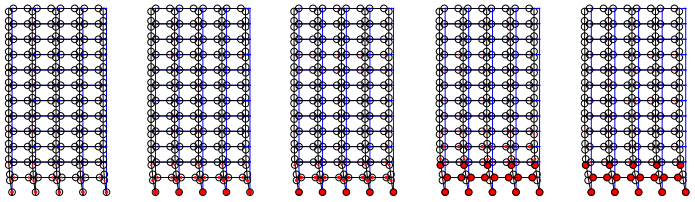

2900001

1.2 1.4 1.6 1.8 2.0

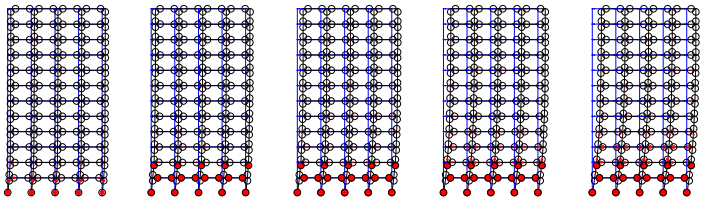

2900002

1.2 1.4 1.6 1.8 2.0

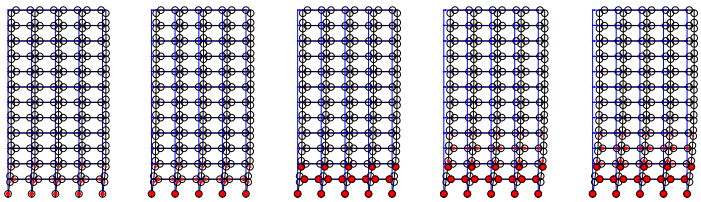

2900003

1.2 1.4 1.6 1.8 2.0

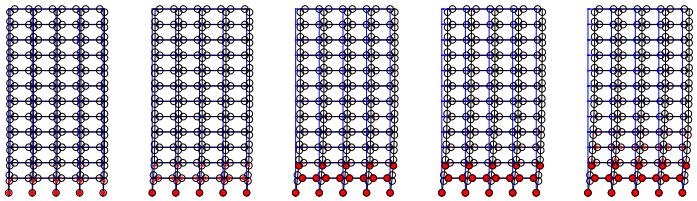

2900004

1.2 1.4 1.6 1.8 2.0

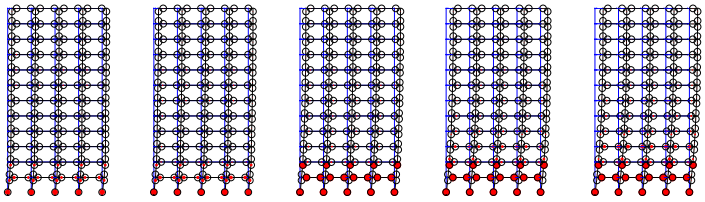

2900005

1.2 1.4 1.6 1.8 2.0

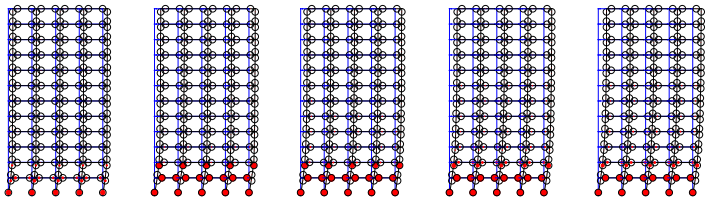

2900006

1.2 1.4 1.6 1.8 2.0

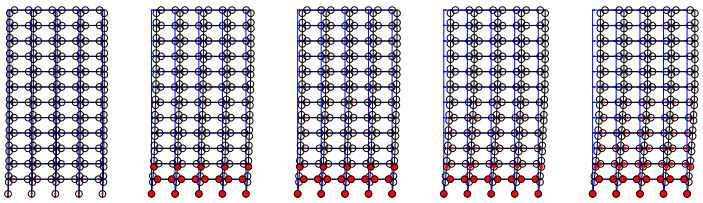

2900007

1.2 1.4 1.6 1.8 2.0

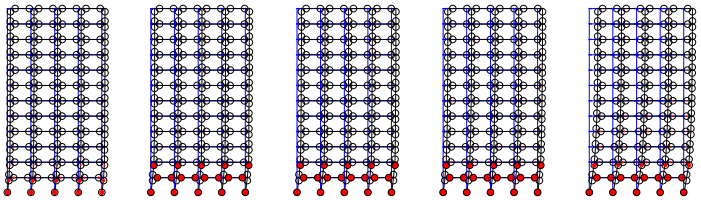

A.2 18-Story Building

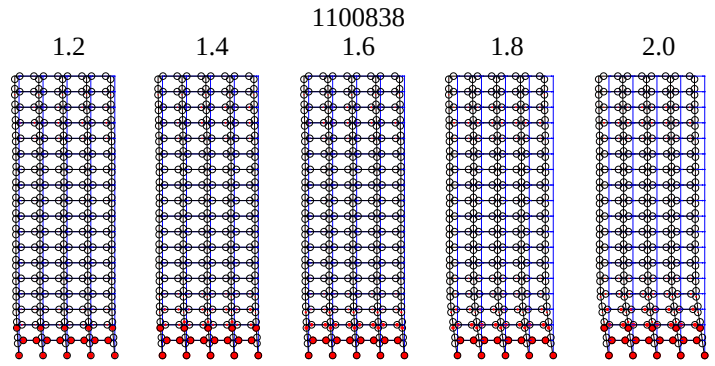

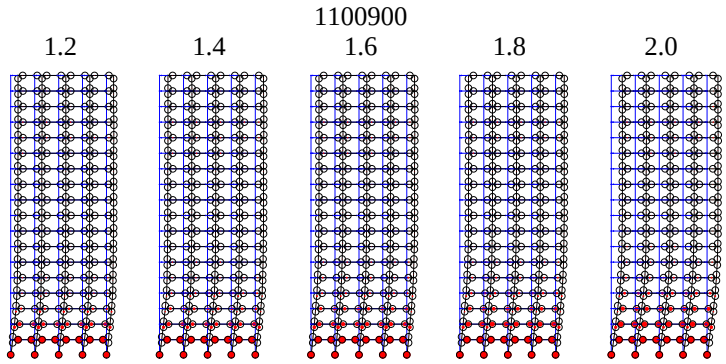

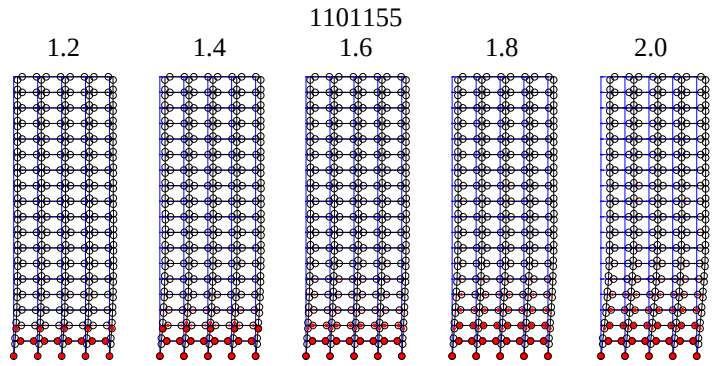

1101163

1.2 1.4 1.6 1.8 2.0

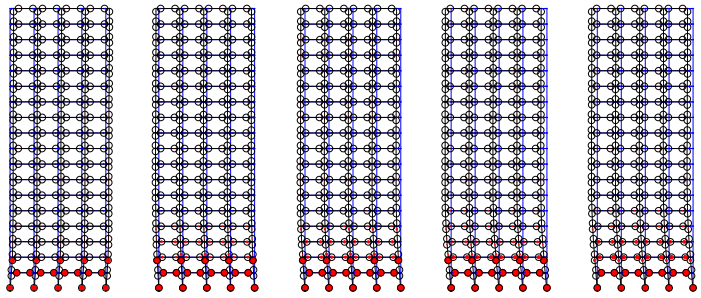

1101515

1.2 1.4 1.6 1.8 2.0

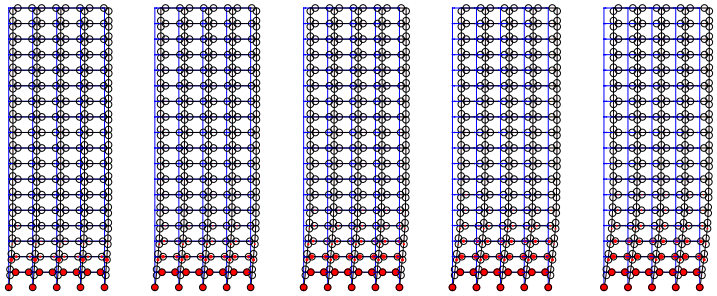

1101546

1.2 1.4 1.6 1.8 2.0

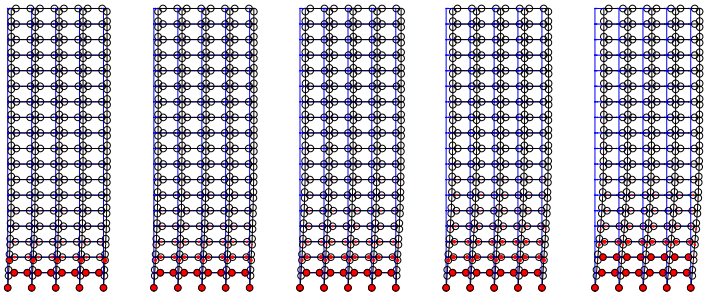

1101792

1.2 1.4 1.6 1.8 2.0

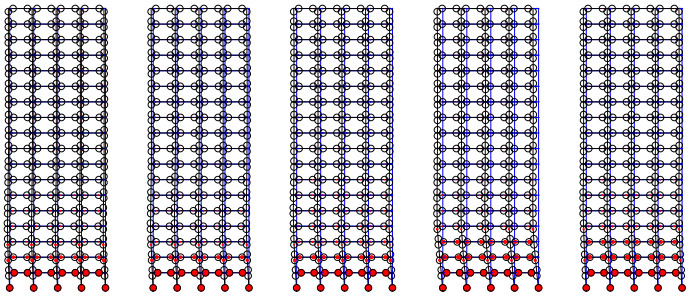

1102114

1.2 1.4 1.6 1.8 2.0

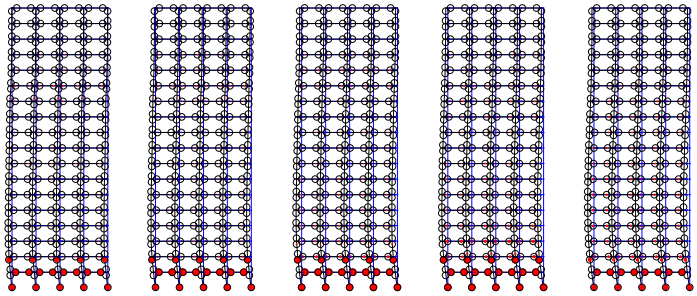

1900001

1.2 1.4 1.6 1.8 2.0

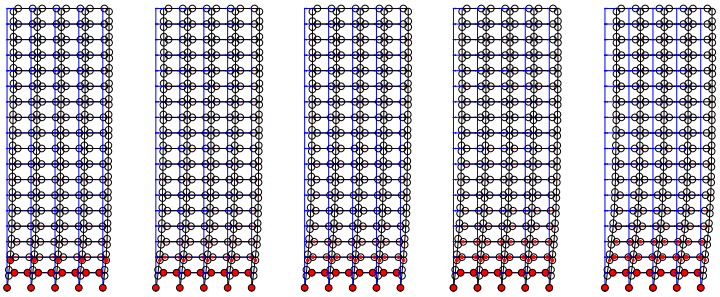

1900002

1.2 1.4 1.6 1.8 2.0

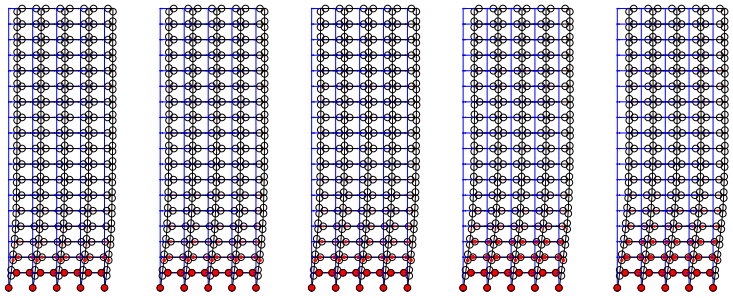

1900003

1.2 1.4 1.6 1.8 2.0

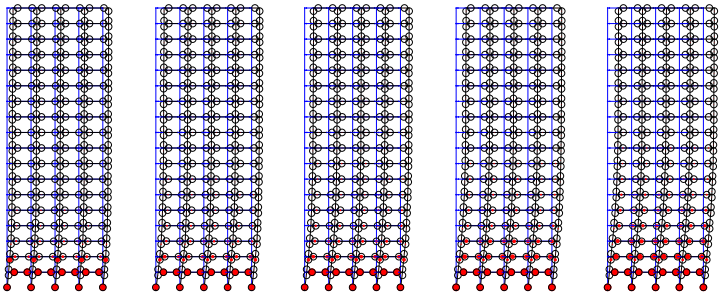

1900004

1.2 1.4 1.6 1.8 2.0

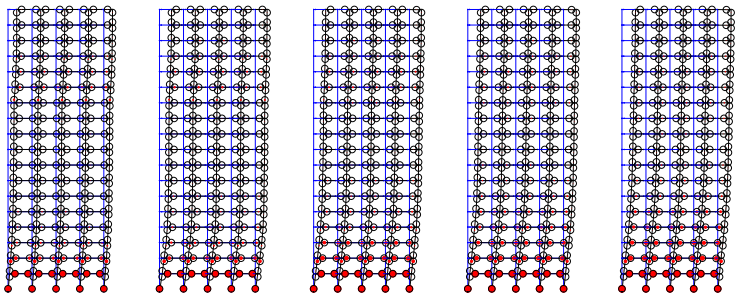

1900005

1.2 1.4 1.6 1.8 2.0

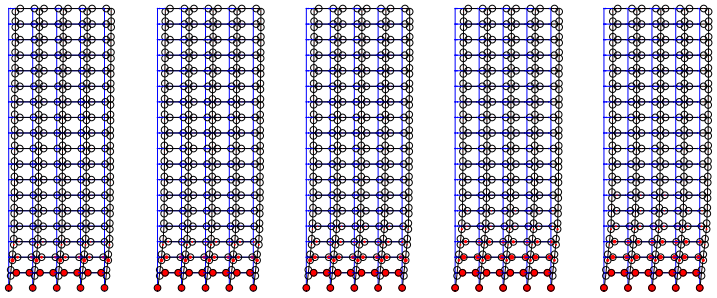

1900006

1.2 1.4 1.6 1.8 2.0

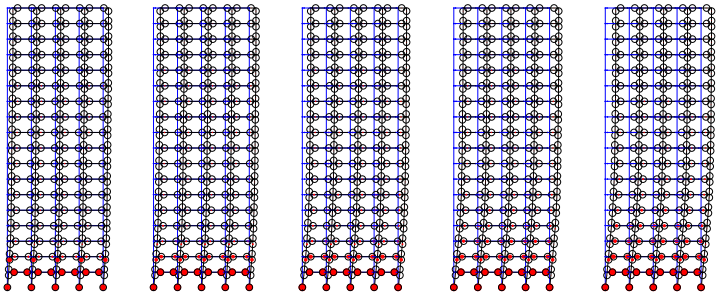

1900007

1.2 1.4 1.6 1.8 2.0

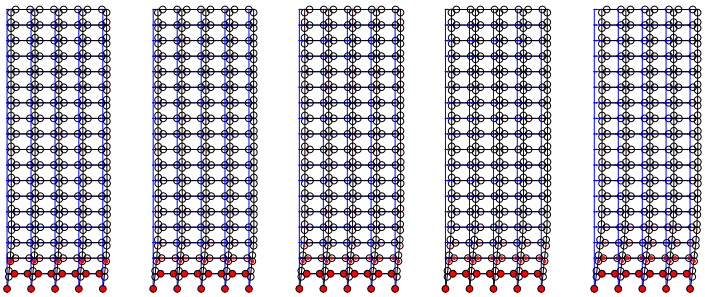

2100838

1.2 1.4 1.6 1.8 2.0

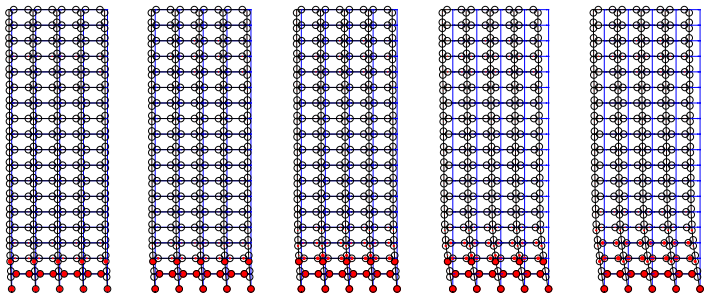

2100900

1.2 1.4 1.6 1.8 2.0

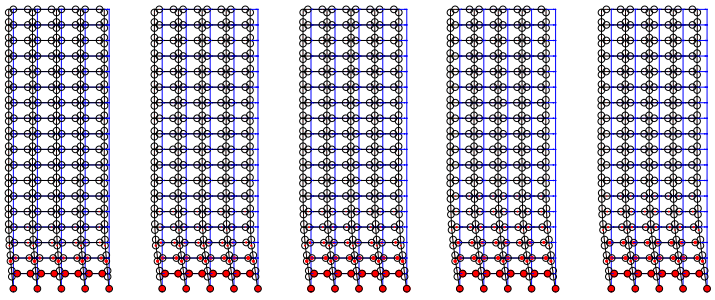

2101155

1.2 1.4 1.6 1.8 2.0

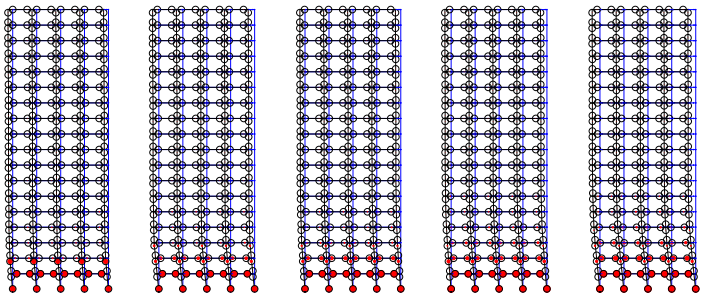

2101163

1.2 1.4 1.6 1.8 2.0

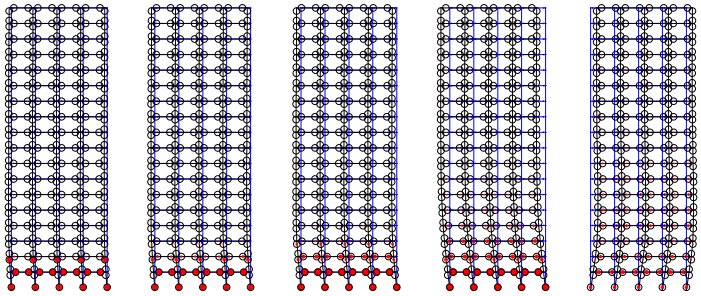

2101515

1.2 1.4 1.6 1.8 2.0

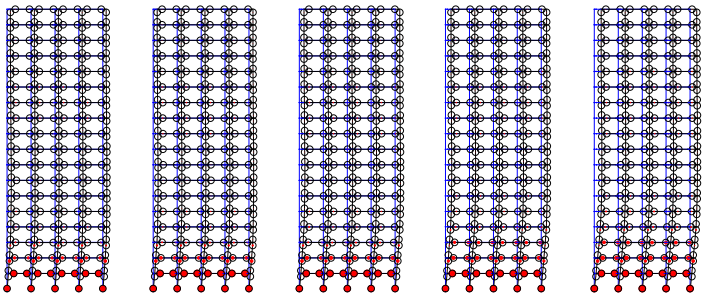

2101546

1.2 1.4 1.6 1.8 2.0

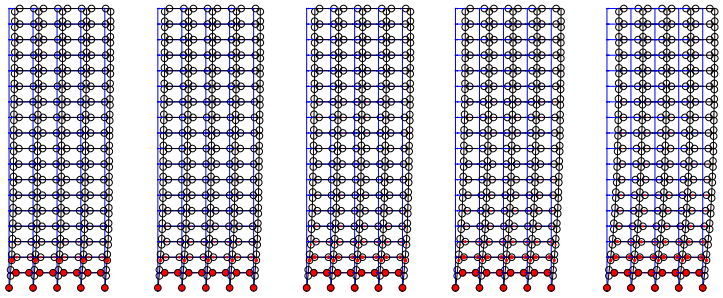

2101792

1.2 1.4 1.6 1.8 2.0

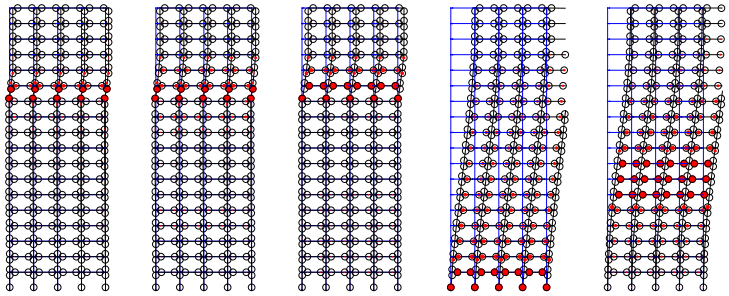

2102114

1.2 1.4 1.6 1.8 2.0

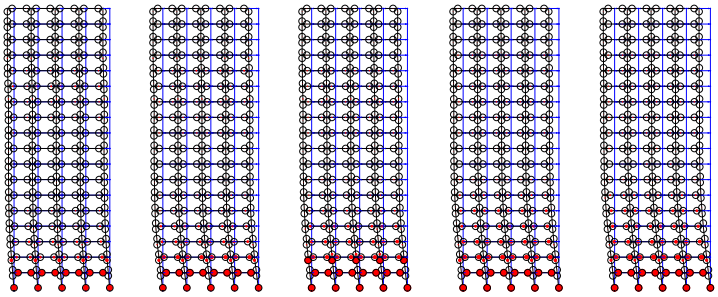

2900001

1.2 1.4 1.6 1.8 2.0

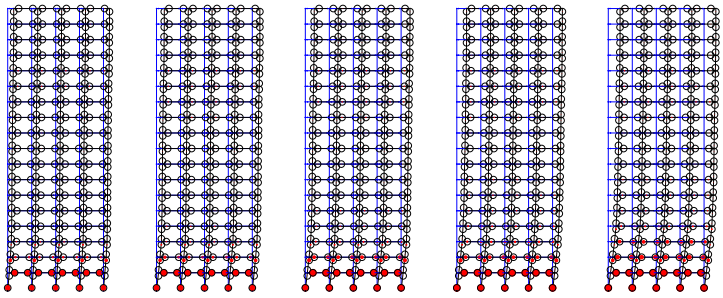

2900002

1.2 1.4 1.6 1.8 2.0

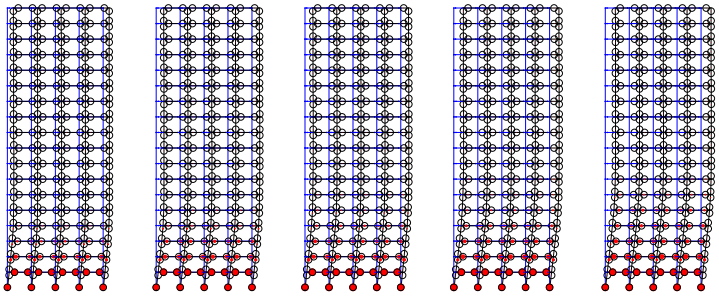

2900003

1.2 1.4 1.6 1.8 2.0

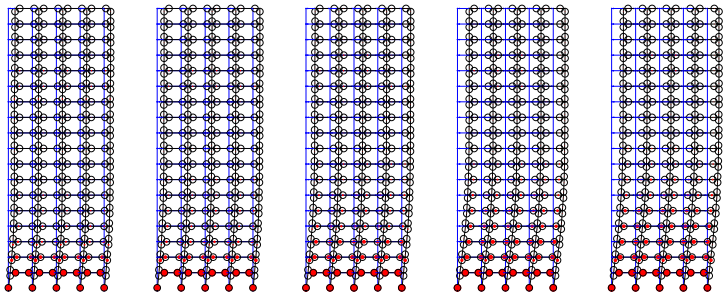

2900004

1.2 1.4 1.6 1.8 2.0

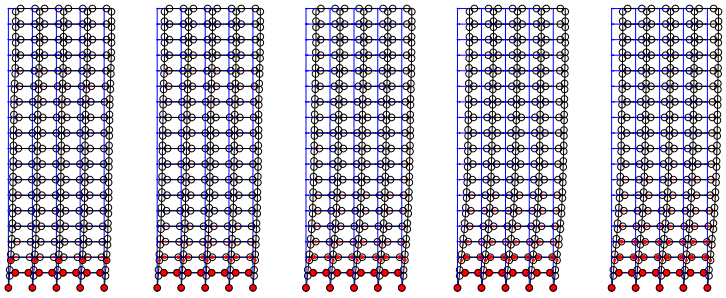

2900005

1.2 1.4 1.6 1.8 2.0

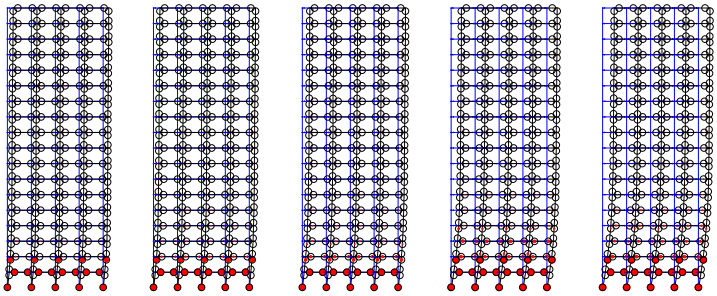

2900006

1.2 1.4 1.6 1.8 2.0

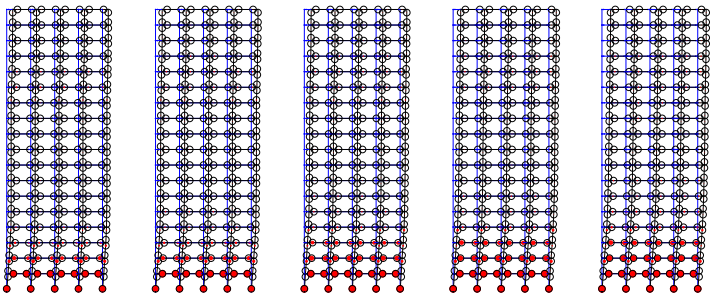

2900007

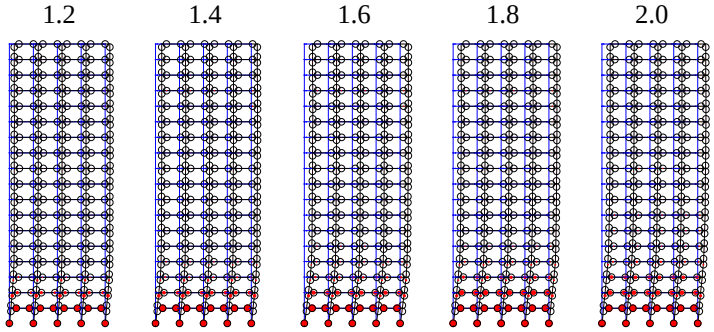

A.3 24-Story Building

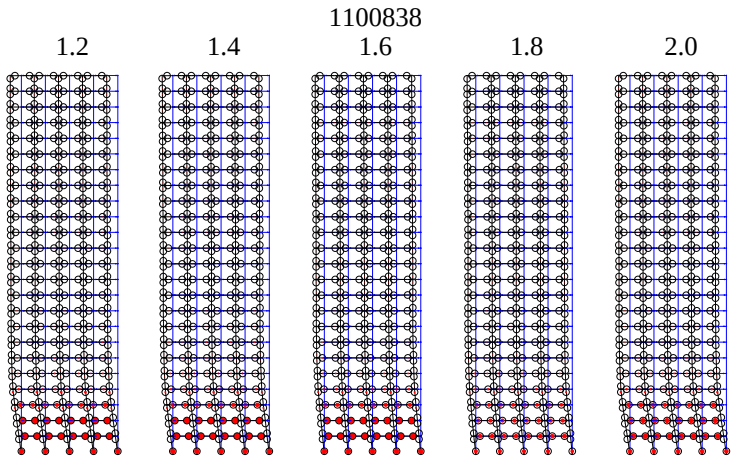

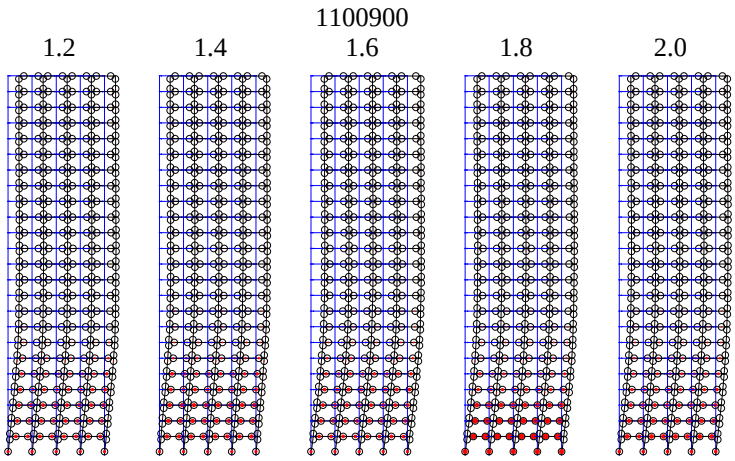

1101155

1.2 1.4 1.6 1.8 2.0

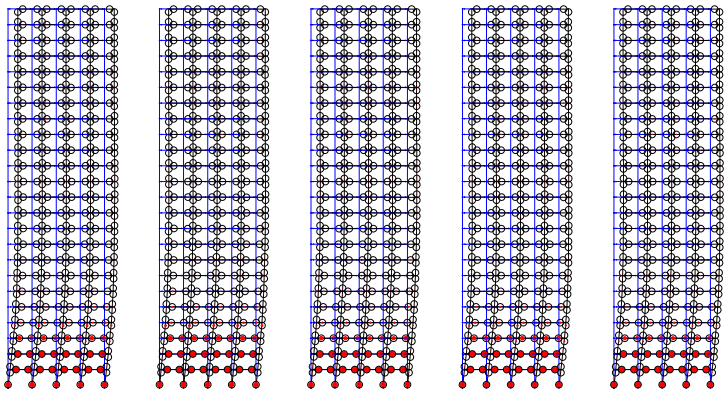

1101163

1.2 1.4 1.6 1.8 2.0

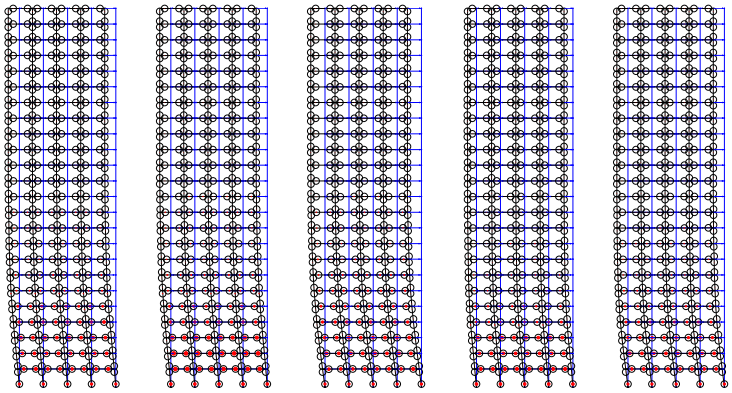

1101515

1.2 1.4 1.6 1.8 2.0

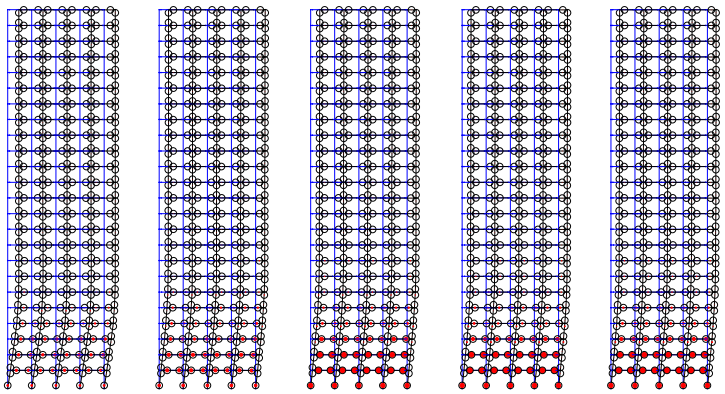

1101546

1.2 1.4 1.6 1.8 2.0

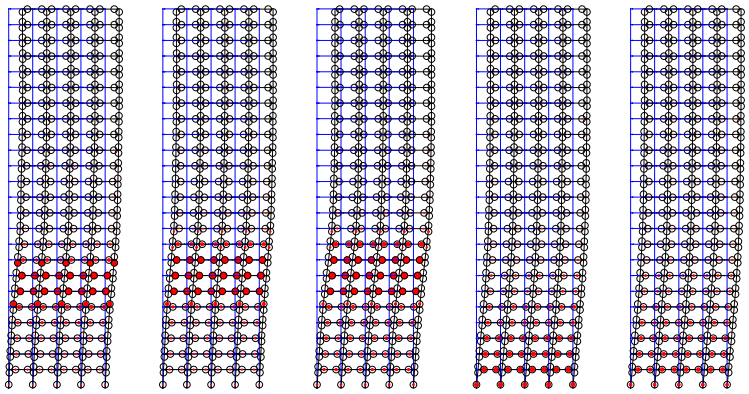

1101792

1.2 1.4 1.6 1.8 2.0

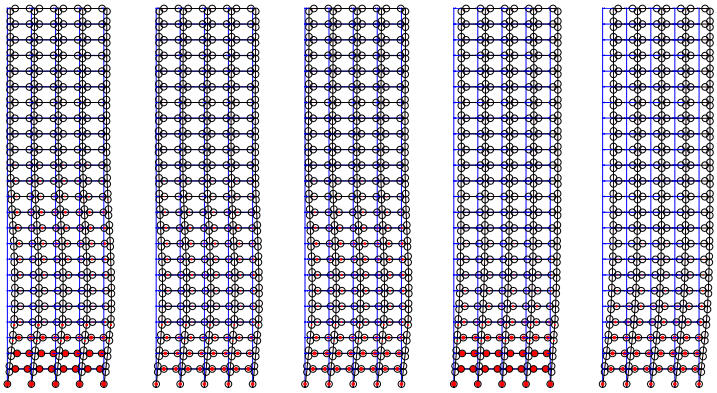

1102114

1.2 1.4 1.6 1.8 2.0

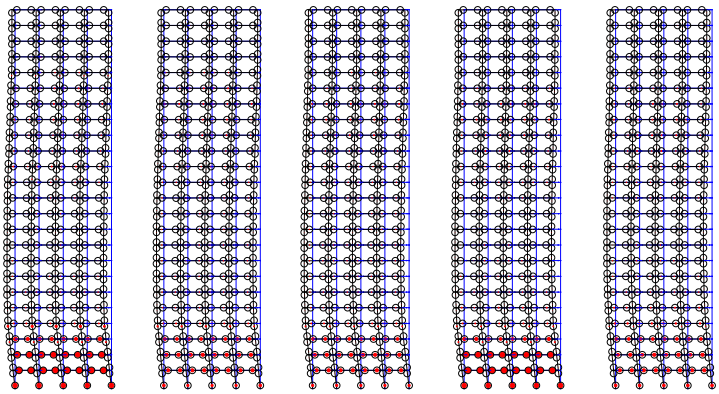

1900001

1.2 1.4 1.6 1.8 2.0

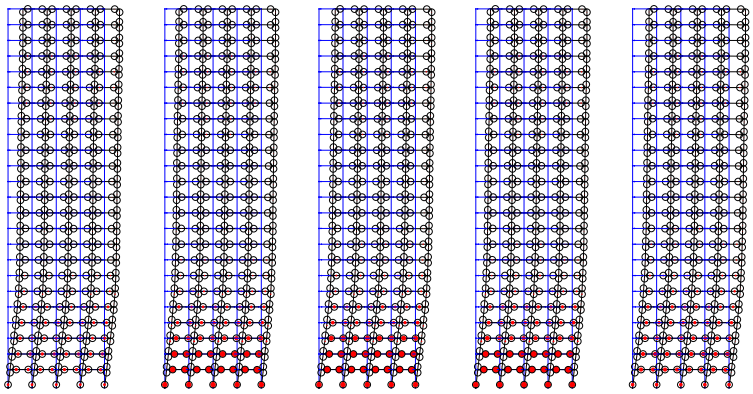

1900002

1.2 1.4 1.6 1.8 2.0

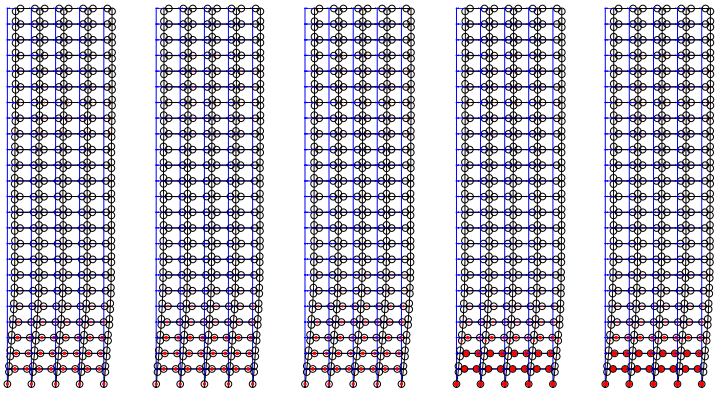

1900003

1.2 1.4 1.6 1.8 2.0

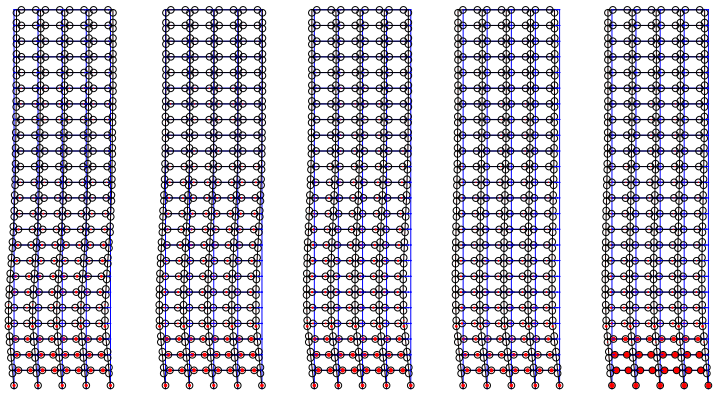

1900004

1.2 1.4 1.6 1.8 2.0

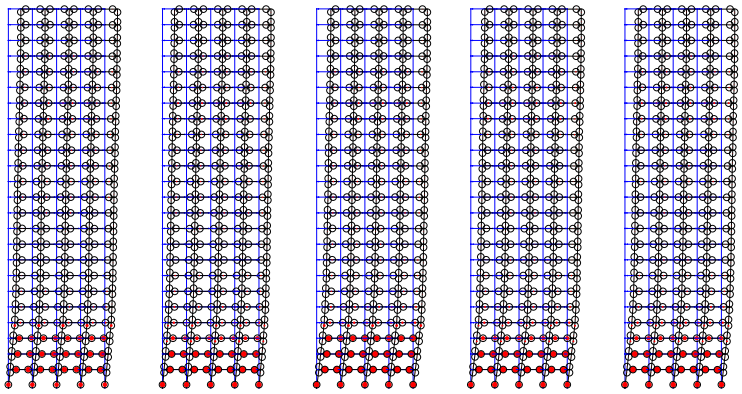

1900005

1.2 1.4 1.6 1.8 2.0

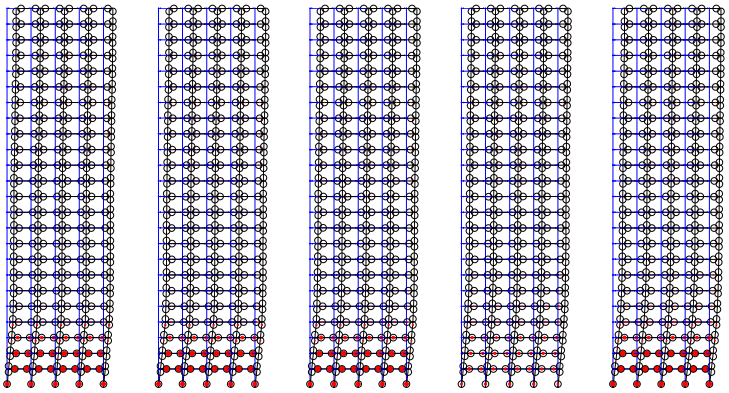

1900006

1.2 1.4 1.6 1.8 2.0

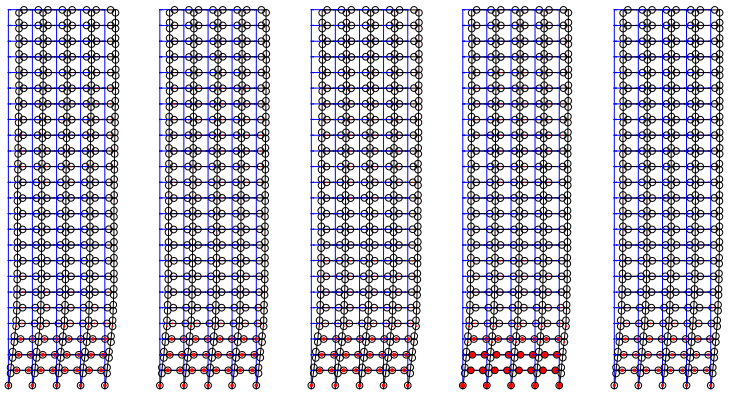

1900007

1.2 1.4 1.6 1.8 2.0

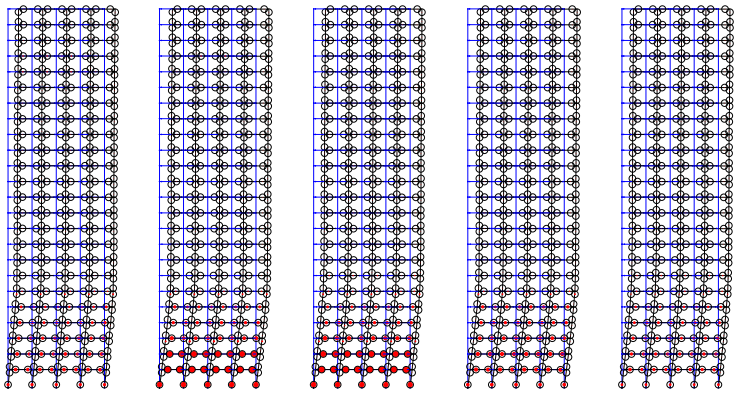

2100838

1.2 1.4 1.6 1.8 2.0

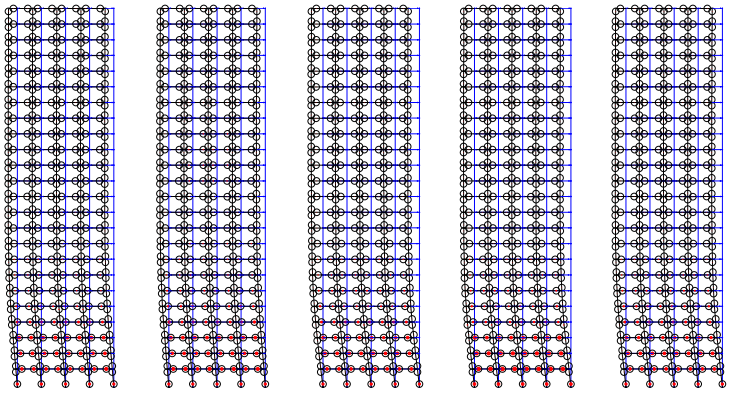

2100900

1.2 1.4 1.6 1.8 2.0

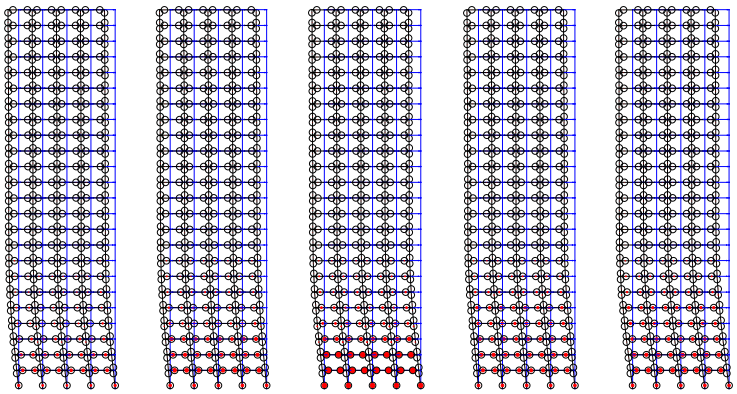

2101155

1.2 1.4 1.6 1.8 2.0

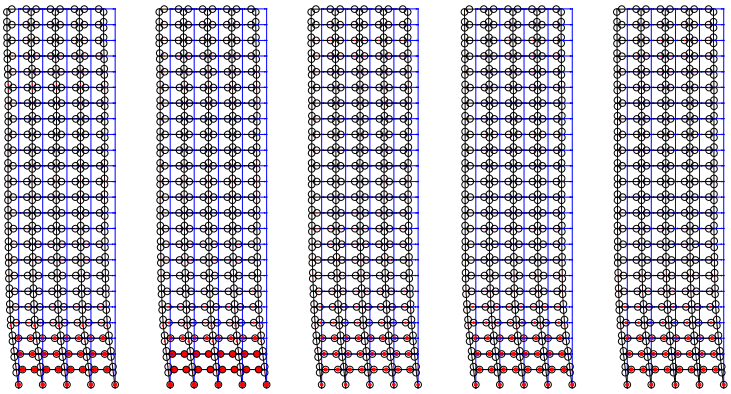

2101163

1.2 1.4 1.6 1.8 2.0

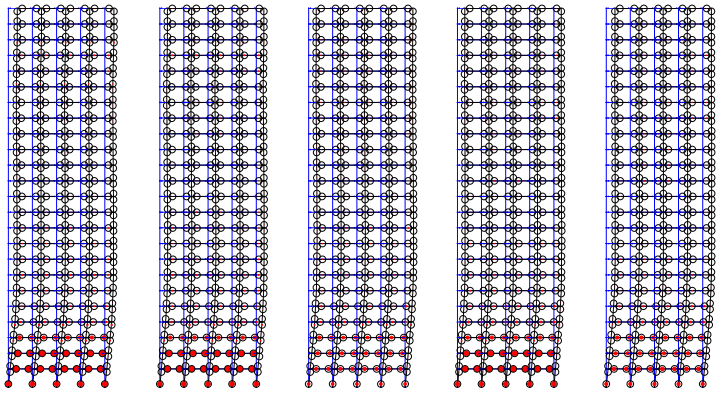

2101515

1.2 1.4 1.6 1.8 2.0

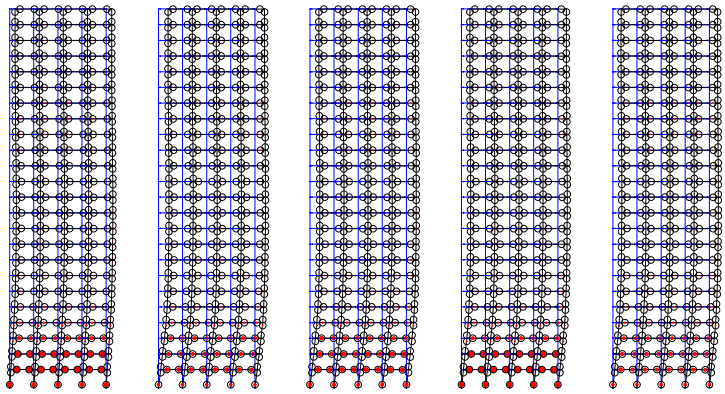

2101546

1.2 1.4 1.6 1.8 2.0

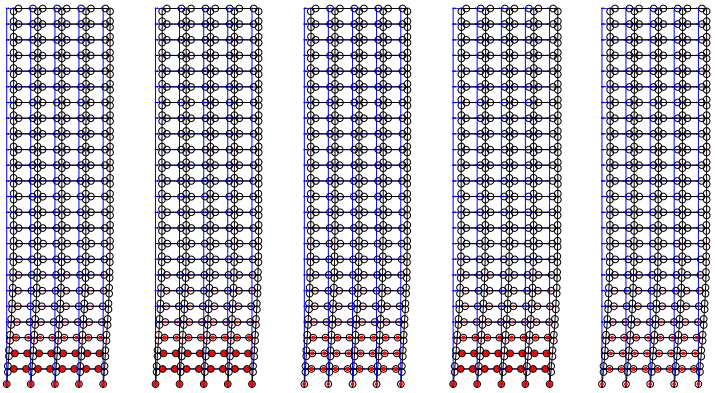

2101792

1.2 1.4 1.6 1.8 2.0

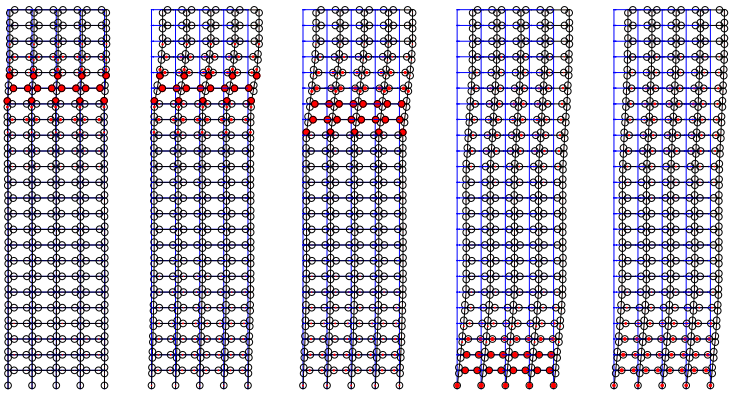

2102114

1.2 1.4 1.6 1.8 2.0

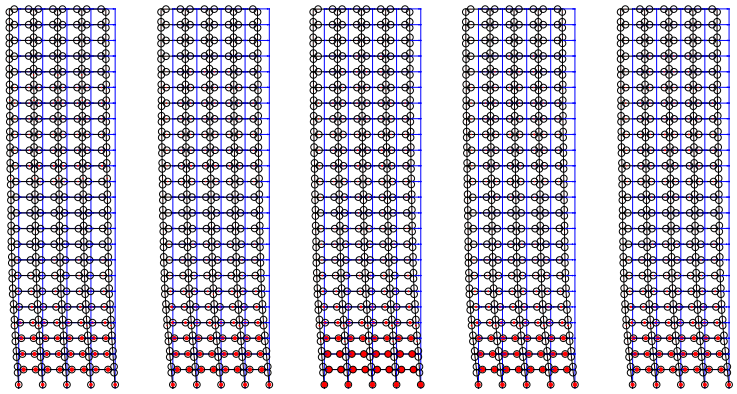

2900001

1.2 1.4 1.6 1.8 2.0

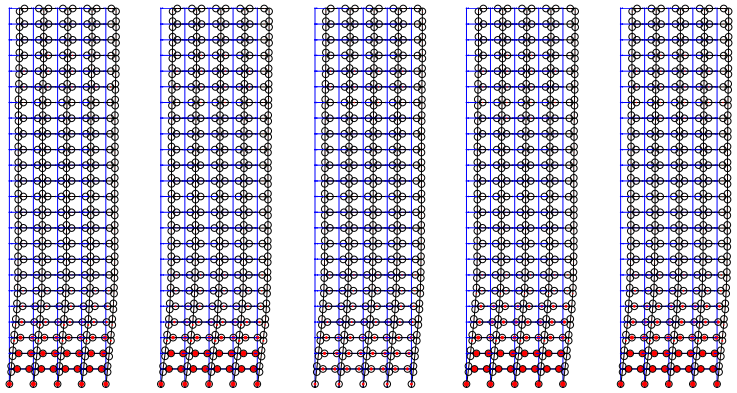

2900002

1.2 1.4 1.6 1.8 2.0

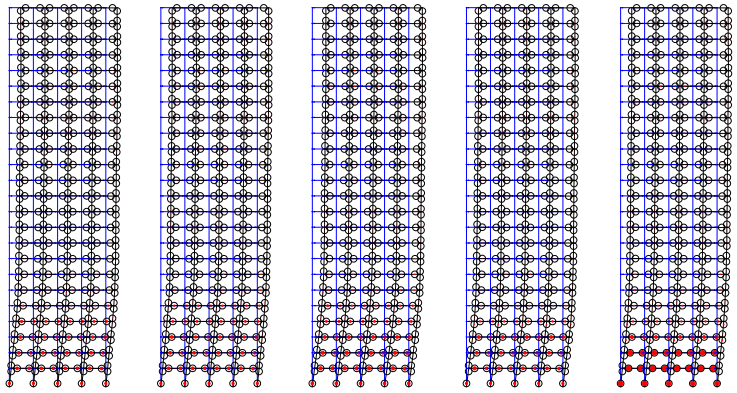

2900003

1.2 1.4 1.6 1.8 2.0

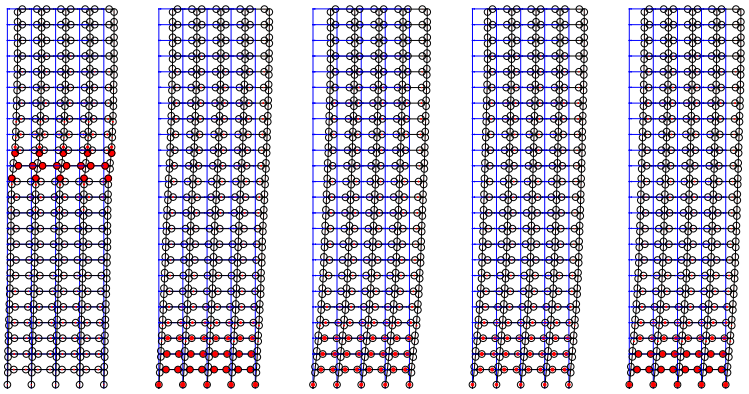

2900004

1.2 1.4 1.6 1.8 2.0

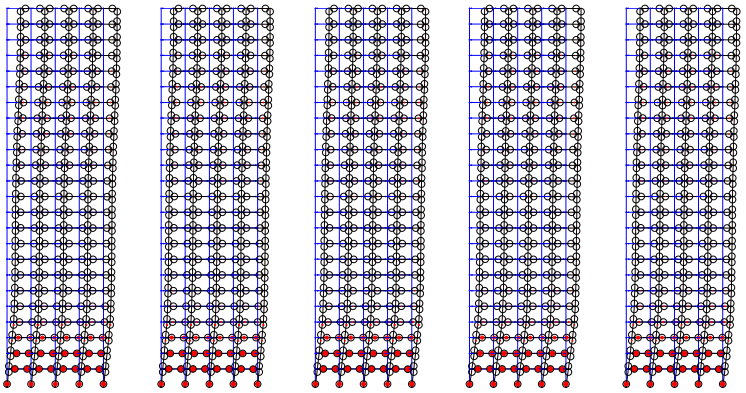

2900005

1.2 1.4 1.6 1.8 2.0

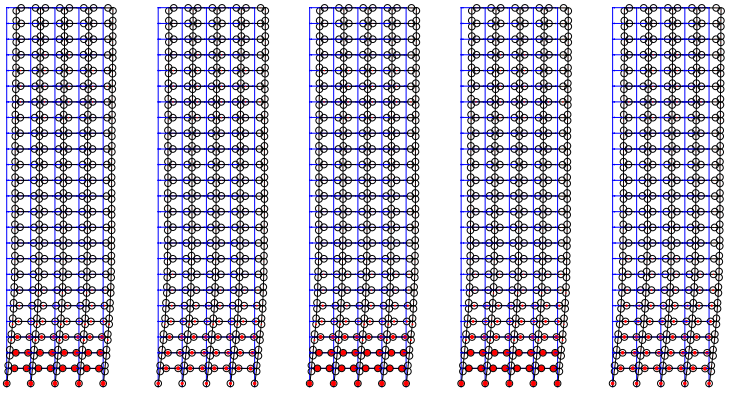

2900006

1.2 1.4 1.6 1.8 2.0

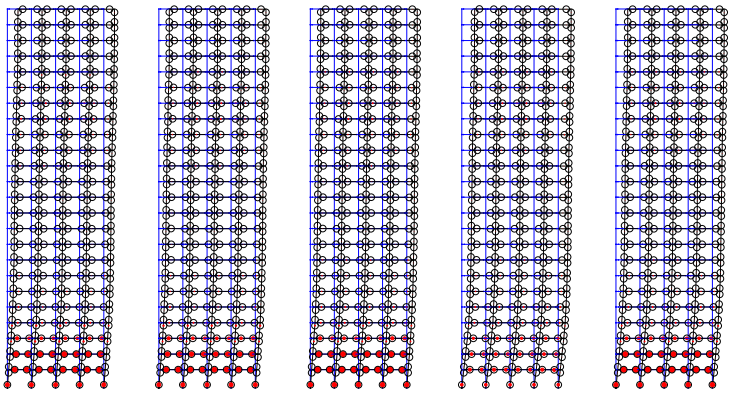

2900007

1.2 1.4 1.6 1.8 2.0